Studies on Synthesis, Structure, and Properties of Metal Coordinated N-Confused Calixphyrin Analogues.

プシュパナンダン, プルネンス

https://doi.org/10.15017/2534410

出版情報：Kyushu University, 2019, 博士（工学）, 課程博士
バージョン：
権利関係：

Doctoral Thesis

Studies on Synthesis, Structure, and Properties of Metal Coordinated N-Confused Calixphyrin Analogues.

Poornenth Pushpanandan

Department of Chemistry and Biochemistry
Graduate School of Engineering
Kyushu University
2019

Table of Contents

Chapter 1. GENERAL INTRODUCTION

1-1. Porphyrin

Porphyrin is a group of aromatic macrocyclic organic compounds, which consists of four pyrrole units connected with each other via α carbon by a methylylidene group. As these macrocycles can chelate different metal ions in their core these isomers of these macrocycles are often seen in natural systems (Figure 1-1). Porphyrin gained initial attention among the researchers due to the key role it

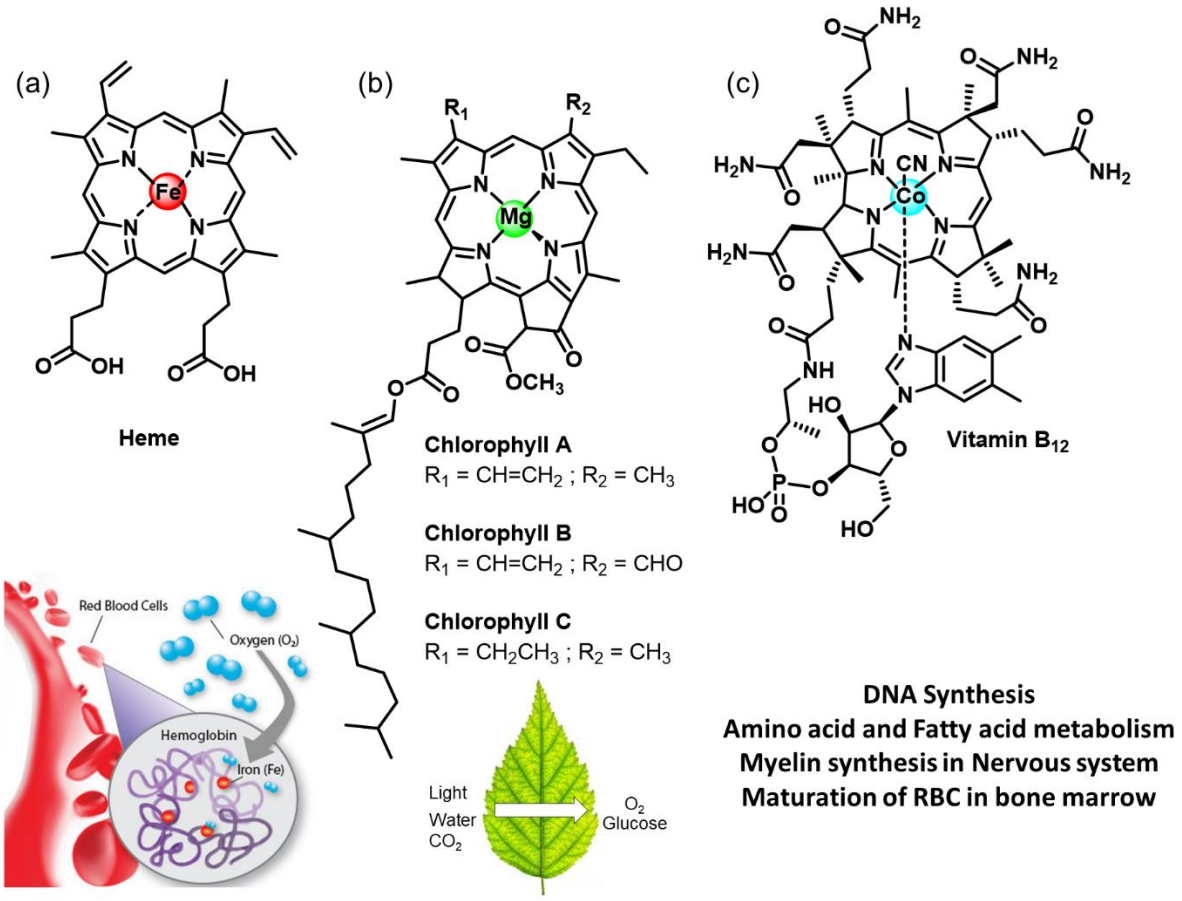

Figure 1-1. Structure of naturally occurring porphyrin derivatives and their functions. (a) Fe (II) porphyrin known as Heme which is present in animals for O_2 transport (b) Mg (II) containing Chlorophyll in plants for photosynthesis (c) Co (III) containing vitamin B_{12} found in most of the cells for multiple purposes.

plays in the natural system. It is well known that red blood cells of animals can transport oxygen due to hemoglobin which has a Fe(II) porphyrin derivative heme in it. The porphyrin derivatives are found in

plants in the chloroplast of a leaf in the form of chlorophyll which helps in photosynthesis. The structure of chlorophyll and heme was discovered by Willstätter and Fisher in the early 20th century for which they received Nobel prize in 1915 and 1930, respectively.[1] Similarly, vitamin B_{12} or cyanocobalamin contains Co(III) porphyrinoid derivative which is involved in the metabolism of every cell in the human body as well as many functions like the synthesis of DNA, helps in the functioning of the nervous system and many more. The vitamin B_{12} structure is similar to that of heme in which there are four nitrogen atoms bonded to the metal, however, the structure is more closely associated with the corrin ring.

The parent porphyrin which has no substitution in the meso position with 18 π electrons is called porphine. These highly conjugated tetrapyrrolic macrocycle consists of two amine like nitrogen in the core which makes it a divalent macrocycle. These aromatic macrocycles show interesting

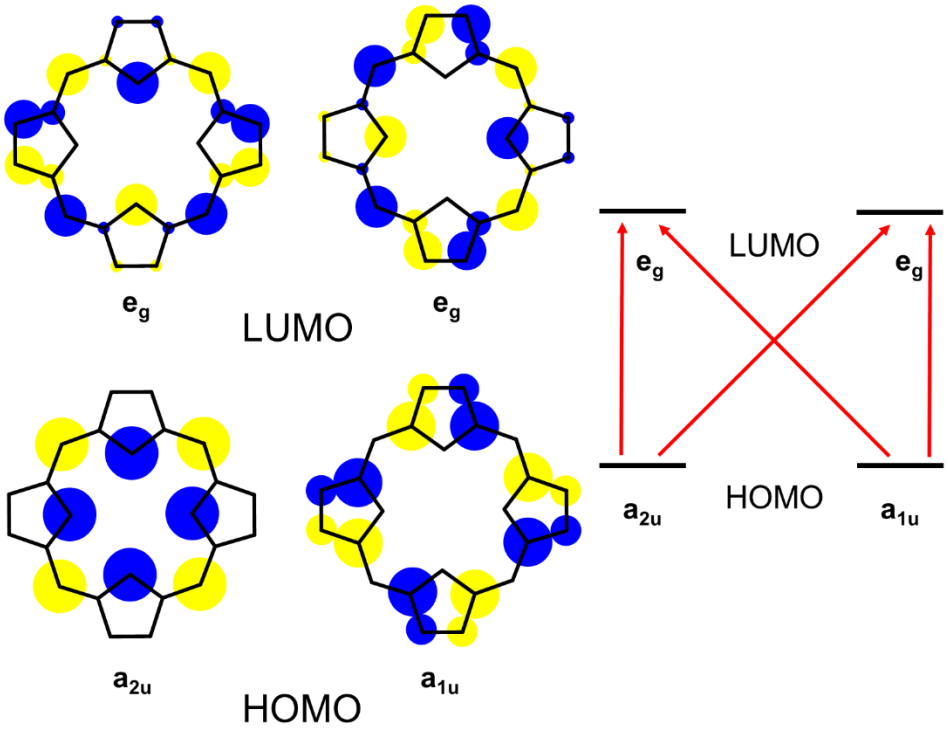

Figure 1-2. Frontier orbital by Gouterman's four orbital model for porphyrins. Porphyrin HOMO's and LUMO's (left) and the orbital diagrams showing possible electronic transitions (right). The HOMO's are represented as degenerate orbitals but the energies are related to substitution on the parent macrocycle.

photophysical properties such as strong absorption in the visible region (400 nm) commonly known as Soret band or B band and weak absorption around 550 nm known as the Q band. The soret band is due to the transition to the second excited state (S_0 to S_2) and Q band is due to the weak transitions to first excited state (S_0 to S_1). The absorptions can be explained by considering the four frontier orbitals, two HOMO and

two LUMO which is put forth by Gouterman and widely known as Gouterman's four orbital model.[2] The fluorescence is only observed majorly from S_1 as the internal conversion (S_2 to S_1) is a very fast reaction in the order of 10^{-15} seconds. Recently, a number of researchers are working on this cyclic conjugated system for utilizing their optical and electronic properties. Porphyrin analogues are synthesized to tailor its properties according to their needs.

1-2. Porphyrin analogues

Over the past 20 years, there has been a growing interest among the synthetic porphyrin chemists to synthesize and study the properties of the structural analogues of porphyrin. The structural modifications result in marked changes in the optical, redox, and ion-coordination properties, making them potentially suitable for a wide range of applications. Porphyrin analogues can be classified into 4 groups, expanded porphyrin, isomeric porphyrin, contracted porphyrin, and core-modified porphyrin (Figure 1-3).[3]

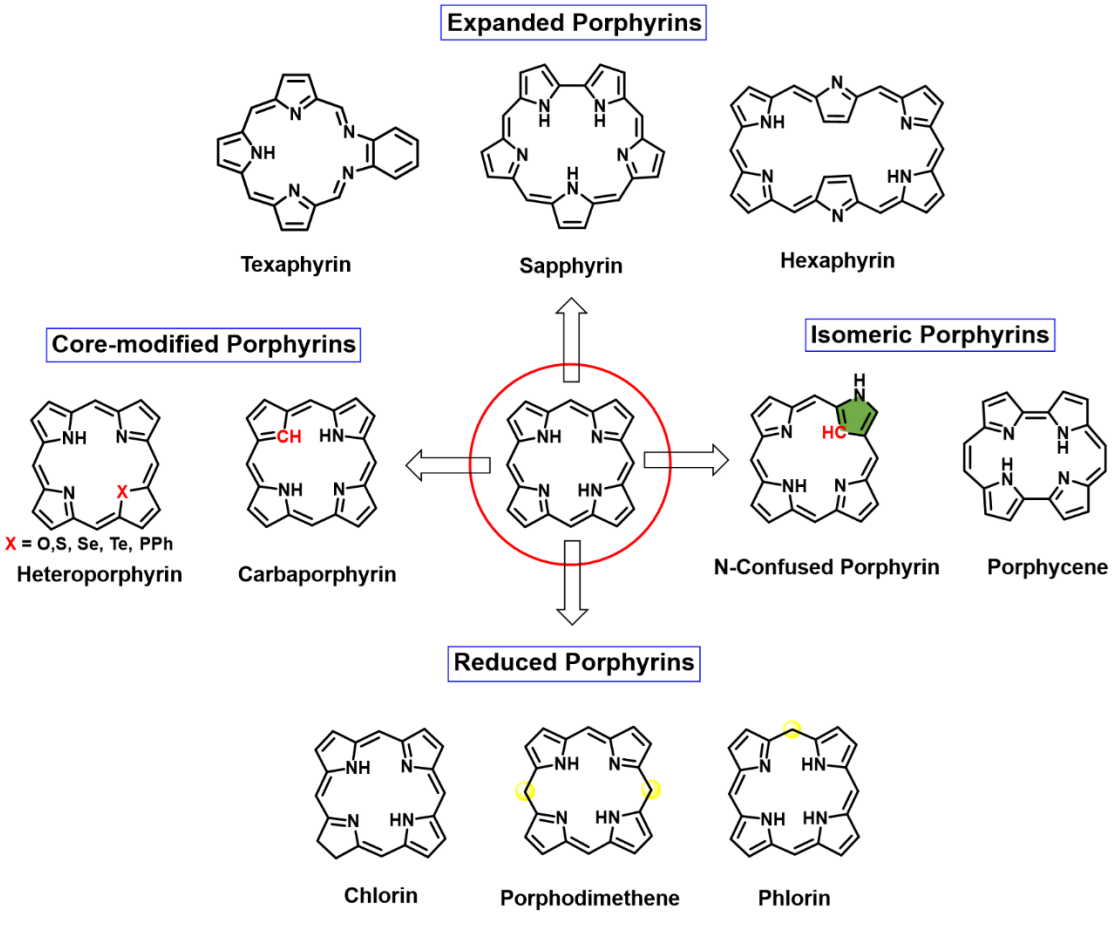

Figure 1-3. Chemical structure of porphyrin analogues.

A great deal of effort has been devoted by synthetic chemists, for designing new and efficient synthetic routes for expanded porphyrins. Expanded porphyrin differing in ring size, ring connectivity, peripheral substitution and core modification is also a major area of research in the section. Expanded porphyrins such as sapphyrin, hexaphyrin, octaphyrin consist of more than four methine carbon and pyrrole rings which makes it a larger macrocyclic conjugated system than that of the porphyrin. This structural modification leads to bathochromically shifted electronic spectra compared to porphyrin. To integrate the extended π conjugation, the molecule shows large cavity size, remarkable structural flexibility and unique multiple anion as well as cation binding properties. In addition, these macrocycles can exhibit aromatic and antiaromatic characteristics due to their flexible conformations and multiple redox states. As representative examples chemical structures of texaphyrins,[4] sapphyrin,[5] and hexaphyrins[6] shown in Figure 1-3 which belongs to the class of expanded porphyrins which possess the potential ability for biochemical applications owing to their unique optical properties and coordination abilities. These class of molecules have also shown the potential application in many fields including anion recognition, functional dyes, magnetic resonance imaging (MRI), theranostic agents and photodynamic therapy (PDT).

Isomeric porphyrins have a cyclic tetrapyrrolic skeleton with the similar molecular formula and can be obtained by rearranging pyrrole and meso-carbons in the porphyrin structure. As representative examples of isomeric porphyrins, N-confused porphyrin, and porphycene are shown in Figure 1-3. Vogel and co-workers reported the first isomeric porphyrin, Porphycene in 1986.[7] They can stabilize metal ions in higher oxidation site due to the flexible coordination site.[8] The spectral characteristics of porphycenes, particularly their strong absorption in the red spectral region and efficient triplet-state formation, make these compounds attractive as sensitizers in PDT. These compounds have found potential applications in catalysis, organic photovoltaics, and as artificial heme component as well.[9] N-Confused porphyrin was first reported independently and almost simultaneously by the Furuta and Latos-Grażyński groups in 1994.[10] Since then, NCP has been widely used for various applications because of their unique coordination and optical properties.[11] The pyrrolic NH from the N-confused pyrrole lies at the periphery of the macrocycle, thus the peripheral NH groups also show coordination properties. The asymmetric structure diffuses the degeneracy seen in the molecular orbitals and HOMO-LUMO energy gap becomes narrower leading to redshifted photophysical properties.[11]

Another important porphyrin analogue is calixphyrin. These are seen as intermediate in the natural porphyrin synthesis. Calixphyrins have one or more sp^3 meso carbons (maximum 3) in tetrapyrrolic systems. My work which I will discuss in the thesis is about this particular porphyrinoid, and will be discussed in detail in the coming sections.

Another important class of porphyrin analogues are core-modified porphyrins in which one (or more) pyrrole N's within the porphyrin macrocycle are replaced by other atoms such as O, S, Se, Te, Si, P, and C. These conjugated porphyrins are termed as heteroatom-containing porphyrins or even sometimes called as carbaporphyrins (when replaced with carbon atom). These class of molecules are the most recent among the porphyrin analogues and provide great opportunity to study the wide range of chemistry which generate potential applications in various fields.[15] The molecular orbitals can be tailored via core-modifications to obtain desired photophysical properties according to the number of heteroatoms substituted. The chemistry of core-modified porphyrins has evolved over the years after the first synthesis in 1970s and since then, many new heteroatom-substituted porphyrinoids such as heteroporphyrins, confused heteroporphyrins, and heterocarbaporphyrins were synthesized and their properties have been widely explored for potential applications.[15] In addition, great efforts have been made in the combination of heteroporphyrins with ring-expanded and contracted porphyrins to further manipulate the metal ion coordination properties.

In addition, there are contracted porphyrin analogues with smaller internal cavities with at least one or more *meso*-carbons or one pyrrole ring less as compared to porphyrin macrocycle. The first corrole was synthesized by Johnson and Kay in 1964 as they are structurally similar to Vitamin B_{12}. Until 1999 very few corrole based systems are reported due to the synthetic difficulties. In 1999, Gross and coworkers reported the facile synthesis of corrole derivatives.[12] Since then hundreds of corrole derivatives and corresponding metal complexes (metallocorroles) were developed to utilize for practical applications in chemistry and biology.[13] Corroles should be the most studied porphyrin analogue due to facile synthesis and advantage in photophysical properties such as strong fluorescence. Other notable examples such as subporphyrins, norcorroles, and isocorroles also belong to the family of contracted porphyrins.[14]

1-3. N-Confused Porphyrin

Linus Pauling and Melvin Calvin predicted the structure and properties of N-confused porphyrin (NCP) in 1944.[16] After 50 years our group and Latos-Grażyński's group independently reported the synthesis and characterization of N-confused porphyrin (NCP) in 1994.[10] Normally in porphyrin the pyrrole rings are connected to each other with a meso carbon and each pyrrole ring is connected to the meso carbon through the α, α' positions of respective pyrroles. However, in NCP one of the four pyrrole rings are connected to meso carbon atoms through α, β' positions to form the tetrapyrrolic macrocycle (Figure 1-4.). Accordingly, NCP is also an isomer of porphyrin which can be categorized to the carbaporphyrins family as well due to the NNNC core.

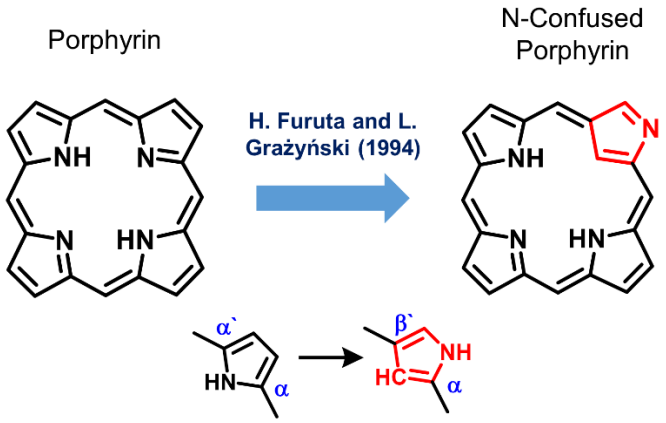

Figure 1-4. Chemical structure of porphyrin and N-confused porphyrin.

NCP shows an asymmetric structure and is accounted for all its properties (Figure 1-4.). These molecules show NH Tautomerism in solution depending on the polarity of solvent or proton its accepting capability of solvent used (Figure 1-5.).[17] For example, the molecule in a less proton accepting solvents such as toluene or CH_2Cl_2, takes a structure with 3 hydrogen atoms in the core. But, the

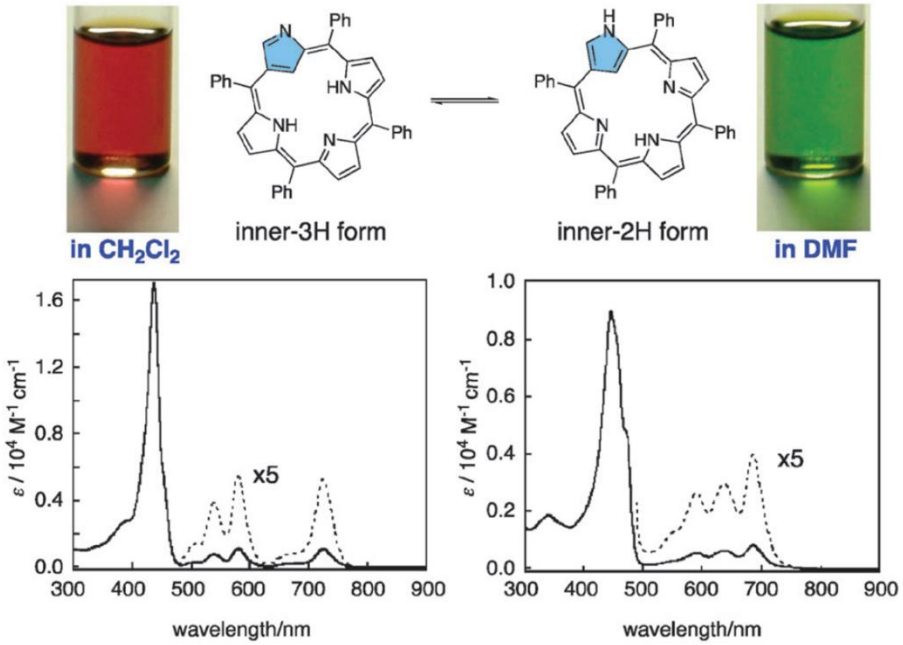

Figure 1-5. NH Tautomerism observed in N-confused porphyrin. Absorption spectra of NCP in CH_2Cl_2 and DMF, respectively.[17]

same molecule in a proton accepting solvents such as DMF or DMSO adopts a structure with 2 hydrogen atoms in the core. In a strong proton accepting solvent (DMF or DMSO) the possibility of stabilizing the overall structure by utilizing outer NH for hydrogen bonding is prominent which is absent in less proton accepting solvents. Interestingly, in a moderate proton accepting solvent mixture of the inner-3H form and the inner-2H form is observed.

The introduction of N-confused pyrrole in the macrocycle results in the loss of degeneracy among HOMO, HOMO-1 and LUMO, LUMO-1. The HOMO is destabilized and LUMO is stabilized substantially leading to a small HOMO-LUMO energy gap due to the asymmetric structure.[18] The calculated electronic distribution in the frontier molecular orbitals are shown in Figure 1-6. In the frontier orbitals of NCP, the lowest two unoccupied orbitals (LUMO) (Figure 1-6.) are both of e_g symmetry and are similar to those of tetraphenylporphyrin (H_2TPP). Because of the decrease in symmetry in the ring the LUMO and LUMO +1 is nondegenerate and separated in energy unlike H_2TPP. The two highest occupied orbitals (HOMO) in NCP is in a_2u and the HOMO-1 is in a_1u symmetry. In H_2TPP it is the other way around. The degenerate HOMO and HOMO-1 in H_2TPP are separated substantially in NCP. Thus stabilizing the LUMO and destabilizing the HOMO orbitals results in a narrower HOMO-LUMO energy gap compared to that of H_2TPP. It is clear from this discussion the difference in the molecular orbital imparted by inversion of a pyrrole ring in the macrocycle will cause significant changes in the electronic features.

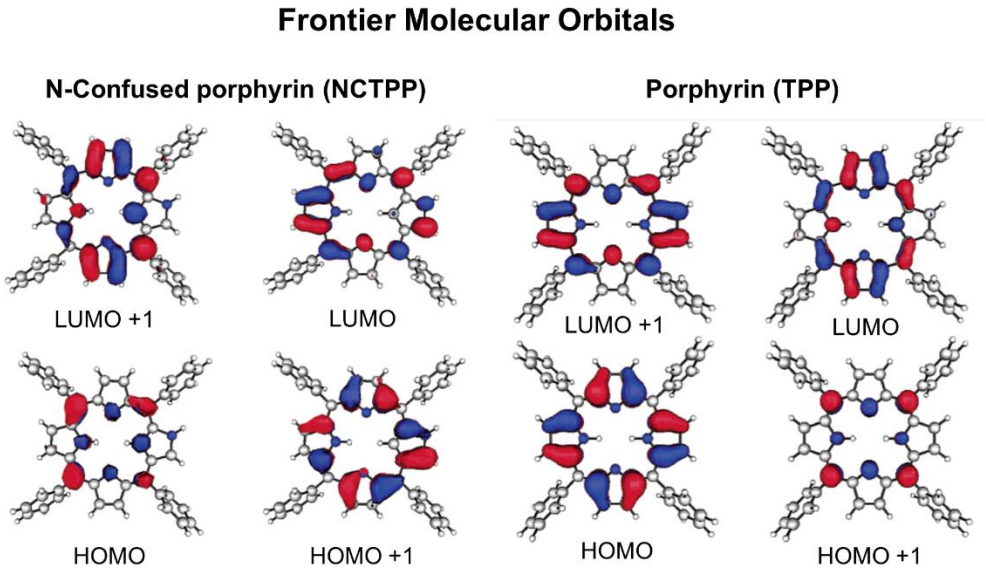

Figure 1-6. Frontier molecular orbitals of NCP and TPP.[18]

With respect to the solvent used the photophysical properties changed due to the predominance of inner-3H form and inner-2H form. This also gathered considerable attention and have been studied in detail.[19] The MOs for both 3H and 2H are ring-based and much similar to those predicted by Gouterman's four

electron four-orbital model for porphyrin. Reported emission quantum yield of NCTPP lower than those of TPP, even the fluorescence lifetime of NCTPP is shorter than TPP.[20] With an increase in interest among researchers for the NCP, many metal complexes have been reported. Figure 1-7 summarizes all the metal complexes of NCP reported till 2019[21] except for alkali and alkali earth metal complexes such as Li complex of NCP reported by Ziegler and co-workers.[22]

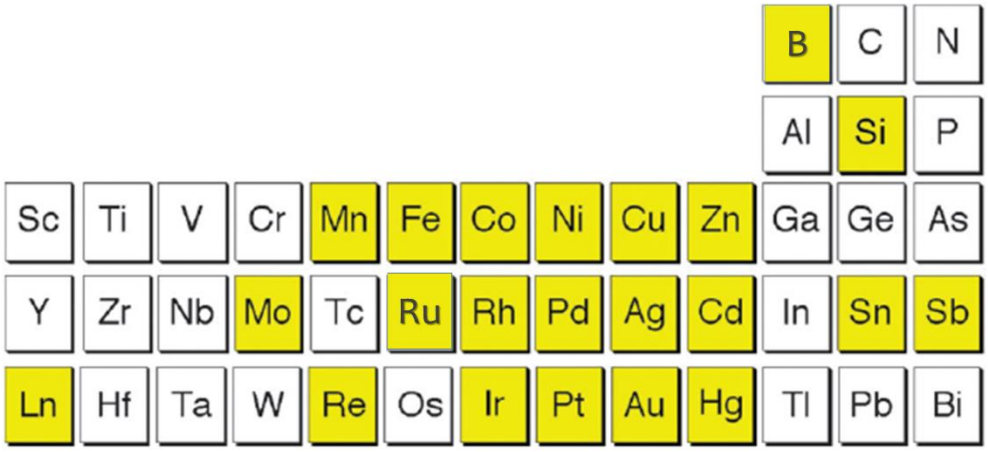

Figure 1-7. Reported NCP metal complexes up to 2019.

1-4. Calixphyrin

All hybrid porphyrin analogs which contain a mixture of sp^2 and sp^3 hybridized meso-carbon can be coined under the class of macrocycle, known as calixphyrin. Structurally it shows characteristics of both porphyrins and calix[4]pyrroles as both metalation and anion binding properties are present.[23] Calixphyrin molecules with 4 pyrrole rings were the early ones to be studied and they are (1) Calix[4]phyrin(**1**.*1*.*1*.*1*) (Figure 1-6. **C4P-1**) which contains one sp^2-hybridized meso carbon atom and all other meso positions are sp^3 hybridized, (2) Calix[4]phyrin(**1**.*1*.**1**.*1*) and Calix[4]phyrin(**1**.**1**.*1*.*1*) (Figure 1-8. **C4P-2**, **C4P-3**) which contains two sp^2-hybridized meso carbon atoms and these can be further classified to either a "cis-" or "trans-like" (i.e., 5,10 or 5,15) fashion across the macrocycle according to the position of the two sp^3 meso carbon atom, (3) Calix[4]phyrin(**1**.**1**.**1**.*1*) (Figure 1-8. **C4P-4**) if it has three sp^2 hybridized meso carbons and only one NH in the coordination core, and Calix[4]phyrin(**1**.**1**.**1**.*1*) (Figure 1-8. **C4P-5**) if three sp^2-hybridized meso carbon atoms and three NH in the coordination core. Many of these calix[4]phyrin analogs are observed as intermediate in the synthesis of porphyrin by condensation of pyrrole and aldehyde.[24] In nature as calix[4]phyrins get oxidized easily to porphyrin, initial synthesis/isolation and studying the properties of calixphyrin were difficult. Initial proof of the formation of these species thus came from the

spectroscopic analysis carried out during synthesis of porphyrin formation or reduction. Most of them were metal complexes of calix[4]phyrin as it is much more stable than the freebase and were the ones to be isolated with far more ease.[25]

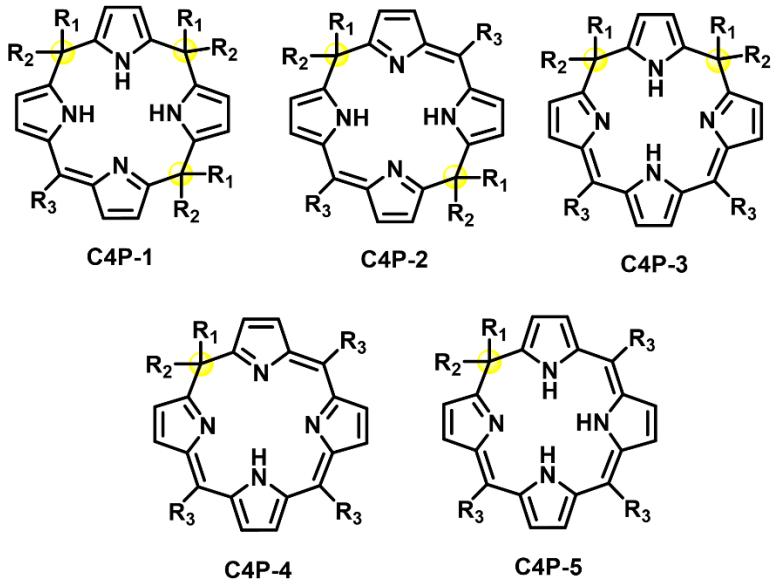

Figure 1-8. Chemical structure of calix[4]phyrin analogs. **C4P-1**, **C4P-2**, **C4P-3, C4P-4,** and **C4P-5**. The sp^3 meso carbons are marked in yellow.

Since its discovery, by systematic studies to understand the electronic and steric effects of the macrocycle which destabilizes the moiety, synthesis of stable non metalated species have evolved. In the past decades, the field of freebase calix[n]phyrin chemistry has grown rapidly and is opening up new opportunities in the area of porphyrin analogues. This in particular, promises to be a unique and different from other porphyrin analogues reported. The structural features of these hybrid systems, containing both sp^2 and sp^3 hybridized bridging meso carbon atoms, makes it intriguing as it offers a flexible framework.

With the development of the calixphyrin analogues such as expanded calixphyrins, nomenclature for these novel class became more significant. The most popular nomenclature is the one coined by sessler and co-workers.[23] The nomenclature system is based on distinguishing between the sp^2 and sp^3 carbon in the meso-position. The naming starts from sp^2 carbon center, and the molecule is named in the direction in which the nearest sp^2 carbon center lies. The sp^3 carbon will be shown in italics and sp^2 carbon in bold numbering. For example, porphodimethene **C4P-2** in Figure 1-8, will be calix[4]phyrin(**1**.*1*.**1**.*1*) accordingly. The number of pyrroles in the macrocycle is represented in the square bracket. Each individual

bold and the italicized number denotes the number of bridging meso centers between each pyrrole subunit. This nomenclature is the most accepted and will be followed throughout the thesis.

1-4-1. Synthesis of calixphyrin

In the biosynthesis of porphyrin from porphyrinogen, porphomonomethene and porphodimethene (Figure. 1-9) are formed as stable intermediates. A cyclic tetrapyrrolic macrocycle, known as porphyrinogen is synthesized enzymatically from its precursor, porphobilinogen (PBG) a reactive intermediate in the biosynthesis of heme. PBG deaminase is an enzyme which acts on porphobilinogen which forms the tetrapyrrolic acyclic preuroporphyrinogen which under the action of uroporphyrinogen III synthase cyclizes to form uroporphyrinogen III. Decarboxylation of uroporphyrinogen III the reaction catalyzed by uroporphyrinogen decarboxylase—forms coproporphyrinogen III. Conversion of coproporphyrinogen III to protoporphyrinogen IX involves oxidative decarboxylation of two propionate side chain rings A and B and their conversion to vinyl groups. Protoporphyrinogen oxidase converts protoporphyrinogen IX to protoporphyrin IX through the formation of porphomonomethene and porphodimethene.

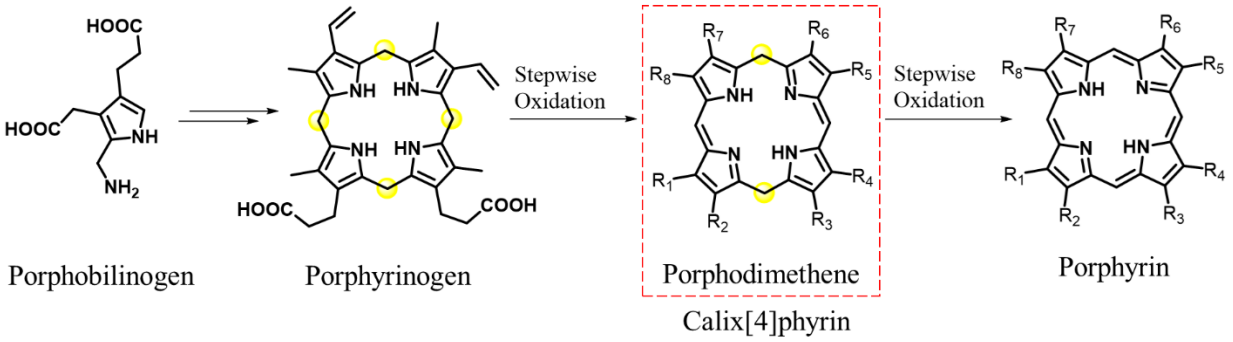

Figure 1-9. Representation of natural synthesis of porphyrin. Calix[4]phyrin is formed as intermediate in the synthesis.

The chemical synthesis of porphodimethene, as an intermediate in the synthesis of porphyrin, involves successive four-electron and six-electron oxidation of porphyrinogen which has sp^3 carbon in all four meso-positions. The oxidation by tetrachloro-1,4-benzoquinone will lead to a less oxidized species or a fully oxidized product, porphyrin. The condensation reaction of pyrrole and aldehyde results in the cyclization of an open-chain tetrapyrrolic compound forming the initial structure, porphyrinogen. The oxidation reaction of naked porphyrinogen occurs in a stepwise factor.[26] In the overall two-electron oxidation step, the dehydrogenation reaction occurs at the methylene position next to the pyrrole ring as it is sterically less hindered, resulting in the porphomonomethene (**C4P-1**) (one sp^2 and three sp^3 carbon) intermediate. Next step is a four-electron oxidation step and there are two pathways for the same. One of which leads to the

formation of the phlorin (**C4P-5**), which is an unstable intermediate and thus oxidized immediately to porphyrin. In the other pathway the porphodimethene (**C4P-3**) (two sp^2 and sp^3 carbon) is formed, which is comparatively stable and can be isolated.

Buchler's procedure, involves reductive alkylation of porphyrin[27] and Floriani's pathway involving de-alkylation of octaalkylcalix[4]pyrrole.[28] But, the most used or facile synthetic strategy is the '2 + 2' MacDonald-like strategy based on the acid-catalyzed condensation of oligopyrroles and ketone developed by sessler and coworkers.[23]

❖ Buchler's Method

Buchler and coworkers synthesized substituted porphodimethenes via reductive alkylation of the corresponding porphyrin (Figure 1-10).[27] As side products many isomeric products are formed by this method and the separation of the compounds are comparatively tedious which adversely affects the yield of the desired product. Moreover, this synthetic method enables us to synthesize only symmetrical porphodimethenes and their metal complexes and was also not effective with all metalated porphyrins with β-pyrrolic substituents. These limitations made it difficult to obtain a range of desired porphodimethenes and restricted the in-depth study of the class of compounds using the method.

❖ Floriani's Method

During the synthesis of porphyrin by oxidizing porphyrinogen, porphodimethenes are formed as the stable intermediates.[28] In Floriani's method porphodimethenes are synthesized from dealkylation of calix[4]pyrroles. (Figure 1-10).

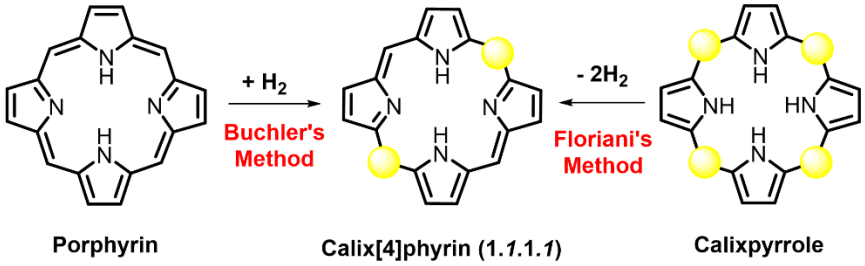

Figure 1-10. Buchler's and Floriani's strategies for synthesizing calixphyrin. The sp^3 hybridized meso carbon is shown as yellow rings.

❖ Sessler's method

By the condensation reaction of dipyrromethane with acetone in acidic condition was developed by Sessler and co-workers to strategically synthesize calix[n]phyrins including higher homologous (n>4).[23, 29] This is the most widely used synthetic method as facile synthesize of calix[n]phyrins which are

manipulated according to our need is possible (Figure 1-11.). Even though various calix[4]phyrin derivatives such as phlorins,[30] isophlorin,[31] 5,10- or 5,15-dihydroporphyrins,[32] porphomethenes,[33] and higher order calix[n]phyrins (n > 4)[34] were reported interest towards chemistry have increased, as the synthesize is more facile with the current methods.

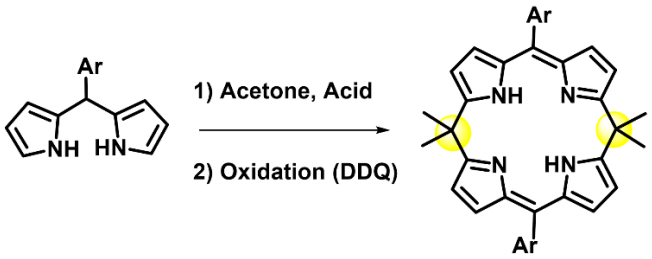

Figure 1-11. Sessler and coworker's strategy for synthesizing calix[n]phyrin. The sp^3 hybridized meso carbon is shown as yellow rings.

These class of molecules with broken aromaticity have shown great potential in the molecular recognition of anionic as well as cationic species. Binding properties of calix[n]phyrins (n ≥ 4) were first recognized and studied by Sessler and co-workers.[35] They found that, by using appropriate acyclic polypyrrolic precursors, it is possible to modify the ratio of oxidized to non-oxidized meso-like carbon atoms in the higher order calix[n]phyrins. By this approach the chemical properties of these macrocycles can be fine-tuned according to our needs. For example; 5,5-10,10-20,20-25,25-octamethylcalix[6]phyrin, being a non-planar species acts as an anion receptor both in solution and in the solid state. The anion binding following protonation is the most common scenario with various other polypyrrolic macrocycles. Metalation of divalent Zn^{II} and Cu^{II} ions of calix[4]phyrin, and trivalent Co^{III} and Ru^{III} ions to calix[6]phyrin and their photophysical properties were among the first ones to be studied using various spectroscopic techniques.[29b]

The first total synthesis of a stable isoporphyrin, calix[4]phyrin-(1.1.1.*1*) without any unwanted conversion into a porphyrin, was obtained through the same strategy. The MacDonald condensation involved dicarboxylic acid substituted dipyrromethane and a diformyl dipyrromethane in the presence of zinc acetate and p-TSA. This resulted in a Zn(II) isoporphyrin with two methyl groups at the sp^3 meso position, **Zn-6** in Figure 1-12.[36] Later, Furuta and Osuka reported the synthesis of an N-confused isoporphyrin system, Figure 1-12.[37] They obtained in 3% yield from the condensation reaction of pyrrole, p-tolualdehyde, and acetone in acidic condition, followed by DDQ oxidation. Due to the lower reactivity of ketone than aldehyde, when acting as an electrophile, it is thought that the N-confusion occurs in the final cyclization step. Crystal structures of Ni(II) and Cu(II) complexes were obtained and it gives more clarity. These structures revealed the existence of dimers in the solid-state, through hydrogen-bonding interactions involving the outward-

facing amide-like moiety present in the calixphyrin-type skeleton. Even though Cu(II) was found to be relatively planar despite the presence of an sp^3 meso carbon, the Ni(II) complex showed a ruffled structure which was normally expected. These metal complexes demonstrated for the first time that complete π-conjugation is not a necessary requirement for metal–carbon bond formation in a polypyrrolic system.[37]

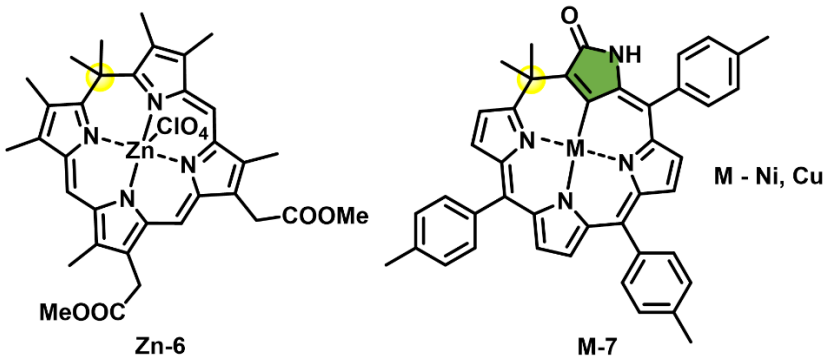

Figure 1-12. Initial reports of metalated stable isoporphyrin. The sp^3 hybridized meso carbon is shown as yellow rings and N-confused pyrrole ring is indicated in green. M is Cu^{II} or Ni^{II}.

1-4-2. Electronic spectral features of Calixphyrin

Calix[4]phyrins show strong soret like band in the range 400-500 nm which is caused by distinct linear conjugated π-systems. Although the appearance of a weak broad shoulder around 520 nm is a characteristic feature of calixphyrin this can't be considered as Q band which is common in porphyrin macrocycle.[29] But in the case of metalated calix[4]phyrin system it shows a close resemblance to corresponding metal porphyrin. UV–Vis absorption spectra show intense Soret like band at 400–420 nm along with weak bands at 520–600 nm. These transitions have been assigned to single excitation from highest occupied π-orbital to lowest unoccupied π* orbitals. Gouterman's four orbital model used in porphyrin is applicable here as the absorption can be explained by mixing the four excited states. Changes in the HOMO-LUMO energy results in the observed difference between metalated calix[4]phyrin and porphyrin absorption spectra as these are the main transitions involved. In the metalated calix[4]phyrins, the Soret band is replaced by a characteristic 'methene' band at lower energy (420–470 nm) with a smaller extinction coefficient. The HOMO and LUMO energies can be modified to tailor the photophysical properties by structural modifications such as introducing core modifications, N-Confused pyrrole rings/increasing the conjugation pathway by synthesizing expanded calix[n]phyrin. These kinds of structural modifications on metalated calixphyrin systems and their properties have been elaborately discussed in the thesis.

1-5. Calixphyrin Analogues

As a class of porphyrinoid macrocycle calixphyrin got much attention due to its anion and cation binding properties. Inspired by porphyrin macrocycle the modifications in porphyrin were applied also to calixphyrin macrocycle for tuning its properties. Till date, many modifications have been introduced to calixphyrin such as core modification, N-confusion, Ring expansion for various applications and structural properties. I will be introducing important calixphyrin analogues in the coming sections.

1-5-1. Core modification in calixphyrin

The motivation for the researchers to design and study core modified calixphyrin macrocycle is gained from its parent molecule porphyrin. In porphyrin moiety modifications of NNNN core by the introduction of a C-H unit or a heteroatom (X = O, S, Se, Te) in place of one of the nitrogen atoms resulted in the synthesis of a class of porphyrinoids such as carbaporphyrinoids and heteroporphyrinoids, which have interesting properties both in terms of potentially binding metal ions as well as its aromatic characteristics. Matano and co-workers reported core-modified phosphole-containing calixphyrins which exhibits characteristic coordination behavior derived from both the phosphole ring and the π-conjugated pyrrole-heterole-pyrrole (N–X–N) subunits (Figure 1-13).[38] The macrocyclic frame in the Pd(II) complex of hybrid calix[4]phyrin becomes flexible at elevated temperatures due to the sp^3 meso carbon and allows interactions between the palladium center and the solvents to stabilize the structure. These core modified complexes have shown its potential as a platform to catalyze the Heck reaction (8-Pd, 8-Rh in Figure 1-13).[39]

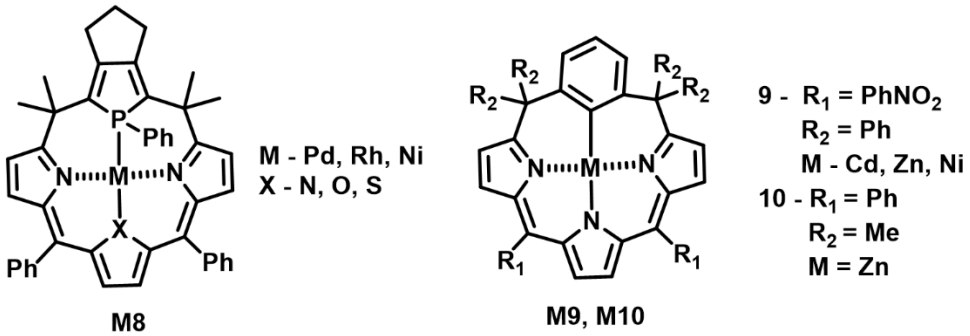

Figure 1-13. Chemical structures of core-modified calixphyrin macrocycles M**8**, **M9**, and **M10**.

In 2004, Stepień and coworkers demonstrated the synthesis of m-benzene ring incorporated porphodimethene and its coordination chemistry with Ni and Cd.[40] Later, Hung and coworkers reported the Zn ion sensing ability of benziporphodimethene.[41] Metal coordinated ligand becomes fluorescent compared to the free base and is selective to Zn by forming 1:1 complex and is significantly higher

compared to other Zn chemosensors. The higher selectivity for the macrocycle is attributed to the flexibility of the free ligand due to the calixphyrin framework and the rigid planar metalated structure which makes this macrocycle a potential candidate in bioimaging and other photophysical applications.

1-5-2. Expanded calixphyrin

In the past 20 years the chemistry of higher-order or "expanded" calix[n]phyrins (n > 4) has got much attention among the calixphyrin analogues. In 2000, Vogel group reported the preparation of expanded calix-phyrin by the acid condensation reaction of dimethyldipyrrylmethane and diformylbipyrrole.[34] This was an accidental discovery as he was trying to synthesize a bimetallic nickel(II) complex of diketo-octaphyrin-(1.1.1.1.0.1.1.1.0). The sp^3 meso carbon helps in stabilizing the spiro-conjugated expanded calixphyrin moiety here. Sessler and co-workers reported the synthesis of calix[6]phyrin and calix[8]phyrin macrocycles that contain a succession of conjugated dipyrromethene subunits linked by MacDonald-like condensation strategy (Figure 1-14).[29b] The presence of sp^3 meso-carbon leads to a bent structure and it was conformed by crystallographic analysis. NMR spectroscopy also supports the hypothesis of flexibility in the solution. They have also studied the metalation behavior of calix[6]phyrin with Co^{III} and Ru^{III} ions in solution. It is well documented that the ring size can be controlled by appropriate solvent conditions. Thus the affinity towards particular anion can be tuned.

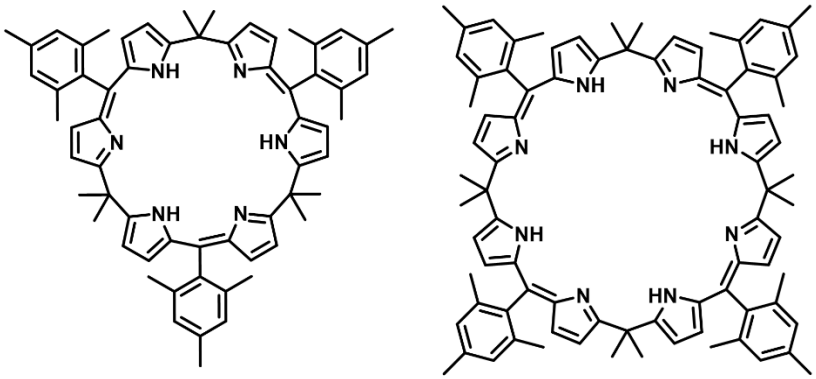

Figure 1-14. Chemical structure of calix[6]phyrin and Calix[8]phyrin reported by sessler.

In 2001 calix[6]phyrin was reported to show anion binding property of calix[6]phyrin. It was synthesized via the acid based condensation reaction of tripyrrane with an aldehyde.[42] Expanded calix[6]phyrin was obtained as the major product with less purification effort. Intramolecular hydrogen bonding possibility was revealed from the X-ray crystallographic analysis as it tightly bound water molecules in its crystal structure. After protonation the complex possesses a strong binding affinity for both in solid state and solution. Anion binding property was studied by carefully studying the UV–Vis absorption spectral change upon addition of tetrabutylammonium salts of chloride, bromide and iodide ions. Moreover,

the crystal structure also showed the binding to anions. Utilizing the same synthetic strategy Furuta et al., developed a new class of expanded N-confused calix[6]phyrin. It will be discussed in details in the next section.

As a core modified analogue of expanded calixphyrin Srinivasan and co-workers, reported the synthesis of calix[2]-4-benzo[4]phyrin by the acid based self-condensation reaction of bis-pyrrolyl benzene and pentafluorobenzaldehyde followed by DDQ oxidation (Figure 1-15.).[43] Many isomers were obtained and have been characterized using ^{1}H NMR, UV-Vis absorption spectroscopy and FAB-MS techniques. X-ray crystallography revealed the unique packed arrangement of meso-pentafluorophenyl groups by forming intermolecular hydrogen bonding. This resulted in enhanced emission characteristics and have found useful as a chemosensor for Hg^{II}. Hg^{II} can be recognized by the ligand as complexation leads to significant fluorescence quenching.

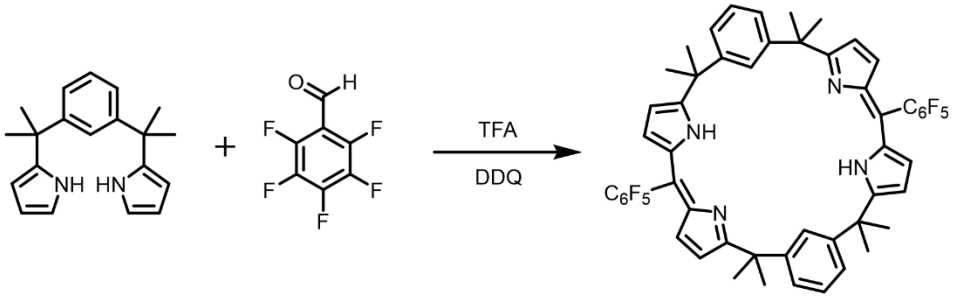

Figure 1-15. Synthesis of core modified calix[2]-4-benzo[4]phyrin.

They continued with their work on the core modified expanded calixphyrin heterocycles and ansa-ferrocene-appended normal.[44] The report was the first report of an ansa-ferrocene incorporated calixphyrin reported. The ansa-ferrocene unit was synthesized by the acid based condensation reaction of 1,1′-bis(diphenylpyrrolylmethyl)ferrocene moiety with arylaldehydes and 2,5-bis-(phenylhydroxymethyl)thiophene and incorporated into the backbone of the macrocycle. No side products were formed and the purification is comparatively easier and characterized using NMR, FAB-MS, UV–Vis and X-ray crystallographic analysis. Dipyrrin and tripyrrin bands were observed in the UV−vis absorption studies according to the structure. Crystal analysis revealed the structural differences of the analogues synthesize. Such as ansa-ferrocene-based calixpyrrole retains the parent calix[4]pyrrole behavior, whereas ansaferrocene-based calixphyrins are partially planar systems and generate curved staircase conformations assemblies. Apart from their intramolecular hydrogen bonding they also show intermolecular hydrogen bonding and forms self-assembled dimers an interesting supramolecular assembly in the solid state (Figure 1-16 a). As further studies in the area they reported the synthesis of calix[2]thia[4]phyrin, and calix[3]thia[6]phyrin (Figure 1-16 b).[45] The synthesis is based on general acid base condensation. The

macrocycle shows anion binding interactions and X-ray crystallographic studies give the unequivocal

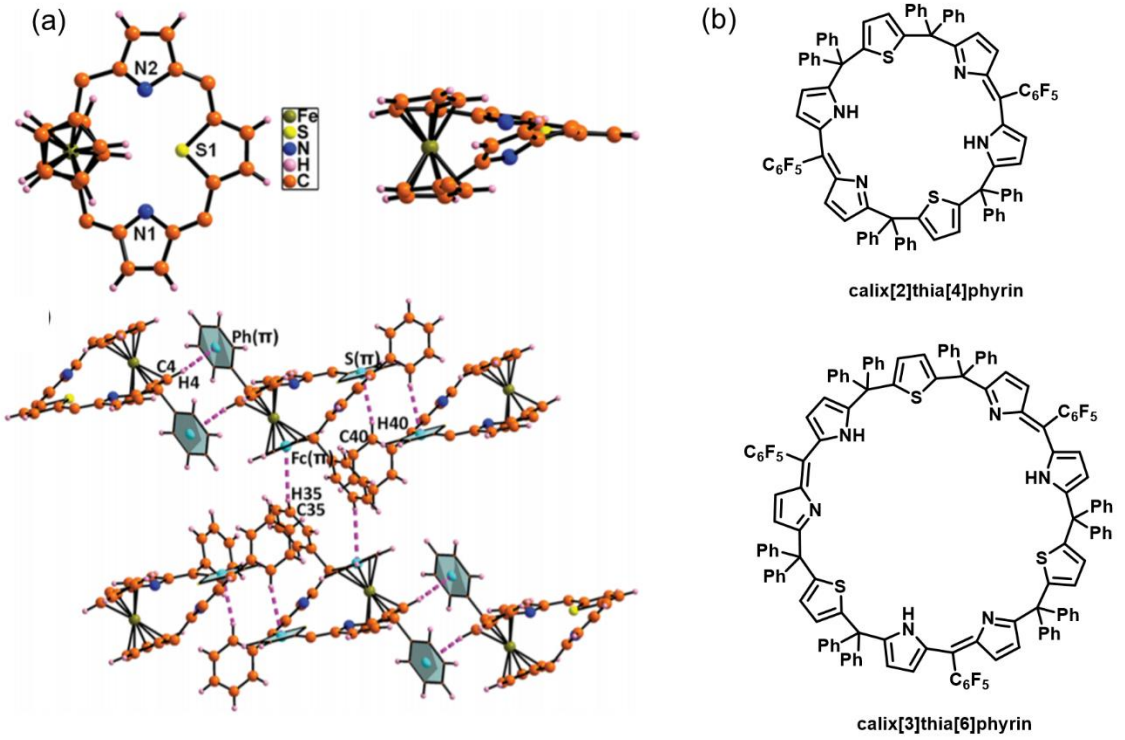

Figure 1-16. (a) X-ray crystal structure of ansa-ferrocene based calixphyrin and the observed hydrogen bonding interaction in the system. (b) Chemical structures of calix[2]thia[4]phyrin, and calix[3]thia[6]phyrin.

support to the claim. Both 1:1 and 1:2 complexes are seen in the solid state study as well as host-guest chemistry and interactions. Interestingly the compound is also showing aggregation induced enhanced emission and can be observed by the difference in its emission intensity according to the temperature. From solid state studies it can be summarized that the effect is due to the restricted intramolecular rotation of meso-aryl substituents present on the sp^3 bridging carbon atoms.

In 2015, Ravikanth et al., reported the synthesis of the expanded dithiacalixphyrin macrocycle.[46] They have three sp^2 and two sp^3 bridging meso carbon centers. Acid-catalyzed condensation of 5,5′-dialkyldipyrromethane with butane-2,3-diyl-bisthiophene-2,5-diyl-bis(p-methoxyphenylmethanol) resulted in the target macrocycle with NNSS coordination core and were confirmed using standard characterization techniques such as NMR, HRMS and X-ray crystallography. X-ray crystallography revealed the flexibility of the macrocycle and retains a boat shaped structure. Metalation and anion binding behavior was studied systematically and the molecule shows selectivity towards fluoride ions. Thus they envisage the potential use of expanded dithiacalixphyrins in optical sensors.

1-5-3. N-confused calixphyrin

As N-confused porphyrin gained wide attention among researchers as a potential ligand for various organometallic compounds researchers started exploring N-confused chemistry in its analogue calixphyrin. Furuta and coworkers first reported Cu and Ni complexes of N-confused calix[4]phyrin in 2001 (Figure 1-12, M-7).[37] Two years later, in 2003, our group observed the agostic interaction between the metal ion and three pyrrolic nitrogen atoms and inner carbon of the confused pyrrole ring in the monomeric and dimeric Zn complexes of N-confused calix[4]phyrin.[47]

Furuta and co-workers also reported a new class of doubly N-confused expanded calixphyrin, calix[6]phyrin and calix[8]phyrin and their metalation.[48] Acid based condensation of pentafluorophenyl-substituted tripyrrane with cyclohexanone or acetone resulted in the target compound. Similar to the expanded calixphyrin reported by sessler the synthesis is comparatively high yielding and can be isolated easily. The macrocycle gave different coordination environment for the metal such as NNNC, NNNC and NNNN, NNCC. These structural isomers have been characterized by X-ray crystallography. The bis-Pt^{II} complexes of calix[6]phyrins have shown phosphorescence in the low energy near infrared (NIR) region at room temperature. Hence, these complexes demonstrated a new platform for their use as IR luminescent dyes. Boron difluoride complexes of N-confused calixphyrins were reported in 2016. The BODIPY ring was constructed through acid-catalyzed self-cyclization of 2-acylated dipyrromethane.[49] BODIPY subunits were arranged in a circular fashion in the N-confused calixphyrins giving rise to a new class of cyclic BODIPY arrays (Figure 1-17.). Interestingly, these array shows solid-state lasing properties with strong luminescence. Thus these molecules show the potential application in organic photonic materials,

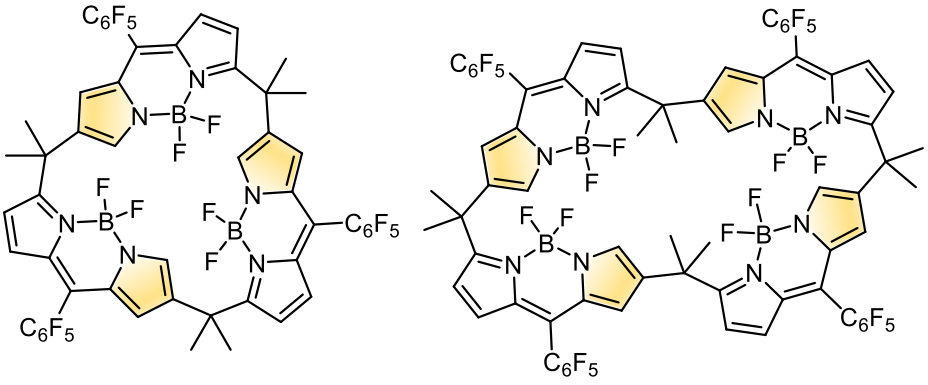

Figure 1-17. Chemical structures of cyclic BODIPY arrays with N-confused calix[6]phyrin and N-confused calix[8]phyrin.

solar-cell dyes and time-gated bio-imaging probes. In 2014 brothers and coworkers, reported mono- and

di-boron complexation with calix[4]phyrin as well as its isomers.[50] The isomers have different bonding site and thus have different coordination environment as it is coordinated to dipyrrin or dipyrromethane. They studied the isomerization pattern using DFT calculations and kinetic studies. Interesting enough, cisoid and transoid geometries have also been observed for unprecedented dipyrrin-bonded and dipyrromethane bonded bis-boron calix[4]phyrin complexes. The mono-boron substituted calix[4]phyrin were considered to be BODIPY analogues. The flexibility in these non-planar macrocycles causes the absence of fluorescence compared to the N-confused analogue. In this thesis I will be discussing about the metalation of N-confused calixphyrin complexes and its photophysical properties. Photosensitizers based on N-confused calixphyrin is discussed in the thesis.

1-6. Triplet Photosensitizers

A photoactive organic chromophore in its ground state will be excited to singlet excited state upon photoexcitation. According to kasha's rule the lowest excited singlet state S_1 will be involved in the subsequent photophysical processes such as relaxing to the ground state by emitting radiation (S_1-S_0 Fluorescence). The excited singlet state (S_1) can undergo spin inversion and populate thee triplet state via intersystem crossing (ISC). The triplet population process is shown in Figure 1-18. Efficient ISC is an essential criterion for an efficient triplet photosensitizer (PS). A good triplet PSs should also show strong absorption of visible or UV light or NIR light to facilitate the excitation and should be a photostable molecule.

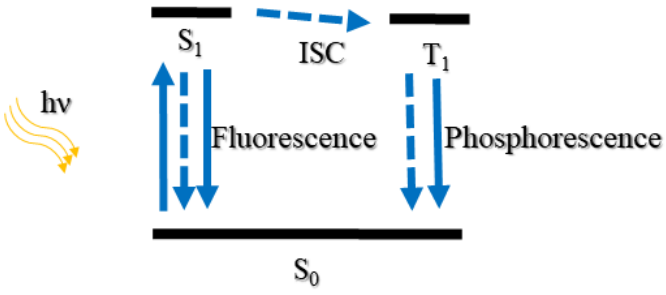

Figure 1-18. Simplified Jablonski diagram to show photoexcitation processes.

Chromophores with the triplet excited state or triplet photosensitizers have found applications in many important areas, such as electroluminescence, phosphorescent bioimaging or molecular sensing, photodynamic therapy for cancer treatment (PDT, by singlet oxygen generation, $^1O_2$), photo-initiated polymerization, photocatalytic organic reactions.[51] In general the fluorescent chromophores are mainly used for luminescence purposes. But triplet PSs are can be used as triplet energy donors such as in

photochemical and photophysical processes, as in PDT, photocatalytic organic reactions, and triplet–triplet annihilation (TTA) upconversion (UC).[52] The major hurdle in this chemistry is to design a triplet PS, i.e. a chromophore with predetermined, efficient ISC as the structural relation to ISC is not yet well established. The principal photophysical processes involved in phosphorescence which is $S_0 - S_1 - T_1$ (Figure. 1-18), is quantum mechanically forbidden which makes the designing of the chromophores more complicated.

One of the widely known concepts is that by enhancing spin orbit coupling (SOC), ISC efficiency can be improved. The nucleus with a positive charge (Z) can accelerate an electron moving with a negative charge to which in turn results in the coupling of spin and magnetic momentum. Thus on increasing the nuclear charge Z the coupling also increases proportionally to Z^4. The heavy atom effect is a concept arising from these known facts. Using a heavy atom in the chromophore design the efficient intersystem crossing can be attained. A Ir, Pt, Pd, Ru, Os, Rh, I, Br, etc are incorporated to the chromophore in this straight forward approach towards efficient triplet PSs.[53] Various transition metal complexes have been prepared utilizing this approach. Chemical structures of some efficient triplet PSs are shown in the Figure 1-19 which utilizes heavy atom effect.[54]

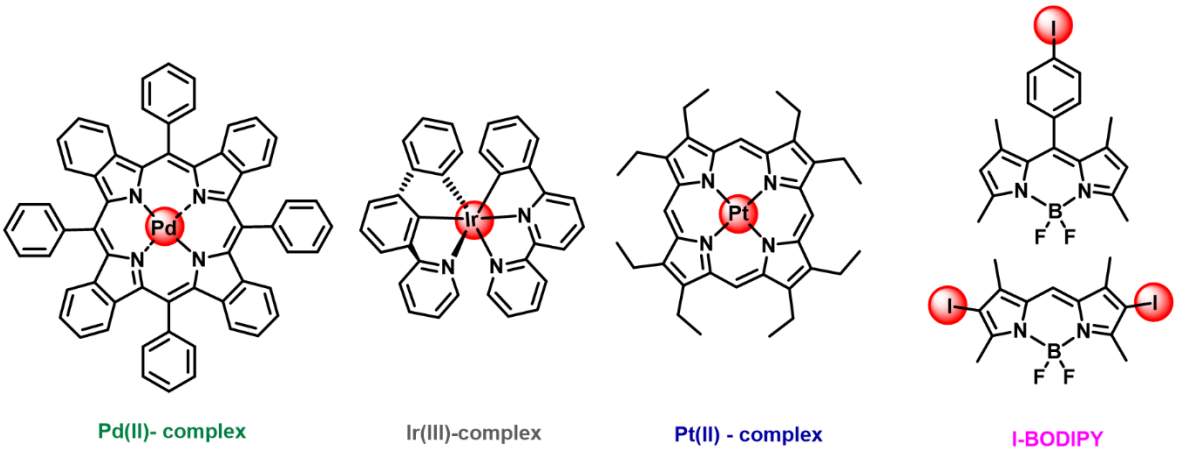

Figure 1-19. Chemical structure of triplet photosensitizers utilizing heavy atom effect.

Among the applications of triplet PSs, photodynamic therapy (PDT) has gained much attention among researchers in the past two decades due to its potential in cancer treatment. Cancer is one of the deadliest diseases and the most common treatments include surgery, radiation therapy and chemotherapy, which results in serious side effects. Photodynamic therapy is a new strategy to kill cancer cells specifically with fewer side effects with many advantages. PDT can be used to kill cancer cells in organs where surgery is impossible or with patients when surgery is not possible. Chemotherapy has shown side effects such as

nausea, vomiting, damage to epithelial surfaces, infertility, swelling of soft tissues, etc. On the other hand, the triplet photosensitizers used for PDT does not show any toxicity.[55] This non-invasive technique is not only used for cancer treatment but also in cardiovascular, dermatological, infectious diseases and as an antibacterial drug. Photodynamic therapy has also found application in insecticide, waste water treatment, catalysis, blood sterilization and so on.[56]

Triplet photosensitizers can sensitize can transfer energy to molecular oxygen in the ground state to sensitize singlet excited states. Molecular oxygen has two excited states $^1\Delta_g$ (22.5 kcal mol^{-1}) and $^1\Sigma^+_g$ (31.5 kcal mol^{-1}) above the ground triplet state. The relaxation of excited $^1\Delta_g$ to triplet ground state of oxygen is spin forbidden and thus it is mostly long lived species.[56] An efficient triplet photosensitizer for photodynamic therapy should have strong absorption in the phototherapeutic window (600-900 nm) and , good triplet state life time. Other criterions are photostability, solubility, facile synthesis for practical purposes. In this thesis the author has worked on improving the characteristics of the chromophore towards this purpose.

1-7. Overview of this Thesis

In this thesis, the author describes the wide scope of modified calixphyrin analogues as the photosensitizing material applications through an N-confusion approach. The implementation of the peculiar pyrrole subunits linking at the α– and β–pyrrole positions in the calixphyrin scaffold afforded specific organometallic environment at the core. Upon metal complexation of these N-confused calixphyrins, the resulting organometallic species stabilized by the strong σ-donating carbon moieties represents fascinating photophysical properties (e.g., red-shift of the energy) and photosensitizing abilities (e.g., singlet oxygen generation). The findings presented in this thesis would provide an important basis for the rational design of photosensitizers used for applications, such as bio-imaging, photodynamic therapy etc. in the future.

In chapter 2, the author will discuss the design and synthesis of organoplatinum calix[4]phyrin complexes. The introduction of N-confused pyrrole to the parent calixphyrin macrocycle lead to the unique molecular orbital perturbations due to the unsymmetrical structure. Further, the coordination environment is also improvised from NNNN of the parent calix[4]phyrin to NNNC and NNCC for the singly and doubly N-confused calixphyrin isomers. The flexibility of the macrocycle in turn helps in smaller coordination sphere and stronger bond formation which can be characterized X-ray crystallography. The structural modifications, tune the molecular orbital to gain bathochromically shifted photophysical properties. Utilizing the heavy metal effect of Pt, the triplet state was efficiently sensitized and can be used for singlet oxygen generation under aerobic conditions.

In chapter 3 the author discusses about designing triplet photosensitizer with good absorption in the phototherapeutic window and photostability by introducing ring expansion modification to form doubly N-confused calix[6]phyrin. Interestingly the modification leads to facile synthesis as well. The structural effect on the excited state dynamics have been studied extensively as the calix[6]phyrin offers two metalation sites with different coordination environment such as NNNC-NNNC, NNNN-NNCC. On complexation with palladium these molecules showed intense absorption profiles in the visible-to-NIR region (500–750 nm) depending on the number of central metals. Moreover, the bis-palladium complexes showed singlet oxygen generation ability with good photostability thus the molecules can be further used for photodynamic therapy applications in the future.

In Chapter 4, the author has summarized the findings in the work and perspectives for future works. According to the structural effect of the core modifications, the number and orientation of the confused pyrrole units embedded in the parent scaffold should be of importance for achieving the desirable optical properties so as to use for photosensitizers. This design principle opens the doors for promising materials in the photodynamic therapy and photocatalysis etc.

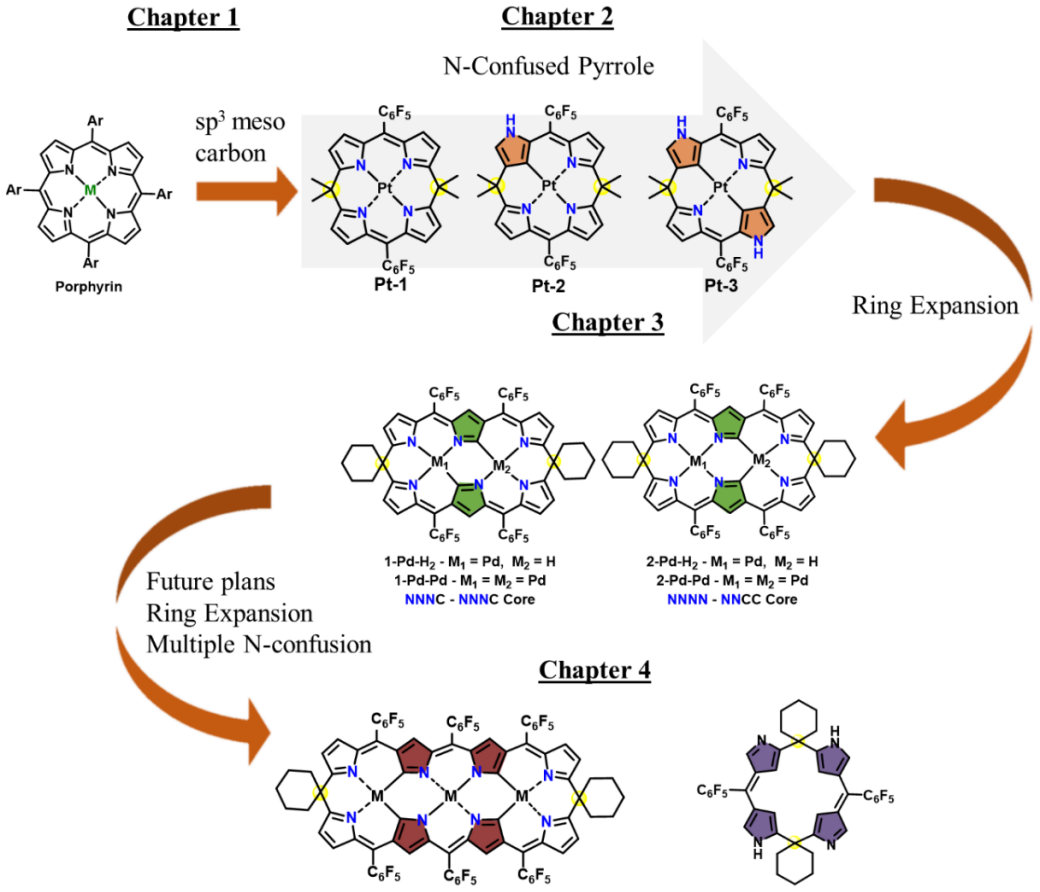

Figure 1-20. The figurative representation of overview of the thesis.

1-8. References

[1] A. R. Battersby, C. J. R. Fookes, G. W. J. Matcham, E. McDonald, *Nature* **1980**, *285*, 17-21.

[2] (a) M. Gouterman, *Journal of Molecular Spectroscopy* **1961**, *6*, 138-163; (b) M. Gouterman, G. H. Wagnière, L. C. Snyder, *Journal of Molecular Spectroscopy* **1963**, *11*, 108-127.

[3] (a) L. Latos-Grazynski, J. Lisowski, M. M. Olmstead, A. L. Balch, *Journal of the American Chemical Society* **1987**, *109*, 4428-4429; (b) J. Mack, *Chemical Reviews* **2017**, *117*, 3444-3478; (c) J. L. Sessler, Z. Gross, H. Furuta, *Chemical Reviews* **2017**, *117*, 2201-2202; dB. Szyszko, M. J. Białek, E. Pacholska-Dudziak, L. Latos-Grażyński, *Chemical Reviews* **2017**, *117*, 2839-2909.

[4] C. Preihs, J. F. Arambula, D. Magda, H. Jeong, D. Yoo, J. Cheon, Z. H. Siddik, J. L. Sessler, *Inorganic Chemistry* **2013**, *52*, 12184-12192.

[5] T. Chatterjee, A. Srinivasan, M. Ravikanth, T. K. Chandrashekar, *Chemical Reviews* **2017**, *117*, 3329-3376.

[6] S. Saito, A. Osuka, *Angewandte Chemie International Edition* **2011**, *50*, 4342-4373.

[7] E. Vogel, M. Köcher, H. Schmickler, J. Lex, *Angewandte Chemie International Edition in English* **1986**, *25*, 257-259.

[8] D. Sánchez-García, J. L. Sessler, *Chemical Society Reviews* **2008**, *37*, 215-232.

[9] (a) J. Waluk, *Chemical Reviews* **2017**, *117*, 2447-2480; (b) G. Anguera, D. Sánchez-García, *Chemical Reviews* **2017**, *117*, 2481-2516.

[10] (a) H. Furuta, T. Asano, T. Ogawa, *Journal of the American Chemical Society* **1994**, *116*, 767-768; (b) P. J. Chmielewski, L. Latos-Grażyński, K. Rachlewicz, T. Glowiak, *Angewandte Chemie International Edition in English* **1994**, *33*, 779-781.

[11] H. Maeda, H. Furuta, in *Pure and Applied Chemistry, Vol. 78*, **2006**, p. 29.

[12] Z. Gross, N. Galili, I. Saltsman, *Angewandte Chemie International Edition* **1999**, *38*, 1427-1429.

[13] (a) I. Aviv-Harel, Z. Gross, *Chemistry – A European Journal* **2009**, *15*, 8382-8394; (b) J. F. B. Barata, M. G. P. M. S. Neves, M. A. F. Faustino, A. C. Tomé, J. A. S. Cavaleiro, *Chemical Reviews* **2017**, *117*, 3192-3253; (c) R. D. Teo, J. Y. Hwang, J. Termini, Z. Gross, H. B. Gray, *Chemical Reviews* **2017**, *117*, 2711-2729.

[14] S. Shimizu, *Chemical Reviews* **2017**, *117*, 2730-2784.

[15] (a) T. Chatterjee, V. S. Shetti, R. Sharma, M. Ravikanth, *Chemical Reviews* **2017**, *117*, 3254-3328; (b) Y. Matano, *Chemical Reviews* **2017**, *117*, 3138-3191; cT. D. Lash, *Chemical Reviews* **2017**, *117*, 2313-2446.

[16] M. O. Senge, *Angewandte Chemie International Edition* **2011**, *50*, 4272-4277.

[17] (a) H. Furuta, T. Ishizuka, A. Osuka, H. Dejima, H. Nakagawa, Y. Ishikawa, *Journal of the*

American Chemical Society **2001**, *123*, 6207-6208; (b) A. Ghosh, *Angewandte Chemie International Edition in English* **1995**, *34*, 1028-1030.

[18] J. P. Belair, C. J. Ziegler, C. S. Rajesh, D. A. Modarelli, *The Journal of Physical Chemistry A* **2002**, *106*, 6445-6451.

[19] (a) E. A. Alemán, J. Manríquez Rocha, W. Wongwitwichote, L. A. Godínez Mora-Tovar, D. A. Modarelli, *The Journal of Physical Chemistry A* **2011**, *115*, 6456-6471; (b) S. Vyas, C. M. Hadad, D. A. Modarelli, *The Journal of Physical Chemistry A* **2008**, *112*, 6533-6549.

[20] (a) J. L. Shaw, S. A. Garrison, E. A. Alemán, C. J. Ziegler, D. A. Modarelli, *The Journal of Organic Chemistry* **2004**, *69*, 7423-7427; (b) S. A. Wolff, E. A. Alemán, D. Banerjee, P. L. Rinaldi, D. A. Modarelli, *The Journal of Organic Chemistry* **2004**, *69*, 4571-4576.

[21] (a) M. Toganoh, H. Furuta, *Chemical Communications* **2012**, *48*, 937-954; (b) T. Yamamoto, K. Mitsuno, S. Mori, S. Itoyama, Y. Shiota, K. Yoshizawa, M. Ishida, H. Furuta, *Chemistry – A European Journal* **2018**, *24*, 6742-6746; (c) A. Młodzianowska, L. Latos-Grażyński, L. Szterenberg, M. Stępień, *Inorganic Chemistry* **2007**, *46*, 6950-6957.

[22] S. Sripothongnak, C. J. Ziegler, *Inorganic Chemistry* **2010**, *49*, 5789-5791.

[23] L. Sessler Jonathan, S. Zimmerman Rebecca, C. Bucher, V. Král, B. Andrioletti, in *Pure and Applied Chemistry, Vol. 73*, **2001**, p. 1041.

[24] (a) D. Dolphin, *Journal of Heterocyclic Chemistry* **1970**, *7*, 275-283; (b) M. O. Senge, S. Runge, M. Speck, K. Ruhlandt-Senge, *Tetrahedron* **2000**, *56*, 8927-8932.

[25] P. N. Dwyer, J. W. Buchler, W. R. Scheidt, *Journal of the American Chemical Society* **1974**, *96*, 2789-2795.

[26] U. Piarulli, C. Floriani, A. Chiesi-Villa, C. Rizzoli, *Journal of the Chemical Society, Chemical Communications* **1994**, 895-896.

[27] (a) M. W. Renner, J. W. Buchler, *The Journal of Physical Chemistry* **1995**, *99*, 8045-8049; (b) A. Botulinski, J. W. Buchler, Y. J. Lee, W. R. Scheidt, M. Wicholas, *Inorganic Chemistry* **1988**, *27*, 927-933.

[28] (a) L. Bonomo, E. Solari, R. Scopelliti, C. Floriani, N. Re, *Journal of the American Chemical Society* **2000**, *122*, 5312-5326; (b) L. Bonomo, E. Solari, R. Scopelliti, C. Floriani, M. Latronico, *Chemical Communications* **1999**, 2227-2228.

[29] (a) C. Bucher, D. Seidel, V. Lynch, V. Král, J. L. Sessler, *Organic Letters* **2000**, *2*, 3103-3106; (b) V. Král, J. L. Sessler, R. S. Zimmerman, D. Seidel, V. Lynch, B. Andrioletti, *Angewandte Chemie International Edition* **2000**, *39*, 1055-1058.

[30] H. Segawa, R. Azumi, T. Shimidzu, *Journal of the American Chemical Society* **1992**, *114*, 7564-7565.

[31] (a) H. Xie, K. M. Smith, *Tetrahedron Letters* **1992**, *33*, 1197-1200; (b) X. Jiang, D. J. Nurco, K. M. Smith, *Chemical Communications* **1996**, 1759-1760.

[32] (a) B. Krattinger, H. J. Callot, *Tetrahedron Letters* **1998**, *39*, 1165-1168; (b) M. Harmjanz, H. S. Gill, M. J. Scott, *Journal of the American Chemical Society* **2000**, *122*, 10476-10477.

[33] J.-M. Benech, L. Bonomo, E. Solari, R. Scopelliti, C. Floriani, *Angewandte Chemie International Edition* **1999**, *38*, 1957-1959.

[34] J. A. Wytko, M. Michels, L. Zander, J. Lex, H. Schmickler, E. Vogel, *The Journal of Organic Chemistry* **2000**, *65*, 8709-8714.

[35] B. Dolenský, J. Kroulík, V. Král, J. L. Sessler, H. Dvořáková, P. Bouř, M. Bernátková, C. Bucher, V. Lynch, *Journal of the American Chemical Society* **2004**, *126*, 13714-13722.

[36] K. M. Barkigia, M. W. Renner, H. Xie, K. M. Smith, J. Fajer, *Journal of the American Chemical Society* **1993**, *115*, 7894-7895.

[37] H. Furuta, T. Ishizuka, A. Osuka, Y. Uwatoko, Y. Ishikawa, *Angewandte Chemie International Edition* **2001**, *40*, 2323-2325.

[38] (a) Y. Matano, T. Miyajima, T. Nakabuchi, H. Imahori, N. Ochi, S. Sakaki, *Journal of the American Chemical Society* **2006**, *128*, 11760-11761; (b) Y. Matano, T. Miyajima, N. Ochi, T. Nakabuchi, M. Shiro, Y. Nakao, S. Sakaki, H. Imahori, *Journal of the American Chemical Society* **2008**, *130*, 990-1002.

[39] Y. Matano, T. Miyajima, N. Ochi, Y. Nakao, S. Sakaki, H. Imahori, *The Journal of Organic Chemistry* **2008**, *73*, 5139-5142.

[40] M. Stępień, L. Latos-Grażyński, L. Szterenberg, J. Panek, Z. Latajka, *Journal of the American Chemical Society* **2004**, *126*, 4566-4580.

[41] C.-H. Hung, G.-F. Chang, A. Kumar, G.-F. Lin, L.-Y. Luo, W.-M. Ching, E. Wei-Guang Diau, *Chemical Communications* **2008**, 978-980.

[42] C. Bucher, R. S. Zimmerman, V. Lynch, V. Král, J. L. Sessler, *Journal of the American Chemical Society* **2001**, *123*, 2099-2100.

[43] P. S. Salini, A. P. Thomas, R. Sabarinathan, S. Ramakrishnan, K. C. G. Sreedevi, M. L. P. Reddy, A. Srinivasan, *Chemistry – A European Journal* **2011**, *17*, 6598-6601.

[44] S. Ramakrishnan, K. S. Anju, A. P. Thomas, K. C. Gowri Sreedevi, P. S. Salini, M. G. Derry Holaday, E. Suresh, A. Srinivasan, *Organometallics* **2012**, *31*, 4166-4173.

[45] G. Karthik, P. V. Krushna, A. Srinivasan, T. K. Chandrashekar, *The Journal of Organic Chemistry* **2013**, *78*, 8496-8501.

[46] E. Ganapathi, T. Chatterjee, M. Ravikanth, *Dalton Transactions* **2015**, *44*, 2763-2770.

[47] H. Furuta, T. Ishizuka, A. Osuka, *Inorganic Chemistry Communications* **2003**, *6*, 398-401.

[48] D.-H. Won, M. Toganoh, Y. Terada, S. Fukatsu, H. Uno, H. Furuta, *Angewandte Chemie International Edition* **2008**, *47*, 5438-5441.

[49] M. Ishida, T. Omagari, R. Hirosawa, K. Jono, Y. M. Sung, Y. Yasutake, H. Uno, M. Toganoh, H. Nakanotani, S. Fukatsu, D. Kim, H. Furuta, *Angewandte Chemie International Edition* **2016**, *55*, 12045-12049.

[50] A. C. Y. Tay, B. J. Frogley, D. C. Ware, P. J. Brothers, *Dalton Transactions* **2018**, *47*, 3388-3399.

[51] (a) Y.-Q. Zou, L.-Q. Lu, L. Fu, N.-J. Chang, J. Rong, J.-R. Chen, W.-J. Xiao, *Angewandte Chemie International Edition* **2011**, *50*, 7171-7175; (b) V. W.-W. Yam, E. C.-C. Cheng, *Chemical Society Reviews* **2008**, *37*, 1806-1813; (c) L. Shi, W. Xia, *Chemical Society Reviews* **2012**, *41*, 7687-7697; (d) A. Kamkaew, S. H. Lim, H. B. Lee, L. V. Kiew, L. Y. Chung, K. Burgess, *Chemical Society Reviews* **2013**, *42*, 77-88; (e) S. O. McDonnell, M. J. Hall, L. T. Allen, A. Byrne, W. M. Gallagher, D. F. O'Shea, *Journal of the American Chemical Society* **2005**, *127*, 16360-16361; (f) V. Fernández-Moreira, F. L. Thorp-Greenwood, M. P. Coogan, *Chemical Communications* **2010**, *46*, 186-202; (g) Q. Zhao, F. Li, C. Huang, *Chemical Society Reviews* **2010**, *39*, 3007-3030; (h) M. Ethirajan, Y. Chen, P. Joshi, R. K. Pandey, *Chemical Society Reviews* **2011**, *40*, 340-362; (i) Y. Chi, P.-T. Chou, *Chemical Society Reviews* **2010**, *39*, 638-655; (j) P. R. Ogilby, *Chemical Society Reviews* **2010**, *39*, 3181-3209.

[52] (a) P. Ceroni, *Chemistry – A European Journal* **2011**, *17*, 9560-9564; (b) T. N. Singh-Rachford, F. N. Castellano, *Coordination Chemistry Reviews* **2010**, *254*, 2560-2573.

[53] (a) J. Zhao, W. Wu, J. Sun, S. Guo, *Chemical Society Reviews* **2013**, *42*, 5323-5351; (b) W.-Y. Wong, *Dalton Transactions* **2007**, 4495-4510.

[54] (a) T. N. Singh-Rachford, A. Haefele, R. Ziessel, F. N. Castellano, *Journal of the American Chemical Society* **2008**, *130*, 16164-16165; (b) Y. Koga, M. Kamo, Y. Yamada, T. Matsumoto, K. Matsubara, *European Journal of Inorganic Chemistry* **2011**, *2011*, 2869-2878; (c) T. Dienel, H. Proehl, T. Fritz, K. Leo, *Journal of Luminescence* **2004**, *110*, 253-257; (d) S. M. Borisov, G. Nuss, W. Haas, R. Saf, M. Schmuck, I. Klimant, *Journal of Photochemistry and Photobiology A: Chemistry* **2009**, *201*, 128-135.

[55] (a) R. Bonnett, G. Martínez, *Tetrahedron* **2001**, *57*, 9513-9547; (b) M. R. Detty, S. L. Gibson, S. J. Wagner, *Journal of Medicinal Chemistry* **2004**, *47*, 3897-3915.

[56] M. C. DeRosa, R. J. Crutchley, *Coordination Chemistry Reviews* **2002**, *233-234*, 351-371.

Chapter 2. Singly and Doubly N-Confused Calix[4]phyrin Organoplatinum(II) Complexes as Near-IR Triplet Sensitizers for singlet oxygen generation.

2-1. Abstract

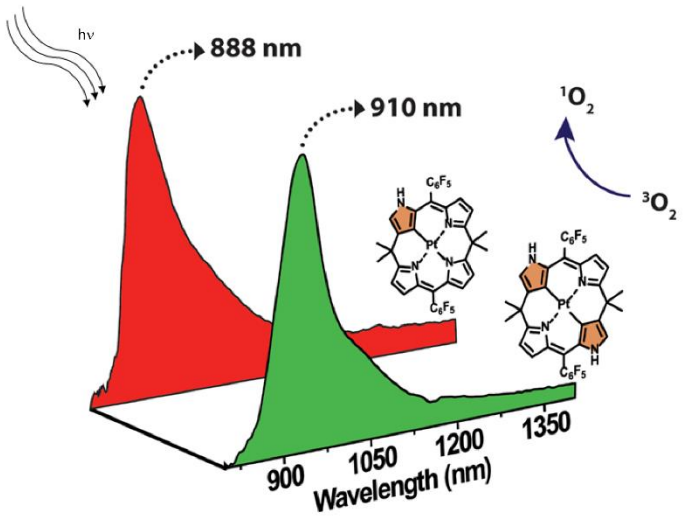

Organoplatinum(II) complexes of calix[4]phyrin analogues, singly N-confused calix[4]phyrin (Pt-2), and doubly N-confused calix[4]-phyrin (Pt-3), were synthesized and characterized. The explicit structures of these organoplatinum(II) complexes were elucidated by single-crystal X-ray diffraction and spectroscopic studies. The introduction of N-confused pyrrole rings to the parent calix[4]phyrin scaffold was found to have profound effects on the photophysical properties, such as the bathochromic shifts of both the absorption and phosphorescence maxima. The triplet excited state properties of these platinum complexes were analyzed by DFT calculations at the B3LYP level. The organoplatinum(II) complexes derived from the deformed scaffolds can serve as potent triplet sensitizers for singlet oxygen generation under aerobic conditions.

2-2. Introduction

Triplet sensitizers have garnered considerable attention owing to their potential applications in electroluminescence,[1] phosphorescence bioimaging,[2] and photocatalysis.[3] The corresponding triplet states formed via intersystem crossing (ISC) upon photoexcitation play an important role in the photodynamic therapy[4] and oxygen sensing,[5] since the triplet energy transfer to the molecular oxygen ($^3O_2$) is the key process for generation of singlet oxygen ($^1O_2$).[6] It would be a general approach that the heavy atom effect of the spin orbit coupling for 4d or 5d metals, such as Ir^{III}, Pt^{II}, Ru^{II}, Os^{II}, etc. allows efficient ISC to the triplet manifold.[7] Therefore, several transition metal complexes were regarded as efficient $^1O_2$ generators being capable of energy transfer to molecular oxygen.[8]

Among these photosensitizers, platinum(II) complexes are one of the promising substitutes, especially for phosphorescence emitters as well as singlet oxygen sensitizers.[9] The most successful examples being as porphyrin-based d^8 platinum complexes, demonstrated high luminescence beyond far red region, and the triplet energies can be tuned by the levels of the molecular orbitals (i.e., HOMO and LUMO).[10-11] To date, many synthetic chemists have devoted much efforts to extend the energy of the triplet states for the sensitizers to the near infrared (NIR) region through the ligand modifications (e.g., peripheral π-extensions and core-expansion with more than 18 π conjugated scaffolds).[12] Increasing the π -conjugation of the ligand moieties, resulted in low solubility and chemical instability of the which hampered the practical use of the designed molecules as a efficient photosensitizers. Therefore, the development of new types of ligand platform for the platinum-based triplet sensitizers has been demanded, and the detailed study on the structure-property relationship for the photoluminescence and singlet oxygen generation efficiency is required.

In this context, the author have introduced a new approach whereby the phosphorescence emission wavelength can be tailored by the ligand modification based on the calixphyrin scaffold. Calixphyrins are a special class of tetrapyrrolic macrocyclic ligands linked by the mixed sp^2 and sp^3 hybridized *meso*-carbons.[13] The sp^3 hybridized *meso*-carbon atoms disrupt the π-electron conjugation, but provide molecular flexibility to adopt a nonplanar (bent) conformation. The unique structure arising from the intrinsically flexible scaffolds is advantageous to the application as molecular sensors,[14] anion-complexing agents,[15] and metal coordination ligands.[16] Sessler and coworkers have developed a general synthetic protocols of calixphyrin derivatives.[17] Matano and coworkers have reported various metal complexes of hybrid calixphyrins with Pd^{II}, Rh^{III}, and Au^{I} ions.[18] Their above findings prompted us to investigate the further coordination chemistry of the calix[4]phyrin analogues for the photosensitizing applications. Prof. Furuta and co-workers have focused on the platinum(II) calixphyrin complexes, where the large spin-orbit

coupling of the heavy-atom platinum(II) ion facilitates rapid ISC ($S_1 \rightarrow T_1$) in the same sense that conventional platinum porphyrin congeners (**Pt-Por**) work as efficient triplet photosensitizers (Figure 1).[19] In order to tune the emission wavelength in the Pt(II)-based emitter, the author has introduced a

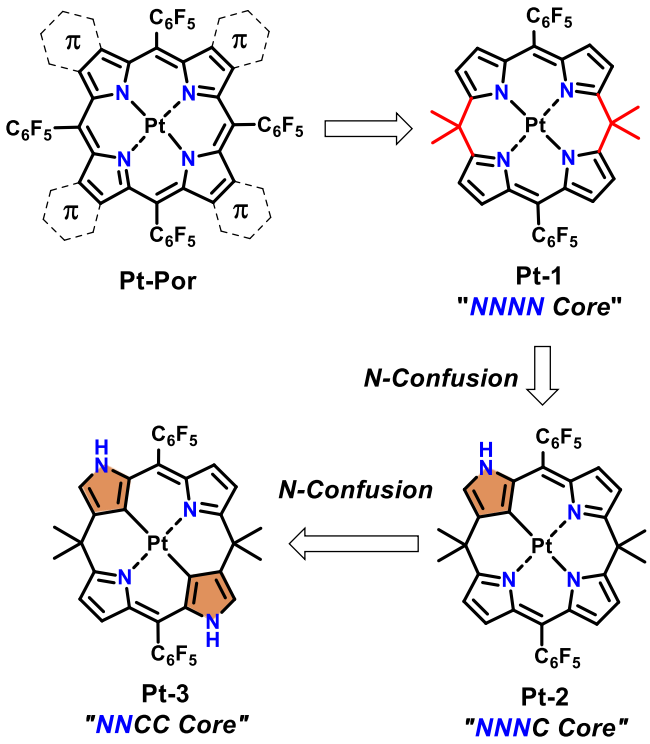

Figure 2-1. Chemical structures of platinum(II) complexes of porphyrin (**Pt-Por**), calix[4]phyrin (**Pt-1**), singly N-confused calix[4]phyrin (**Pt-2**), and doubly N-confused calix[4]phyrin (**Pt-3**).

peculiar pyrrole unit, *so-called* N-confused pyrrole rings into the parent calix[4]phyrin scaffold, which allows replacement of the inner nitrogen atom by carbon atom to procure organometallic coordination environment for Pt(II) ion.[20] Importantly, such electronic perturbation induces a lowering of the HOMO level energies of the organoplatinum complexes (**Pt-2** and **Pt-3**, depicted in Figure 2-1) according to the density functional theory (DFT) calculations (*vide infra*).[21] Consequently, a narrow HOMO-LUMO energy gap can be achieved without extending the π-conjugations of the ligand. In addition, the strong Pt-C bonding interactions between the aromatic cyclometalated compounds and the transition metal elements generates the robust organometallic complexes, thereby the non-radiative decay could be suppressed.[22] The resulting organoplatinum species stabilized by the *NNNC* and *NNCC* chelating environments in **Pt-2** and **Pt-3**, respectively, should work as the π-π* based NIR phosphorescence emitters as well as the singlet oxygen generators.

The author here presents the synthesis and structural characterization of novel organoplatinum(II) calix[4]phyrin complexes, **Pt-n** (n = 2, 3) as near infrared (NIR) triplet sensitizers for the generation of singlet oxygen ($^1\Delta_g$). As opposed to the regular calixphyrin complex, **Pt-1**, the species with a modified core revealed the bathochromic shifts of the phosphorescence beyond 900 nm at room temperature. The detailed photophysical properties along with the kinetic parameters of **Pt-2** and **Pt-3** were analyzed systematically by spectroscopic and theoretical means. In addition, the efficiency of the photosensitized singlet oxygen generation was evaluated for the platinum complexes used in this work.

2-3. Synthesis of Organoplatinum Calix[4]phyrin Complexes.

The synthetic route for the desired complexes is given in Scheme 2-1. Unlike the regular calix[4]phyrin derivative **1** and its platinum species **Pt-1** (Scheme S1 in the supporting information), the N-confused calix[4]phyrin analogues **2** and **3** were synthesized by using N-confused acylated dipyrromethanes (**8**, **9**, and **10**). As reported, the derivative **8** was formed by the acylation reaction of an N-confused dipyrromethane (**7**) in 49% yield.[23] In this reaction, another monoacylated product (i.e., acylated at the α-position of the regular pyrrole ring) **9** as well as the diacylated one **10** was also obtained under the respective conditions in 2 and 8% yields, respectively. Both the dipyrromethanes **8** and **9** are positional isomers and hence reveal similar ^{1}H NMR spectral features in $CDCl_3$ and the identical *m/z* values by the fast atom bombardment (FAB) mass spectrometry (Supporting Information). The explicit structures of these acylated N-confused dipyrromethanes **8** and **9** were determined by X-ray crystallographic analysis (Figure S2-9 and Table S2-1). These results indicate that, monoacylation of **7** predominantly occurs at the 2-pyrrolic position (not 5-pyrrole position) of the N-confused pyrrole ring. Likewise, the diacylated derivative **10** was fully characterized by X-ray crystallography and the NMR spectroscopy, revealing that the acyl substituents are positioned at 2-positions of the *confused* and *regular* pyrrole rings, respectively (Figure S2-9 and Table S2-1).

Using the aforementioned precursors **8** and **10**, the synthesis of singly N-confused calix[4]phyrin (**2**) and doubly N-confused calix[4]phyrin (**3**) was achieved (Scheme 2-1). The reduction of the carbonyl group in **8** by sodium borohydride gave the corresponding carbinol derivative, quantitatively. Subsequent acid catalyzed self-cyclization, followed by 2,3-dichloro-5,6-dicyano-1,4-benzoquinone (DDQ) oxidation in CH_2Cl_2 afforded the target calix[4]phyrin derivative **3** in 7% yield. The highest yield for the product **3** was achieved by using stronger Lewis acid, BF_3 etherate rather than lanthanide-acid $Y(OTf)_3$.[23] Interestingly, the dipyrromethane possessing an acyl group, **9** also afforded the corresponding analogue **3** under the identical conditions, though the overall yield of **3** was relatively lower (i.e., 4%) in this case.

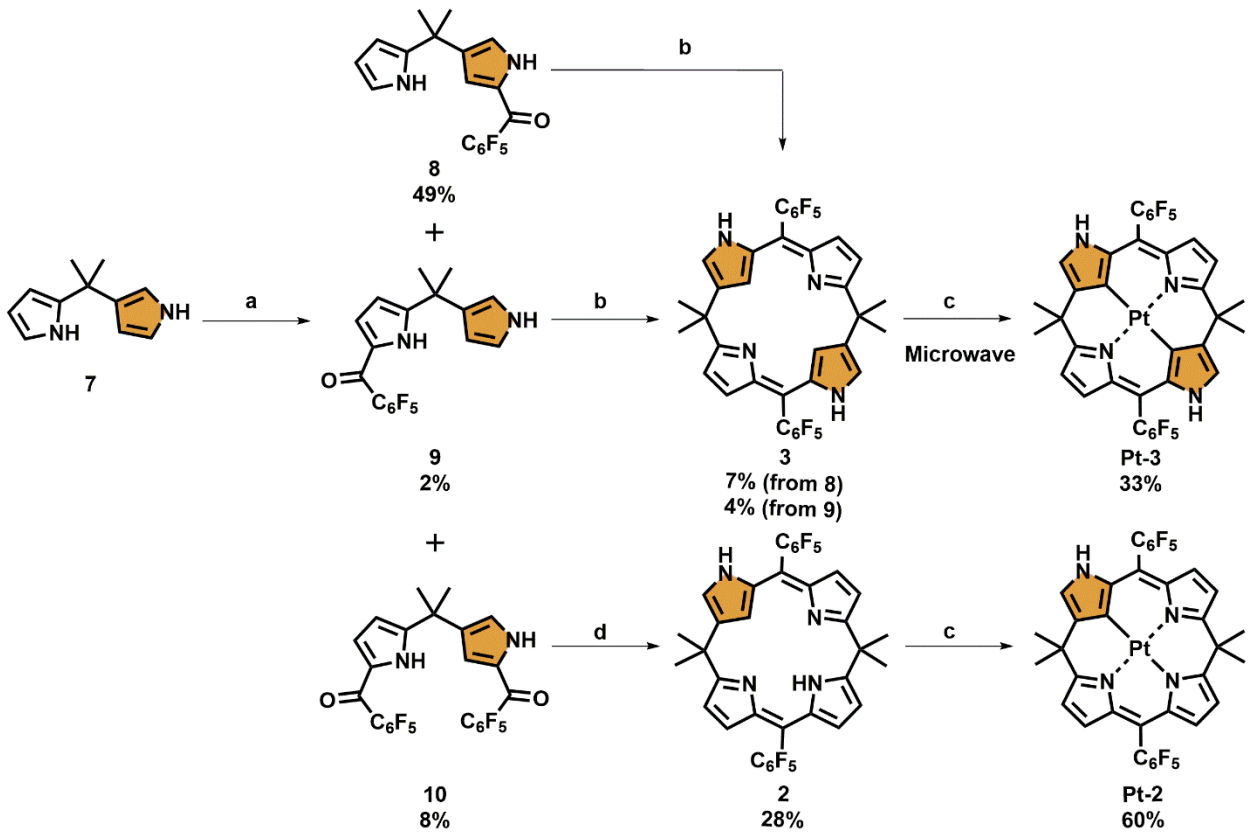

Scheme 2-1. Synthesis of N-Confused Calix[4]phyrins **2** and **3** and the Platinum(II) Complexes **Pt-1**, **Pt-2**, and **Pt-3**. [a]Reagents and conditions: (a) EtMgBr, THF, room temperature and S-2-pyridyl pentafluorobenzothioate, THF, −78 °C; (b) (i) $NaBH_4$, THF/MeOH; (ii) $BF_3{\cdot}OEt_2$, CH_2Cl_2; (iii) DDQ, CH_2Cl_2; (c) $PtCl_2(PhCN)_2$, 1,2-dichlorobenzene; (d) (i) $NaBH_4$, THF/MeOH; (ii) 5,5-dimethyldipyrromethane, $BF_3{\cdot}OEt_2$, CH_2Cl_2; (iii) DDQ, CH_2Cl_2

In the case of singly N-confused calix[4]phyrin, **2** the unsymmetrical [2+2] type condensation between the reduced product of **10** and regular-type dipyrromethane (**11**) afforded the corresponding macrocycle in 28% yield (Scheme 2-1). The obtained products **2** and **3** were characterized by ^1H and ^{19}F NMR and high resolution (HR) mass spectroscopies (Supporting Information). The characteristic NH and β-CH resonances, assigned for the confused pyrrole rings of **3** were observed at 10.68 and 8.98 ppm, respectively.[23] In contrast, as to the C_S unsymmetrical structure of **2**, the two sets of NH and CH signals were seen in the spectrum (Figure S2-4). As reported for **Pt-1c** (a Pt calix[4]phyrin derivative possessing *meso*-cyclohexyl groups), the singly N-confused calix[4]phyrin derivative **2** afforded the corresponding organoplatinum complex **Pt-2** upon refluxing with two equivalent amount of platinum(II) dichloride in dichlorobenzene for 12 h (Scheme 2-1).[24] The synthesis of doubly N-confused congener **Pt-3** was unsuccessful under the identical conditions and even at higher temperature with excess amount of metal salts presumably due to the difficulty in the formation of the carbon-platinum bonds via double inner CH

activation. However, **Pt-3** was finally obtained with the aid of microwave irradiation at 200 °C in 33% yield. All the derivatives were purified by silica gel column chromatography and recrystallized from suitable solvents for the photophysical experiments.

2-4. X-ray Crystallographic Analysis

The molecular structures of **Pt-2**, **Pt-3** were unambiguously identified by X-ray crystallographic analysis (Figure 2-2 and Table S2-2 in the Supporting Information). Similarly, to the structures of **Pt-1** (the preliminary structure, Figure 2-2 (a)) and the derivative bearing meso-cyclohexyl groups (**Pt-1c**; Figure S2-10 in the supporting information), the doubly N-confused **Pt-3** has also a gable-type distortion occurring at the two sp^3 hybridized meso-carbon atoms (5,15-positions). The bent angle between dipyrrin planes (11 atoms) of **Pt-3** was estimated to be 142.14° with a mean deviation of 0.390 Å from the macrocyclic plane (defined by 25 atoms of the macrocyclic core including the platinum metal center) (Figure S2-12 in the Supporting Information).

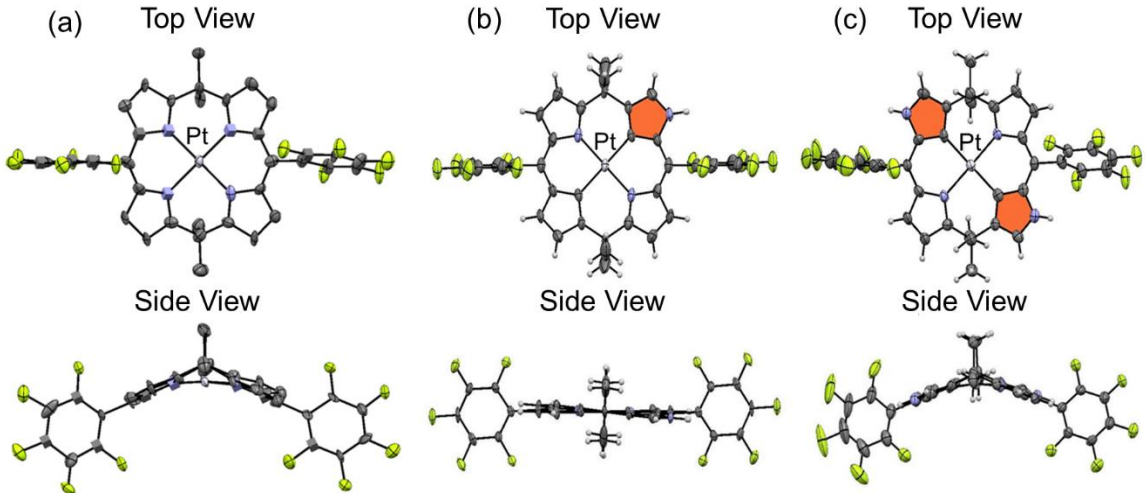

Figure 2-2. Top and side views of the preliminary structure of (a) **Pt-1**. Top and side views of the X-ray crystal structures of (b) **Pt-2** and (b) **Pt-3** are given with 50% probability thermal ellipsoid. The co-crystallized solvent molecule(s) are omitted for clarity. The confused rings are highlighted in orange.

The average bond length of **Pt-3** between the inner carbon atoms and the platinum center is shorter than that between the nitrogen atoms and platinum (2.003 vs 2.034 Å, respectively) (Table 2-1). This strong

Pt−C covalent interaction may be due to the intrinsically strong σ-donor character derived from the inner carbon atoms of the confused pyrrolic rings. In contrast, the singly N-confused Pt-2 shows a relatively pseudoplanar structure rather than a bent geometry (Figure 2-2). This could originate from the crystallographic disorder of the confused pyrrole moiety present in **Pt-2** according to the distinct molecular symmetry. Therefore, the difficulty in identification of the exact nitrogen atom positions of the confused pyrrole rings of the analysis of **Pt-2** also hampered us in investigating the detailed bonding nature around the platinum center.

Table 2-1. Selected bond parameters of **Pt-2**, **Pt-3** and **Pt-1C.**[a]

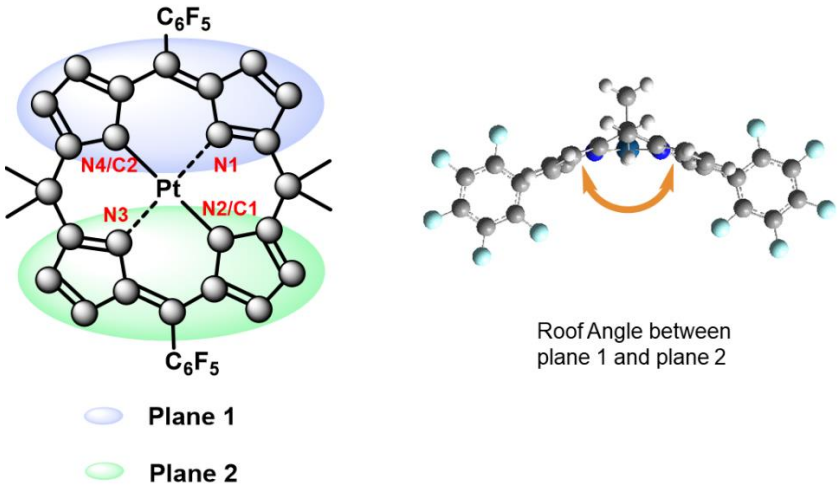

Calix[4]phyrin complexes	Bond length in Å				Bent angle (°)	Mean Deviation (Å)
	Pt-N1	Pt-N2/C1	Pt-N3	Pt-C2/N4		
Pt-2	2.042	2.034	2.042	2.034	180	0.03
Pt-3	2.038(7)	2.005(8)	2.030(7)	2.002(8)	142.14	0.21
Pt-1c[a]	1.995(5)	1.978(5)	1.996(6)	1.994(4)	134.35	0.28

[a] The data was analyzed using the structure; ref [24]. [b]The bent angles (o) between the half skeleton of the dipyrrin planes are estimated. [c]The mean deviation (Å) values were defined using the 24 atoms (gray circle) of the core skeleton of the complexes.

2-5. Studies on Molecular orbital and Optical properties

To gain further structural insight into the platinum complexes, theoretical calculations were performed by using DFT calculations (B3LYP/LACVP** level). The bent structures for the complexes are

energetically favorable, and the bent angle defined by the dipyrrin planes becomes larger as the number of N-confused pyrrole ring(s) in the parent structure increases (137.5°, 143.4°, and 149.5° for **Pt-1**, **Pt-2**, and **Pt-3**, respectively) (Table 2-2). This could be a direct consequence of the short Pt–C/N bond lengths of the complexes. The energy difference, ΔE between the bent and (transient) coplanar structures of the complexes are estimated to be 7.05, 3.45, and 1.21 kcal mol^{-1} for **Pt-1**, **Pt-2**, and **Pt-3**, respectively (Table 2-2). This result indicates that the flipping of the dipyrrin planes in the complexes occurs easily in solution. The optimized structures and the energetic profile of the complexes with the bent and co-planar geometries for (a) **Pt-1**, (b) **Pt-2**, and (c) **Pt-3** obtained by the B3LYP calculations are shown in Figure 2-3.

Table 2-2. Relative Energy Difference between Bent and Planar Structures of Pt-1, Pt-2, and Pt-3 obtained from DFT calculations (B3LYP/LACVP level)**

Compound	ΔE_{Bent} (kcal/mol)	ΔE_{Planar} (kcal/mol)	$\Delta\Delta E_{\text{Bent/Planar}}$ (kcal/mol)
Pt-1	0	7.05	7.05
Pt-2	12.94	16.39	3.45
Pt-3	35.48	36.69	1.21

The ^{1}H NMR and mass spectrometry also supports the proposed structure of the organoplatinum complexes, **Pt-2** and **Pt-3** (Figures S2-5–S2-6). Both the platinum(II) complexes exhibited nearly identical mass numbers; *m/z* = 894.1258 and 894.1261 ($[M]^+$ = 894.1254 calculated for $C_{36}H_{21}F_{10}N_4Pt$) because of the isomeric forms of the structures. The singly N-confused calix[4]phyrin **Pt-2** has a lower C_1 symmetry, which gives rise to inequivalent peripheral CH resonances in the low field region. One broad signal appearing at δ = 11.37 ppm can be assigned to an outer NH proton by a D_2O exchange experiment (Figures S2-7–S2-8). The ^{1}H NMR spectrum of **Pt-3** shows a simple resonance feature for peripheral CHs and NHs, which suggests the C_2 symmetry. Moreover, a higher degree of symmetry for **Pt-3** was proven by the ^{19}F NMR spectrum (Figure S2-6).

The resulting N-confused analogues **Pt-2** and **Pt-3** demonstrated the characteristic optical features (Figure 3). As the number of the confused pyrrole ring(s) in the scaffold increases, the low-energy absorption bands

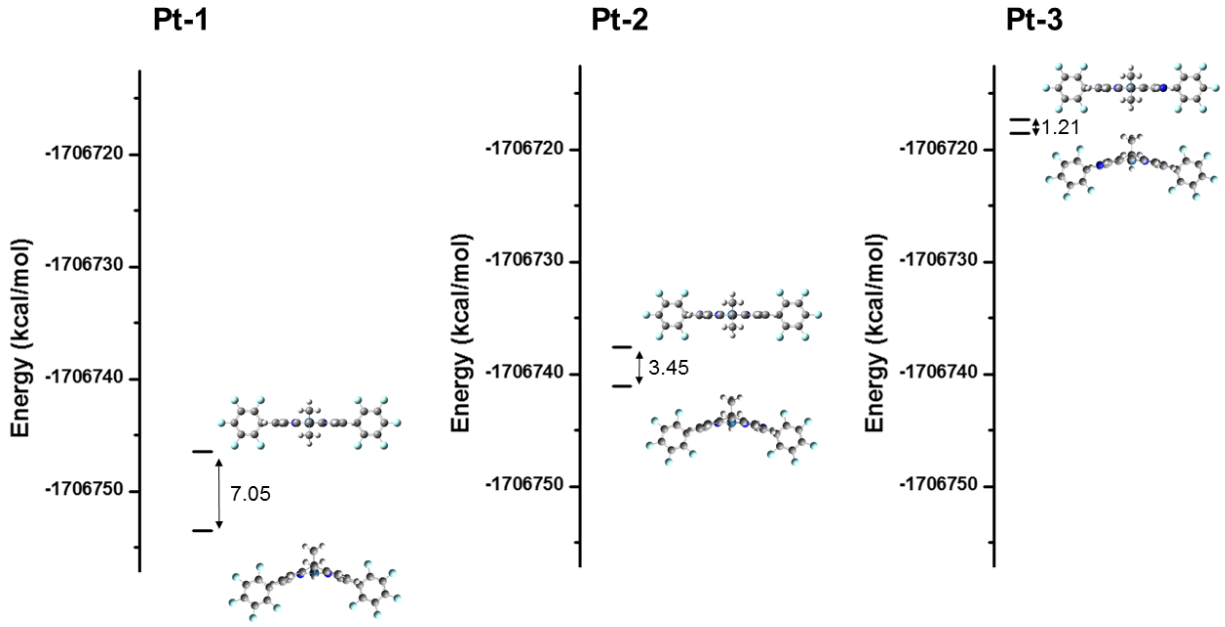

Figure 2-3. Optimized structures and the energetic profile **(**in kcal/mol) of the complexes with bent and co-planar geometries for (a) **Pt-1,** (b) **Pt-2**, and (c) **Pt-3** obtained by B3LYP calculations**.**

are red shifted in CH_2Cl_2. The intense absorption band for **Pt-2** also broadens compared to that of **Pt-1** (full width at half maximum (fwhm): 2.0 x 10^9 cm^{-1} for **Pt-1** and 1.8 x 10^9 cm^{-1} for **Pt-2**). The split peaks at 429 and 477 nm are seen in the absorption spectrum of **Pt-3**. These spectral features were also represented in the time-dependent (TD) DFT simulated spectra with the oscillator strengths (*f*) of the complexes decreasing in the order, **Pt-1** > **Pt-2** > **Pt-3** (Figures S2-13–S2-15 and Tables S2-3–S5).

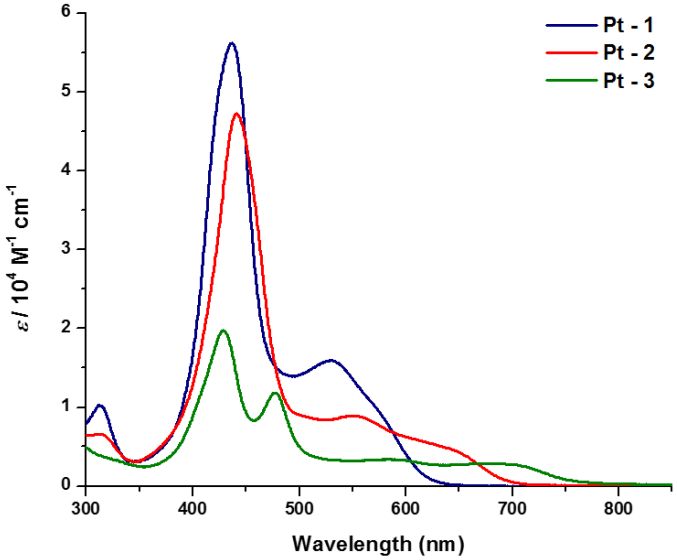

Figure 2-4. Absorption spectra of the platinum(II) complexes (**Pt-1**, **Pt-2**, and **Pt-3**) in CH_2Cl_2.

In order to evaluate the narrower HOMO-LUMO energy gaps of the complexes, **Pt-2** and **Pt-3** than that of **Pt-1**, the electrochemical properties were examined by cyclic voltammetry in DMF containing 0.1 M tetrabutylammonium hexafluorophosphate ($TBAPF_6$) as the supporting electrolyte (Figure 2-5). The irreversible oxidation waves were observed at E_{pa} = 0.96 and 0.87 V (vs ferrocene/ferrocenium couple) for **Pt-2** and **Pt-3**, respectively, which are anodically-shifted for **Pt-1** (E_{pa} = 1.47 V). The reversible reduction waves were observed at E_{pc} = –1.08 and –1.12 V, respectively. In this trend, the lower oxidation potentials for the N-confused analogues were observed, and the HOMO-LUMO energy gaps were estimated to be 2.04 and 1.99 eV for **Pt-2** and **Pt-3**, respectively, while the complex **Pt-1** has a 2.72 eV gap. The red shifted absorption band of **Pt-3** is well consistent with the electrochemical energy gap (Figure 2-5).

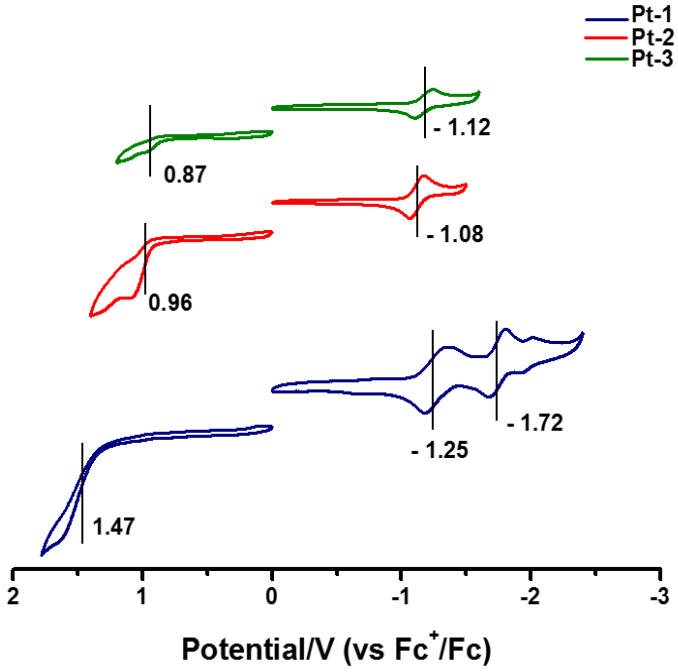

Figure 2-5. Cyclic voltammograms of the platinum(II) complexes (1 mM) in 0.1 M $TBAPF_6$/DMF, scan rate = 100 mV/s.

The MO diagrams of the complexes represent the supportive trend in the energy gaps (Figure 2-6). Upon introduction of the N-confused pyrrole rings (in **Pt-2** and **Pt-3**), remarkable destabilization of the HOMO energies occurs, which induces the broken degeneracies in the HOMO pairs (HOMO and HOMO-1). In contrast, the energies of the LUMOs are not apparently altered, even though the electronic distribution is perturbed significantly in **Pt-2**. Thus, the HOMO-LUMO energy gap decreases as the number of N-confused pyrrole units in the parent macrocycle is increased, e.g., **Pt-1** (2.82 eV) > **Pt-2** (2.61 eV) > **Pt-3** (2.53 eV). The above results are in good agreement with the similar trend as seen in the N-confused

porphyrin systems: e.g., the energy gaps of regular, singly N-confused, and doubly N-confused analogues.[25] The HOMO-2 level is also destabilized similar to the HOMO in **Pt-2** and **Pt-3**. In fact, in **Pt-3** HOMO-1 and HOMO-2 are degenerate which can be accounted to the low-energy excitations shown by the molecule.

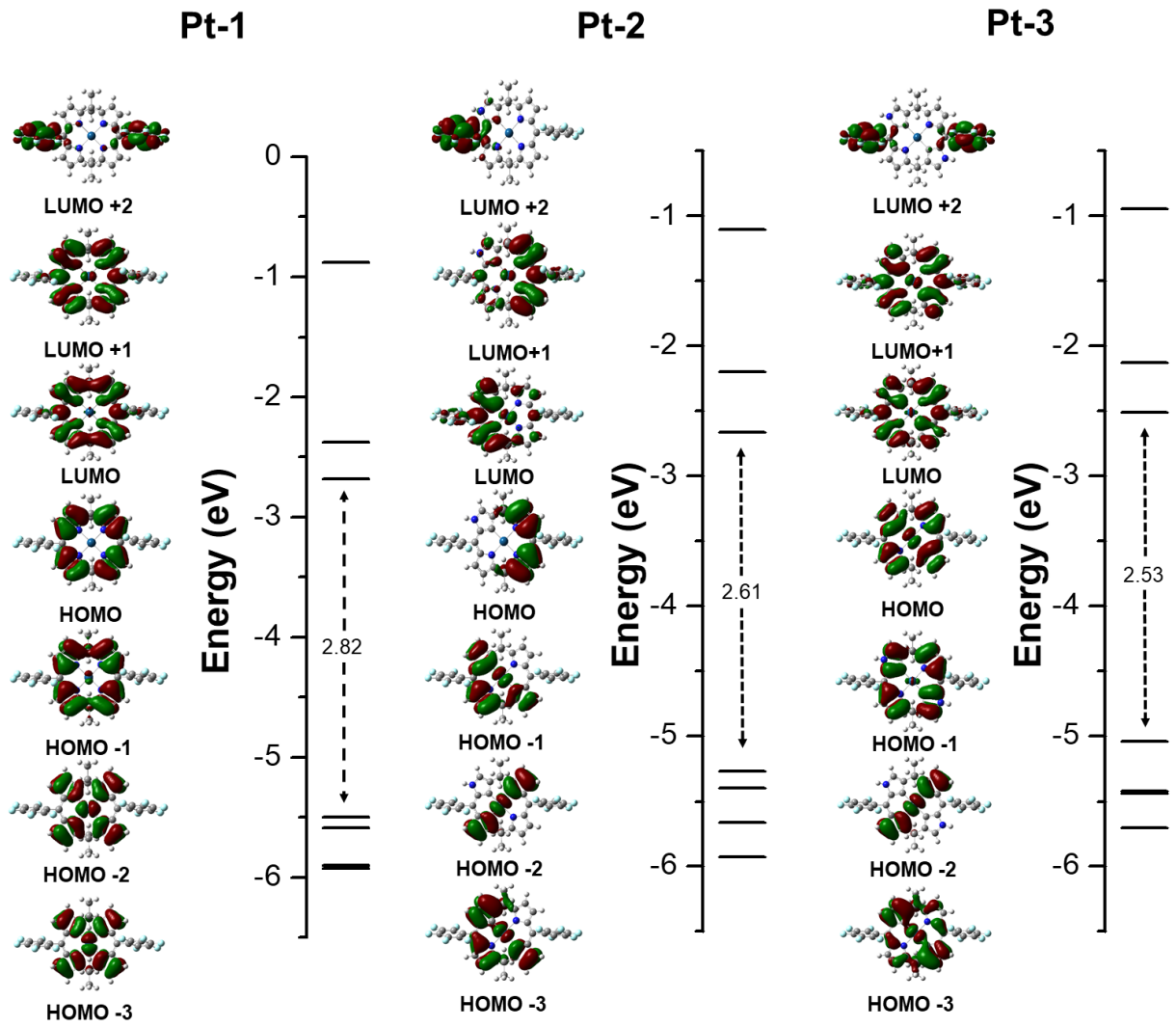

Figure 2-6. Molecular orbital energy diagram of (a) **Pt-1**, (b) **Pt-2**, and (c) **Pt-3** obtained from DFT calculations (B3LYP/LACVP**).

As is the case with **Pt-1c**, the organoplatinum complexes, **Pt-2** and **Pt-3** in deaerated dichloromethane showed phosphorescence in the NIR region at room temperature (Figure 2-7 and Table 2-3).[24] The actual emission from the solution under the 445 nm excitation was captured on an NIR camera (Figure S2-19). The emission peaks were redshifted with increasing the number of N-confused pyrrole in the scaffold. The lifetimes (τ_{PL}) of the phosphorescence determined by the time-correlated single photon counting (TCSPC)

were 8760, 315, and 350 ns, respectively (Figure S2-16 – S2-18). Such observations suggest that the emissions should be attributed to the excited triplet state due to the internal heavy atom effect.[26] In addition, the phosphorescence quantum yields (Φ_{PL}) were estimated to be 0.0189 (for **Pt-1)**, 0.0052 (for **Pt-2**), and 0.0073 (for **Pt-3**). The corresponding triplet energies E_T were estimated to be 1.39 (888 nm) and 1.36 eV (910 nm), for **Pt-2** and **Pt-3**, respectively.[27] These are well consistent with the values calculated by the TD-DFT method; E_T = 1.38 and 1.33 eV, respectively. Accordingly, the radiative (k_r) and nonradiative rate constants (k_{nr}) were estimated by assuming that the quantum yield of intersystem crossing is unity, as these complexes are non-fluorescent (Table 2-3). Our analysis suggests that the efficient nonradiative decay channel (a large k_{nr}) is active in this system. Compared to **Pt-3**, the relatively large k_{nr} for **Pt-2** cannot be explained by the energy gap law, $k_{nr} = \alpha \exp(-\beta \Delta E)$, which indicates that the constant k_{nr} increases with a decrease in the energy gap (ΔE) between the radiative excited state and the ground state (with α and β being constant).[28] The flexible and nonplanar geometry (with a large molecular bent angle) of **Pt-2** is expected to promote the nonradiative deactivation in the excited state[29] although further experiments need to be performed to discuss the excited state dynamics of the complexes in more detail.

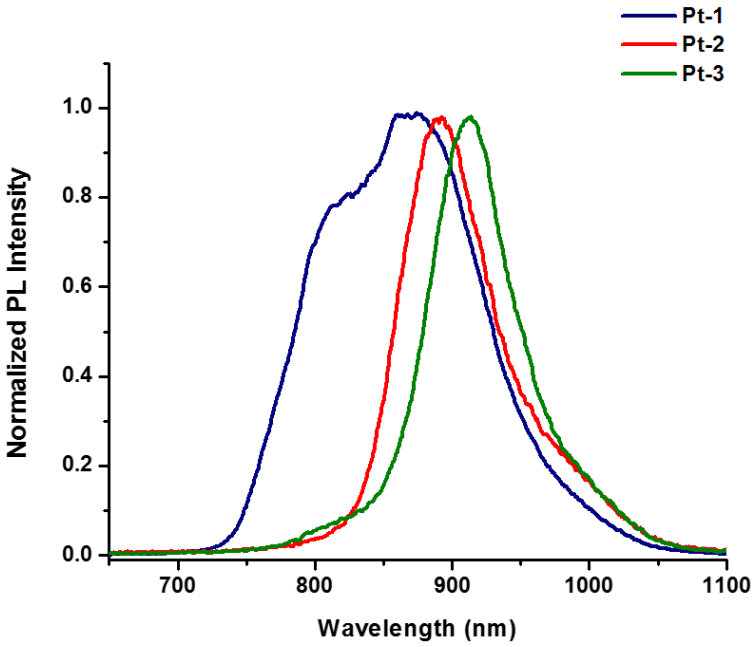

Figure 2-7. Normalized phosphorescence spectra of **Pt-1**, **Pt-2**, and **Pt-3** at room temperature in CH_2Cl_2; λ_{ex} = 445 nm.

As a matter of fact, the organoplatinum complexes **Pt-2** and **Pt-3** can play as the photosensitizers for generation of singlet oxygen. The $^1O_2$ generated in the oxygen saturated solution can be observed by the characteristic spectral profile of the NIR luminescence at 1275 nm (Figure S2-26).[30] Consequently, the

sensitizing abilities of the photosensitizers were determined in methanol through an established photochemical method, that is, by monitoring the reaction of singlet oxygen trap using 1,3 diphenylisobenzofuran (DPBF) in the presence of the complexes as a function of photo irradiation time and absorption intensity.[31] The absorption band of DPBF around 418 nm decayed with increasing illumination time, whereas no reduction in the absorbance in the Q band region of the platinum complexes was observed, which indicates the high photo-stability of the complexes (Figures S2-22–S2-27). The relative oxygen generation efficiency was determined using Rose Bengal (Φ_Δ = 0.76 in CH_3OH) as a reference dye (Figures S2-22–S2-27).[6] The complexes were found to be efficient generators of singlet oxygen with Φ_Δ's of 0.65, 0.42, and 0.45 for **Pt-1**, **Pt-2**, and **Pt-3**, respectively (Table 2-3). Therefore, in descending order, the relative singlet oxygen production yields are **Pt-1** > **Pt-3** > **Pt-2**. These results suggest on one hand that the long lived triplet excited state of the photosensitizers was in general favorable for the singlet oxygen sensitization. On the other hand, the triplet state population is facilitated by the efficient ISC due to the spin-orbit coupling. However, the efficiency of singlet oxygen generation ($^1O_2$) by a photosensitizer should depend not only on the ISC pathway but also on the efficiency of the energy transfer from the triplet to ground state level of the oxygen (ΔE = 0.5572, 0.4044, and 0.3554 eV for **Pt-1**, **Pt-2** and **Pt-3**, respectively). The efficiency of $^1O_2$ generation is consistent with the trends of lifetime measurements also with the energy difference between the triplet state of the triplet sensitizer and the singlet oxygen state.

Table 2-3. Summary of the Photophysical Parameters for the Platinum Complexes[a]

Complex	λ_{abs} (nm) (ε/ 10^4 M^{-1} cm^{-1})[b]	λ_{em} (nm)	Φ_{PL}[c] (1×10^{-2})	τ_{PL} (ns)[d]	k_r (1×10^3 s^{-1})	k_{nr} (1×10^5 s^{-1})	Φ_Δ[e]
Pt-1	437 (5.59)	866	1.89	8760	2.15	1.1	0.65
Pt-2	442 (4.72)	888	0.52	315	16.6	3.1	0.42
Pt-3	429 (1.98)	910	0.73	350	20.9	2.8	0.45

[a] Measured in CH_2Cl_2. [b] Value of the absorption maximum. [c] Quantum yield was calculated using **Pt-1c** (Φ_{PL} = 0.013 in CH_2Cl_2, λ_{ex} = 445 nm) as reference 24. [d] Determined by TCSPC method with excitation at 532 nm. [e] Singlet oxygen quantum yield was obtained in MeOH using Rose Bengal (Φ_Δ = 0.76 in MeOH) as the standard.

2-6. CONCLUSION

In summary, novel organoplatinum(II) complexes of singly and doubly N-confused calix[4]phyrins, **Pt-2** and **Pt-3**, have been successfully synthesized and characterized. These complexes possess isoelectronic

structures formed by the implementation of the peculiar pyrrole units in the calix[4]phyrin scaffold. This structural modification resulted in the alteration of the photophysical properties; on increasing the number of N-confused pyrrole rings in the parent ligand, remarkable bathochromic shifts in their absorption and phosphorescence were observed. The organoplatinum complexes are also stable and capable of photosensitizing the singlet oxygen generation. The relatively high singlet oxygen generation efficiencies of the complexes studied in this work would be suitable to use as potential agents for photodynamic therapy applications.

2-7. EXPERIMENTAL SECTION

2-7-1. Materials and Instruments. All reactions were performed in dried vessels under Ar or N_2. Commercially available solvents and reagents were used without further purification unless otherwise mentioned. CH_2Cl_2 was dried by passing through a pad of alumina. Dry 1,2-dichlorobenzene was purchased from KANTO and used as received. Thin-layer chromatography (TLC) was performed on aluminum sheet coated with silica gel 60 F_{254} (Merck). Preparative separation was performed by silica gel flash column chromatography (KANTO silica gel 60N, spherical, neutral, 40–50 μm) or silica gel gravity column chromatography (KANTO Silica Gel 60N, spherical, neutral, 63–210 μm). ^{1}H and ^{19}F NMR spectra were recorded in $CDCl_3$ and DMSO-d_6 solutions on a JEOL ECX500 NMR spectrometer (500 MHz for ^{1}H and 470 MHz for ^{19}F). Chemical shifts were reported relative to $CDCl_3$ (δ = 7.26 ppm) and $(CD_3)_2SO$ (δ = 2.50 ppm) for ^{1}H in parts per million. Trifluoroacetic acid (0.02% in $CDCl_3$ and $(CD_3)_2SO$) was used as an external reference for ^{19}F (δ = –76.5 ppm). UV−vis−NIR absorption spectra were measured on a Shimadzu UV-3150PC spectrometer. Fluorescence spectra were recorded on an SPEX Fluorolog-3-NIR spectrometer (HORIBA) with NIR-PMT R5509 photomultiplier tube (Hamamatsu) in a 10 mm quartz fluorescence cuvette. High resolution mass (HRMS) spectra were obtained in fast atom bombardment (FAB mode) with 3-nitrobenzyl alcohol (NBA) as a matrix on a JEOL LMS-HX-110 spectrometer. Microwave experiments were carried out in a dedicated Anton Paar Monowave-300 reactor with continuous irradiation power of 0–850 W. The reactions were performed in a G-30 glass vial sealed with Teflon septum and placed in a microwave cavity.

2-7-2. Singlet Oxygen quantum yields. Singlet oxygen quantum yields (Φ_Δ) were determined in MeOH by using a comparative method with Rose Bengal as the standard compound and DPBF as the singlet oxygen scavenger.[31] Solutions were prepared in the dark and irradiated at a crossover wavelength. Photoirradiation was carried out using an Ekspla NT-342B laser system that consists of an Nd:YAG laser

(355 nm, 135 mJ/4–6 ns) that pumps an optical parametric oscillator (OPO, 30 mJ/4–6 ns) to provide a wavelength at which the standard and sample solutions have the same optical density.

2-7-3. Time-resolved spectroscopy. Time-resolved phosphorescence measurement was performed in the time-correlated single photon counting mode using a NIR-sensitive photomultiplier (Hamamatsu H10330-75). The excitation source was a 532-nm frequency-doubled passive-Q-switched Nd:YAG laser delivering a 1-μJ sub-ns (< 0.7 ns) pulse train at a repetition rate of 8 kHz.

2-7-4. Theoretical Calculations. DFT calculations were performed with the Gaussian09 program package without symmetry treatment.[32] Initial structures were based on the X-ray crystal structure of the related compounds. The geometries were fully optimized using Becke's three-parameter hybrid functional combined with the Lee−Yang−Parr correlation function-al, denoted as the B3LYP level of DFT, with the 6-31G(d, p) and LanL2DZ (for Pt) basis set for all calculations.[33] Experimental absorption spectra were analyzed by the time-dependent DFT (TD-DFT) calculations with the same level. Ground-state geometries were verified by the frequency calculations, where no imaginary frequency was found.

2-7-5. X-ray Crystallography. Single-crystal X-ray structural analyses for **8**, **9**, **10**, **Pt-1**, **Pt-2**, and **Pt-3** were performed on a Saturn equipped with a CCD detector (Rigaku) using MoKα (graphite, monochromated, λ = 0.71069 Å) radiation. The data were corrected for Lorentz, polarization, and absorption effects. SHELXS-2014/7 and refined using the SHELXS-2014/7 program. All the positional parameters and thermal parameters of non-hydrogen atoms were refined anisotropically on F^2 by the full matrix least-squares method. Hydrogen atoms were placed at the calculated positions and refined using a riding model on their corresponding carbon atoms.

2-7-6. Synthesis of Platinum(II) Complexes. All the platinum(II) calix[4]phyrin complexes (**Pt-1**, **Pt-2**, and **Pt-3**) were prepared by following a similar protocol.[24] The synthetic procedures of the precursors and the detailed characterized data of **Pt-1**, **Pt-2**, and **Pt-3** are given in the Supporting Information.

Synthesis of Pt-1. Compound **1** (20 mg, 0.028 mmol) and $Pt(PhCN_2)Cl_2$ (26 mg, 0.056 mmol) in 1,2-dichlorobenzene (10 mL) was stirred at 150 °C for 12 h. 1,2-dichlorobenzene was distilled using high vacuum pump. The mixture was then separated with an alumina column and further purified using a silica gel column (Hexane/CH_2Cl_2).

Pt-1: Yield 17 mg (65%); ^{1}H NMR ($CDCl_3$, ppm): δ = 6.50 (d, J = 4.5 Hz, 4H), 6.47 (d, J = 4.5 Hz, 4H), 1.92 (s, 12H); ^{19}F NMR ($CDCl_3$, ppm): δ = –138.28 (d, J = 22.0 Hz, *m*-F), –152.49 (t, J = 20.9 Hz, *p*-F), –160.86 (t, J = 20.2 Hz, *o*-F); HRMS (FAB^+): *m/z* = 894.1257 (found); 894.1254 (calcd for $C_{36}H_{21}F_{10}N_4Pt$) error; +0.1 ppm; UV-vis-NIR [CH_2Cl_2, λ_{max}/nm (ε/ 10^4 M^{-1} cm^{-1})]: 437 (5.62), 529 (15.92). Elemental analysis calcd for (%) $C_{36}H_{20}F_{10}N_4Pt$ **Pt-1**: C 48.39; H 2.26; N 6.27; found: C 48.88 (1.01%); H 2.45(8.4%); N 6.19 (1.2%).

Synthesis of Pt-2. Singly N-confused calix[4]phyrin, **2** (20 mg, 0.028 mmol) and $Pt(PhCN_2)Cl_2$ (26 mg, 0.056 mmol) in 1,2-dichlorobenzene (10 mL) was stirred at 150 °C for 12 h. The mixture was then separated with alumina column chromatography, affording a yellow solution and further purified using silica gel column chromatography (Hexane/CH_2Cl_2) to get **Pt-2**.

Pt-2: 15 mg (60%); ^{1}H NMR (DMSO-d_6, ppm): δ = 11.37 (s, 1H), 7.69 (s, 1H), 6.78 (d, J = 4.3 Hz, 2H), 6.73–6.66 (m, 4H), 1.76 (s, 6H), 1.63 (s, 6H); ^{19}F NMR (DMSO-d_6, ppm) δ = –140.52 (d, *J* = 23.8 Hz, *m*-F), –142.01 (d, *J* = 24.0 Hz, *m*-F), –154.61 (t, *J* = 21.5 Hz, *p*-F), –154.95 (t, *J* = 20.8 Hz, *p*-F), –161.93 (m, *o*-F), –162.21 (m, *o*-F); HRMS (FAB$^+$): *m/z* = 894.1258 (found); 894.1254 (calcd for $C_{36}H_{21}F_{10}N_4Pt$) error; +0.4 ppm; UV-vis-NIR [CH_2Cl_2, λ_{max}/nm (ε/ 10^4 M^{-1} cm^{-1})]: 442 (4.73). Elemental analysis calcd for (%) $C_{36}H_{20}F_{10}N_4Pt$ **Pt-2**: C 48.39; H 2.26; N 6.27; found: C 47.96 (0.8%); H 2.29(1.3%); N 6.21 (0.9%).

Synthesis of Pt-3. Doubly N-confused calix[4]phyrin, **3** (40 mg, 0.057 mmol) and $Pt(PhCN)_2Cl_2$ (54 mg, 0.114 mmol) were added to 1,2-dichlorobenzene (20 mL) and stirred at 200 °C for 15 min with microwave instrument under argon atmosphere. The reaction mixture was passed through alumina column followed by purification using a silica gel column (Hexane/ CH_2Cl_2) to obtain a dark colored solid, **Pt-3**.

Pt-3: 17 mg (33%); ^{1}H NMR (DMSO-d_6, ppm): δ = 11.14 (s, 1H), 7.78 (d, J = 2.7 Hz, 1H), 6.83 (d, J = 4.7 Hz, 1H), 6.77 (d, J = 4.6 Hz, 1H), 1.60 (s, 6H); ^{19}F NMR (DMSO-d_6, ppm): δ = –140.83 (d, J = 22.0 Hz, *m*-F), –155.57 (s, *p*-F), –162.36 (s, *o*-F); HRMS (ESI$^+$): *m/z* = 894.1261 (found); 894.1254 (calcd for $C_{36}H_{21}F_{10}N_4Pt$) error; +0.7 ppm; UV-vis-NIR [CH_2Cl_2, λ_{max}/nm (ε/ 10^4 M^{-1} cm^{-1})]: 429 (1.97), 477 (1.18). Elemental analysis calcd for (%) $C_{36}H_{20}F_{10}N_4Pt$ **Pt-3**: C 48.39; H 2.26; N 6.27; found: C 47.29 (2.2%); H 2.34 (3.5%); N 6.04 (3.6 %).

Synthesis of acylated N-confused dipyrromethane (8, 9 and 10). A solution of ethyl magnesium bromide (6.027 mmol) in THF was added to a solution of N-confused dipyrromethane (**7**) (500 mg, 2.87 mmol) in THF (20 mL) under N_2 atmosphere. The resulting solution was stirred for 30 min at room temperature. A solution of *S*-2-pyridyl pentafluorobenzothioate (875 mg, 2.87 mmol) in THF (15 mL) was added at –78 °C. The resulting mixture was stirred at –78 °C and then the temperature was increased gradually to room temperature and stirring was continued for 1 h. The reaction was quenched by water. Then, the mixture was washed with water and CH_2Cl_2. After solvent was removed, the mixture was purified by column chromatography using silica gel (Hexane/CH_2Cl_2) to afford the separated fractions of **8**, **9**, and **10**, respectively. Compound **8** was characterized previously.[23]

9: 21 mg (2%); ^{1}H NMR ($CDCl_3$, ppm): δ = 8.99 (br s, 1H, NH), 8.18 (br s, 1H, NH), 6.82 (dd, *J* = 5.1, 2.4 Hz, 1H), 6.69 (dd, *J* = 4.1, 2.1 Hz, 1H), 6.60 (s, 1H), 6.20 (dd, *J* = 4.0, 2.6 Hz, 1H), 6.15 (dt, *J* = 2.5, 1.7 Hz, 1H), 1.66 (s, 6H); ^{19}F NMR (DMSO-d_6, ppm): δ = –140.17 (d, *J* = 24.3 Hz), –151.84 (d, *J* = 39.2 Hz),

–160.41 (d, J = 24.7 Hz); HRMS (FAB$^+$): m/z = 368.0966 (found); 368.0948 (calcd for $C_{18}H_{13}F_5N_2O$) error; +4.9 ppm.

10: 129 mg (8%): ^{1}H NMR (DMSO-d_6, ppm): δ = 12.33 (br s, 1H, NH), 12.04 (br s, 1H, NH), 7.26 (s, 1H), 6.83 (s, 1H), 6.71 (s, 1H), 5.92 (s, 1H), 1.60 (s, 6H); ^{19}F NMR (DMSO-d_6, ppm): δ = –142.51 (d, J = 142.8 Hz), –153.28 (d, J = 98.2 Hz), –160.86 (d, J = 86.2 Hz); HRMS (FAB$^+$): m/z = 562.0771 (found); 562.0739 (calcd for $C_{25}H_{12}F_{10}N_2O_2$) error; + 5.7 ppm.

Synthesis of singly N-confused calix[4]phyrin (2). $NaBH_4$ (660 mg, 17.5 mmol) was added to a solution of diacylated N-confused dipyrromethane (200 mg, 0.35 mmol) in dry THF/MeOH (40/8 mL). The mixture was stirred at room temperature for 1 h under N_2 atmosphere. The reaction was quenched by water, washed with CH_2Cl_2 and water, and dried over anhydrous sodium sulfate. After evaporating the solvent, resulting white solid was dissolved in anhydrous CH_2Cl_2 and 5,5-dimethyl dipyrromethane (61 mg, 1 equiv) was added to this solution. After stirring the solution for 5 min BF_3•OEt_2 was added and then the mixture was stirred at room temperature for 1 h under N_2 atmosphere. Then, 2,3-dichloro-5,6-dicyano-1,4-benzoquinone (DDQ) (238 mg, 3 equiv) was added and the mixture was stirred at room temperature for 40 min. The reaction mixture was passed through an alumina column to remove excess DDQ and purified by column chromatography using silica gel (Hexane/CH_2Cl_2).

2: 70 mg (28%); ^{1}H NMR (DMSO-d_6, ppm): δ = 12.16 (s, 1H), 10.90 (s, 1H), 9.22 (s, 1H), 7.02 (dd, J = 2.9, 1.5 Hz, 1H), 6.85 (d, J = 4.5 Hz, 1H), 6.73 (d, J = 4.6 Hz, 1H), 6.69 (d, J = 4.5 Hz, 1H), 6.66 (d, J = 4.6 Hz, 1H), 6.26 (dd, J = 3.6, 2.4 Hz, 1H), 6.20 (dd, J = 3.9, 2.4 Hz, 1H), 1.71 (s, 6H), 1.67 (s, 6H); ^{19}F NMR (DMSO-d_6, ppm): δ = –139.93 (s), –141.41 (s), –154.76 (d, J = 201.1 Hz), –161.61~ –162.62 (m); HRMS (FAB$^+$): m/z = 707.1727 (found); 707.1763 (calcd for $C_{36}H_{23}F_{10}N_4$) error; –5.1 ppm.

Synthesis of doubly N-confused calix[4]phyrin (3). $NaBH_4$ (770 mg, 20 mmol) was added to a solution of acylated N-confused dipyrromethane (**8**/**9**) **(**300 mg, 0.814 mmol) in dry THF/ MeOH (12/3 mL). The mixture was stirred at room temperature for 1 h under N_2 atmosphere. The reaction was quenched by water, washed with CH_2Cl_2 and water, then dried over anhydrous sodium sulfate. After the solvent was removed, white solid was obtained. CH_2Cl_2 (100 mL) was added to the solid and the mixture was stirred at room temperature for 5 min. BF_3•OEt_2 (20 μL, 0.16 mmol) was added and the mixture was stirred at room temperature for 1 h under N_2 atmosphere. Then, DDQ (554 mg, 2.4 mmol) was added and the mixture was stirred at room temperature for 45 min. The reaction mixture was passed through an alumina column to remove excess DDQ and purified by silica gel column chromatography (MeOH/CH_2Cl_2: 0–3%).

3: 40 mg (7.0% from **8**) (4% from **9**); Spectroscopic data were well matched with the reported values.[23]

2-8 Supporting Data

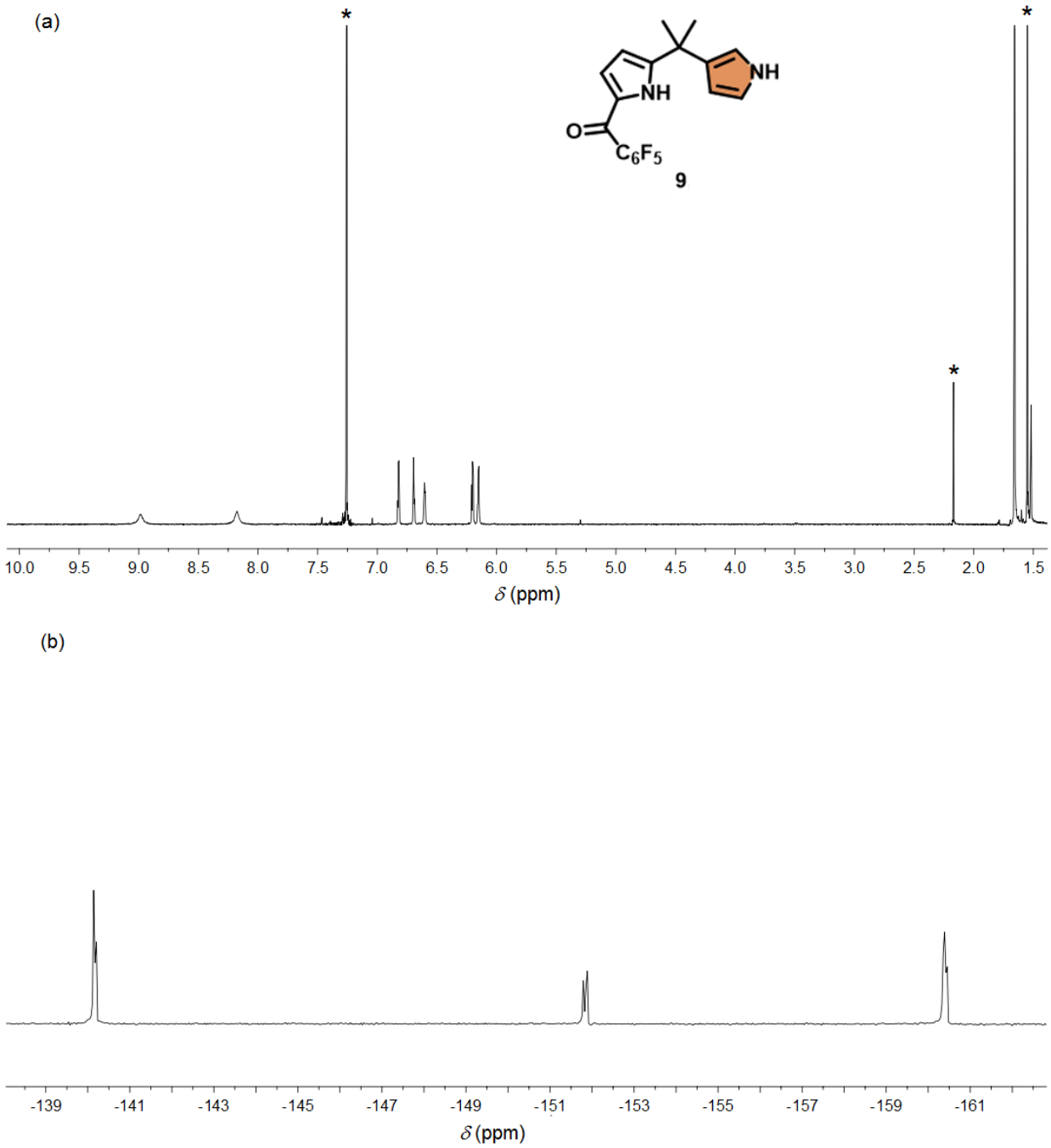

Figure S2-1. (a) ^{1}H and (b) ^{19}F NMR spectra of **9** in $CDCl_3$. Asterisks indicate the peaks of residual solvent and impurities.

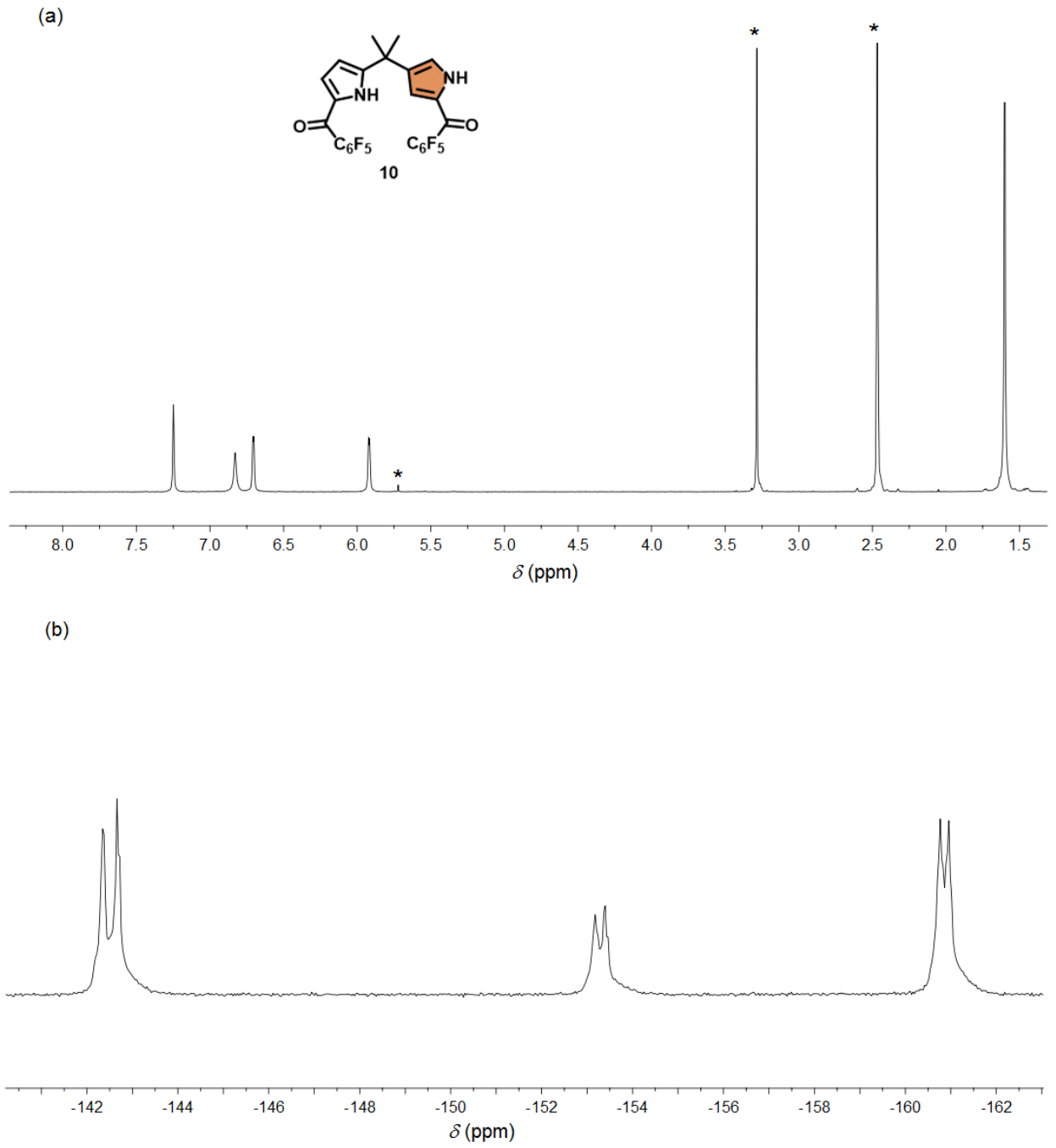

Figure S2-2. (a) ^{1}H NMR and (b) ^{19}F NMR spectra of **10** in $CDCl_3$. Asterisks indicate the peaks of residual solvent and impurities.

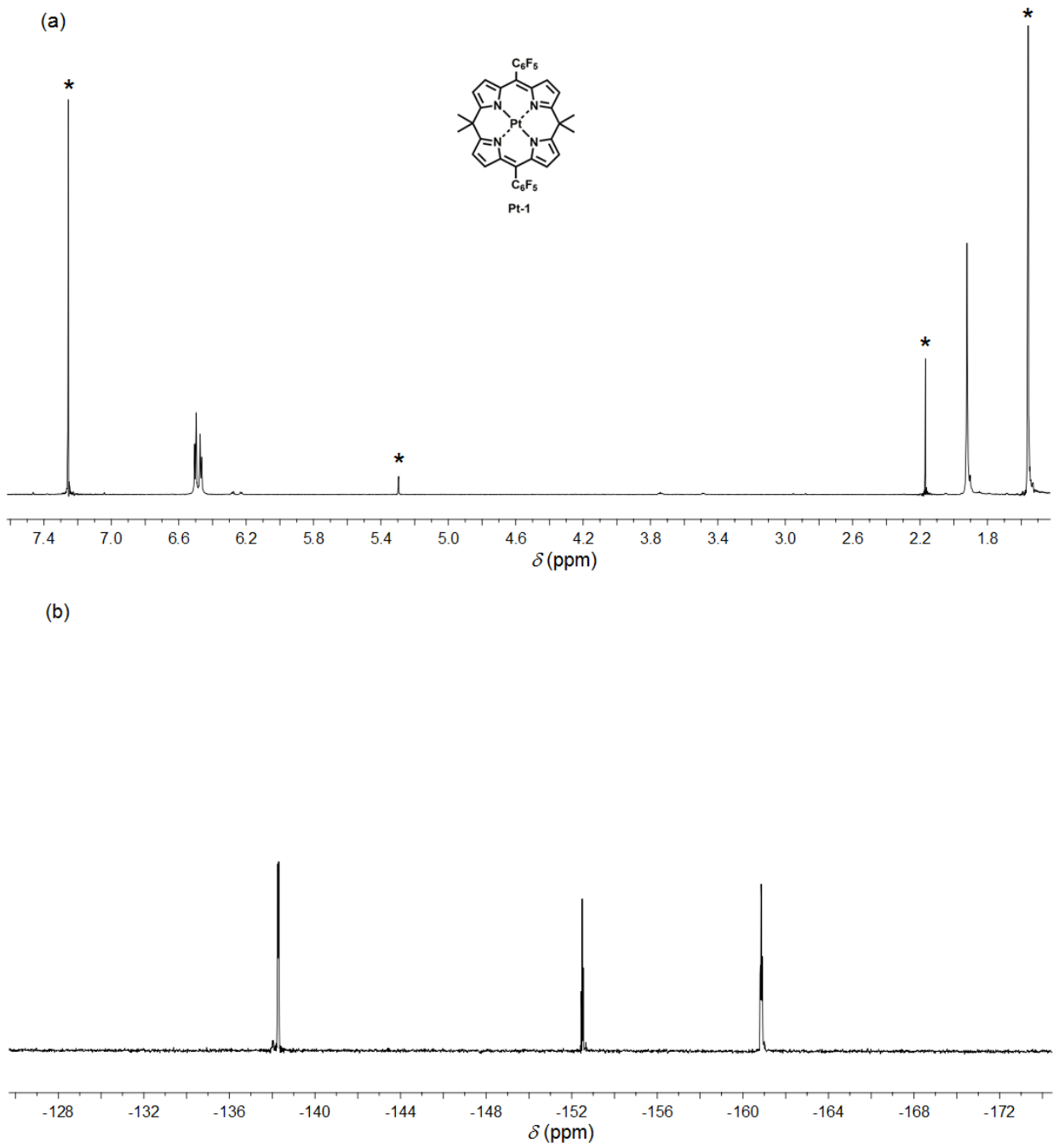

Figure S2-3. (a) ^{1}H NMR and (b) ^{19}F NMR spectra of **Pt-1** in DMSO-d_6. Asterisks indicate the peaks of residual solvent molecule(s) and impurities.

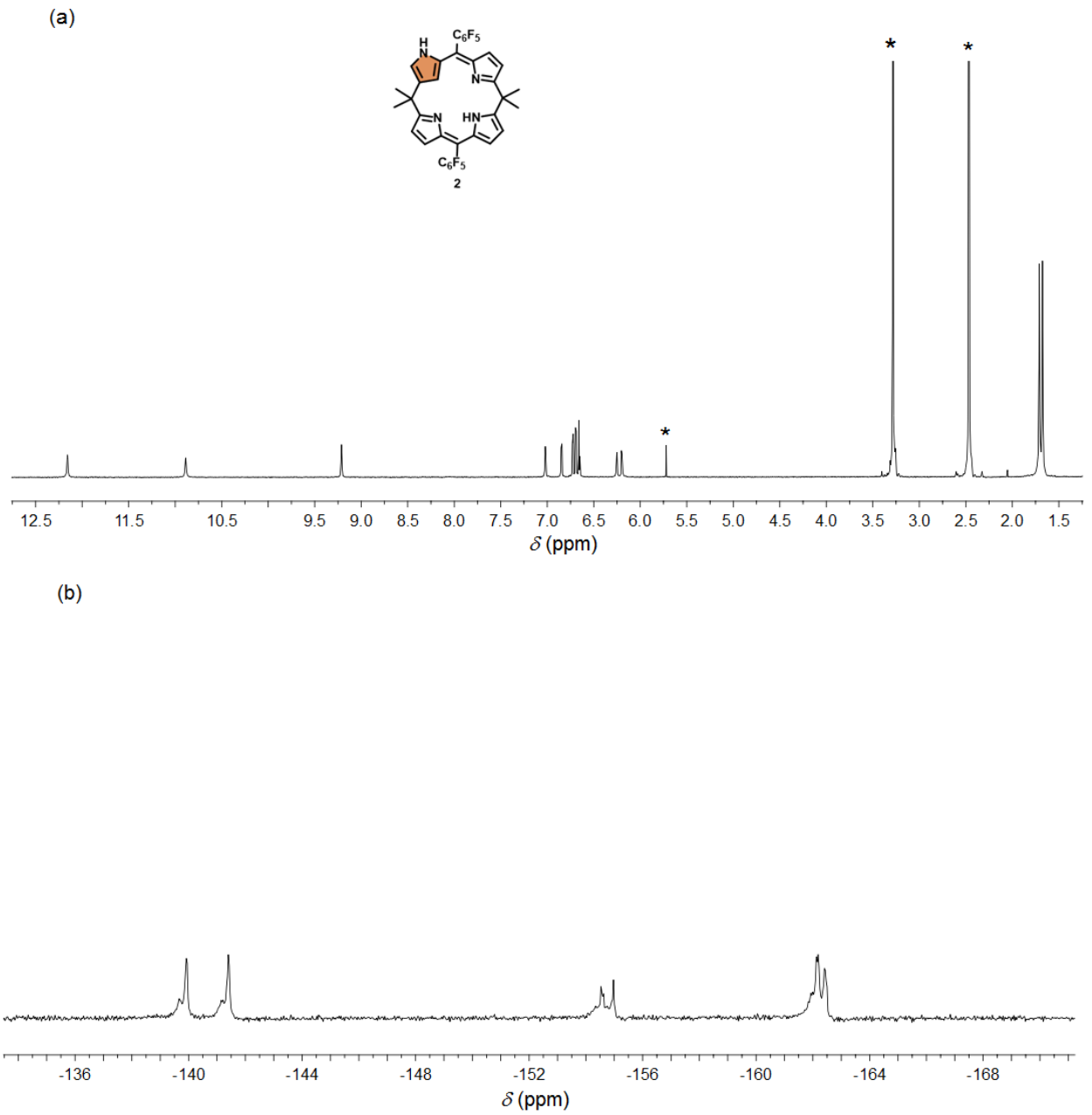

Figure S2-4. (a) ^{1}H NMR and (b) ^{19}F NMR spectra of **2** in DMSO-d_6. Asterisks indicate the peaks of residual solvent molecule(s) and impurities.

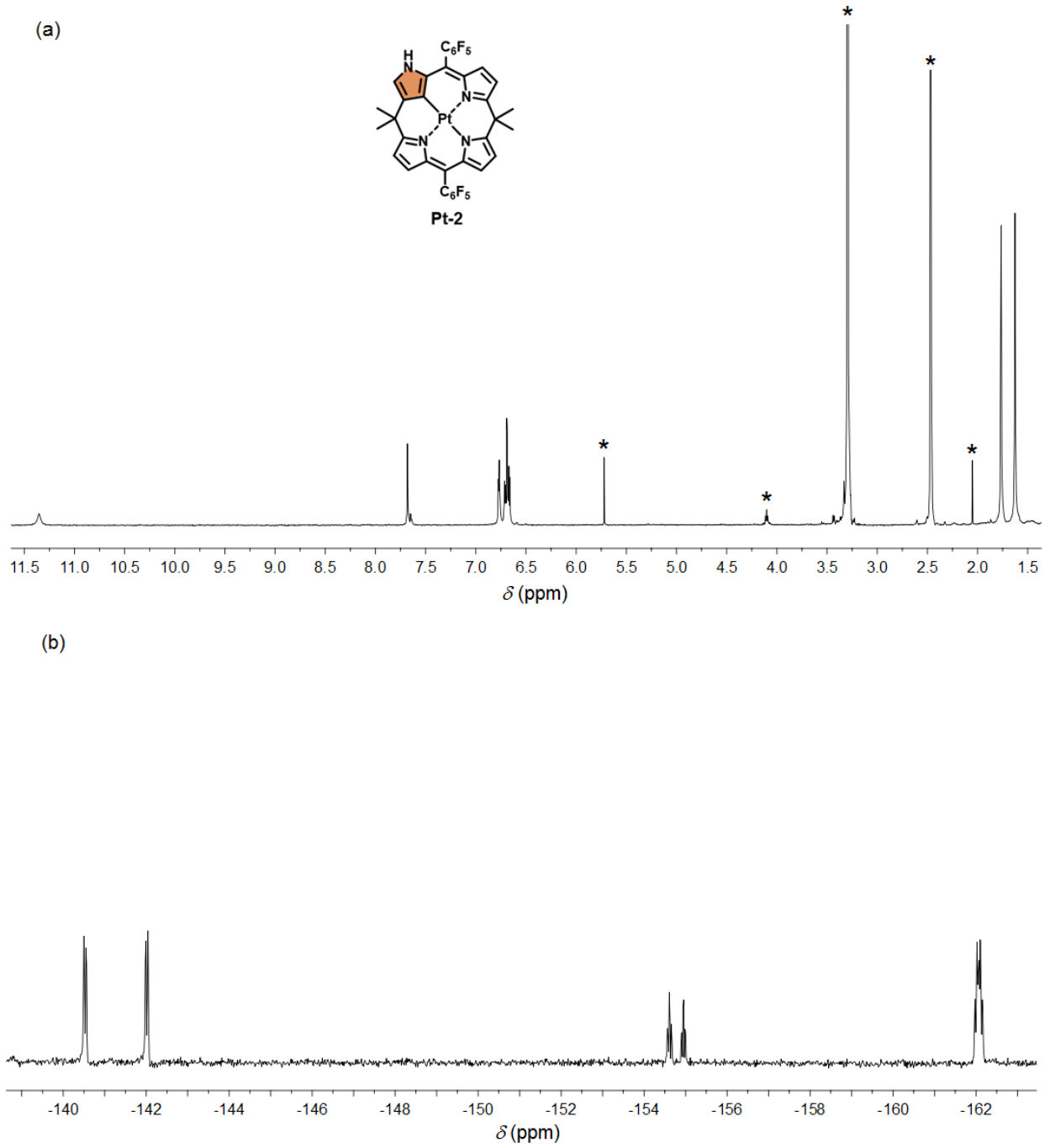

Figure S2-5. (a) ^{1}H NMR and (b) ^{19}F NMR spectra of **Pt-2** in DMSO-d_6. Asterisks indicate the peaks of residual solvent molecule(s) and impurities.

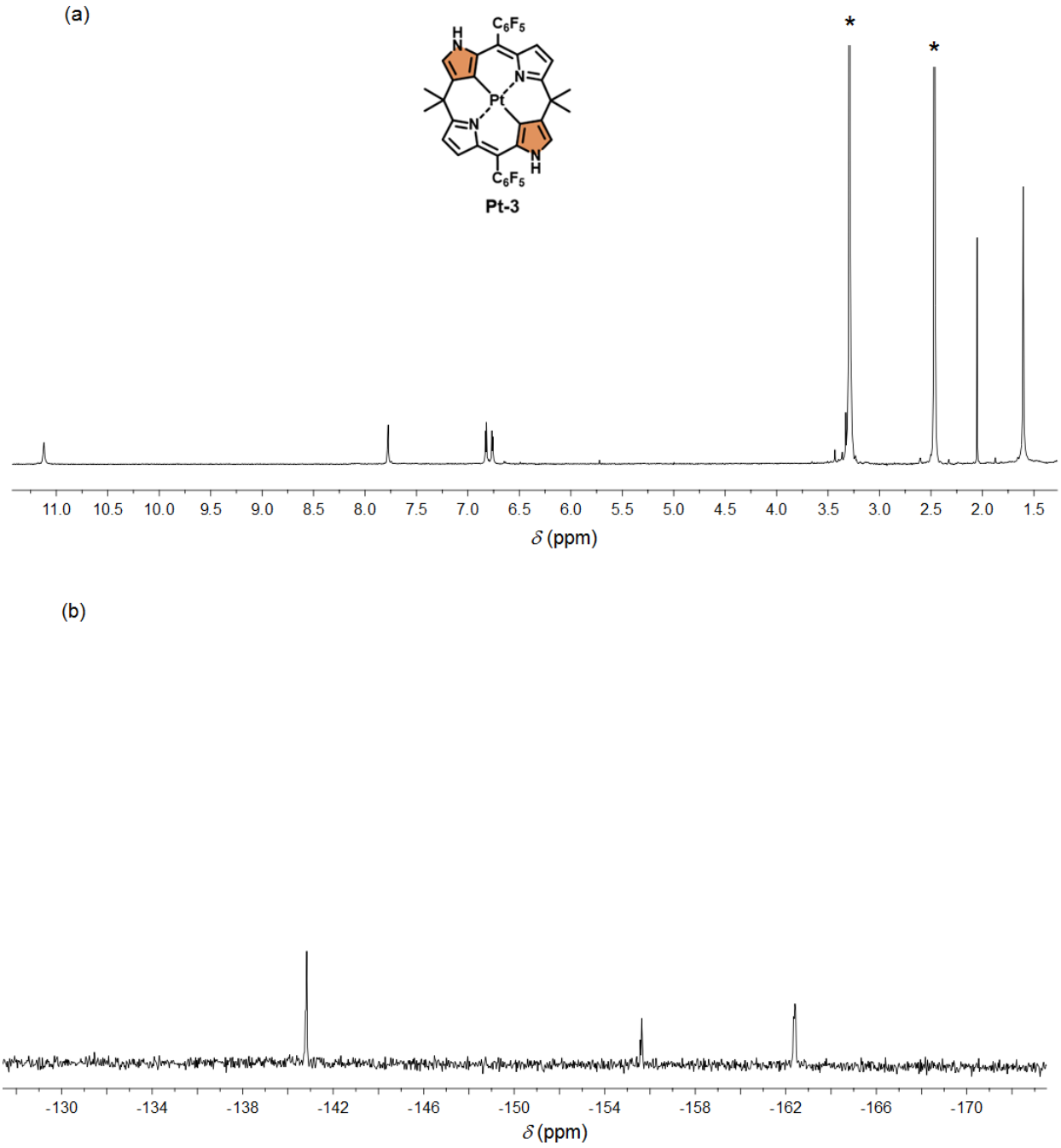

Figure S2-6. (a) ^{1}H NMR and (b) ^{19}F NMR spectra of **Pt-3** in DMSO-d_6. Asterisks indicate the peaks of residual solvent molecule(s) and impurities.

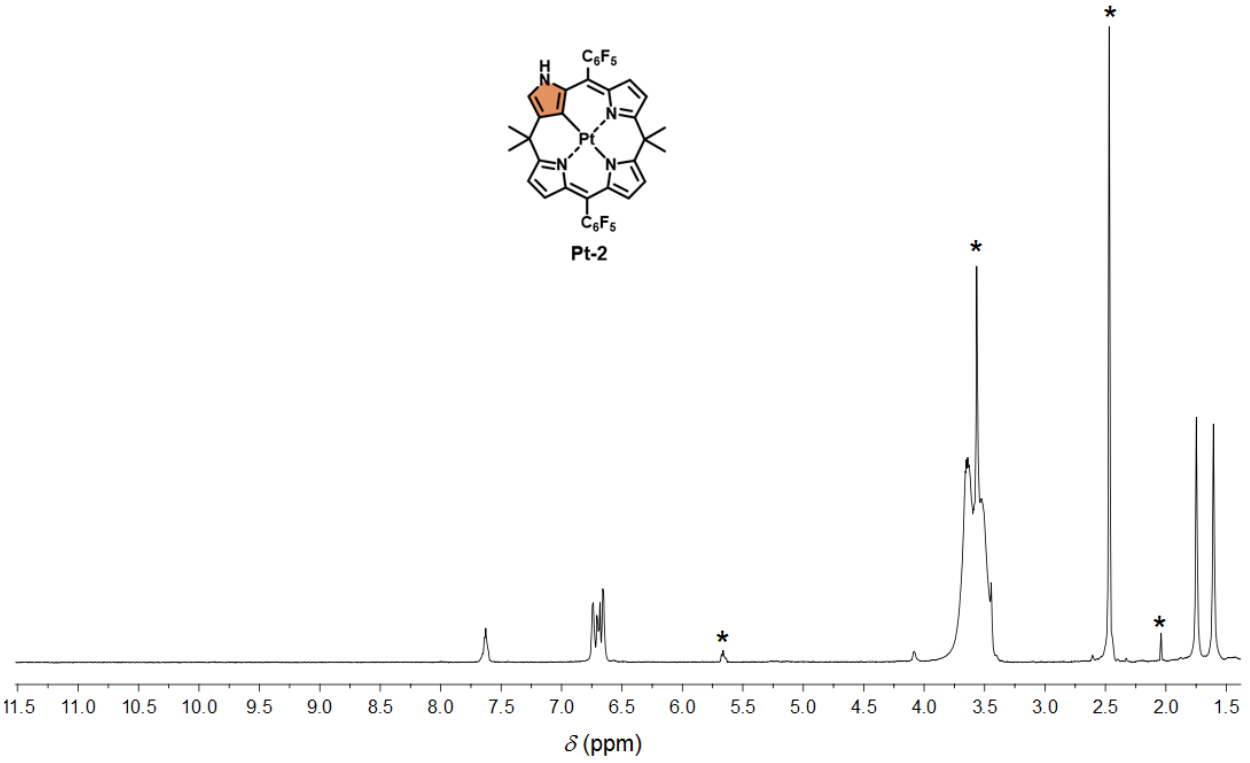

Figure S2-7: ^{1}H NMR spectrum of **Pt-2** in DMSO-d_6 after addition of D_2O. The outer NH peak (11.37 ppm) is disappeared.

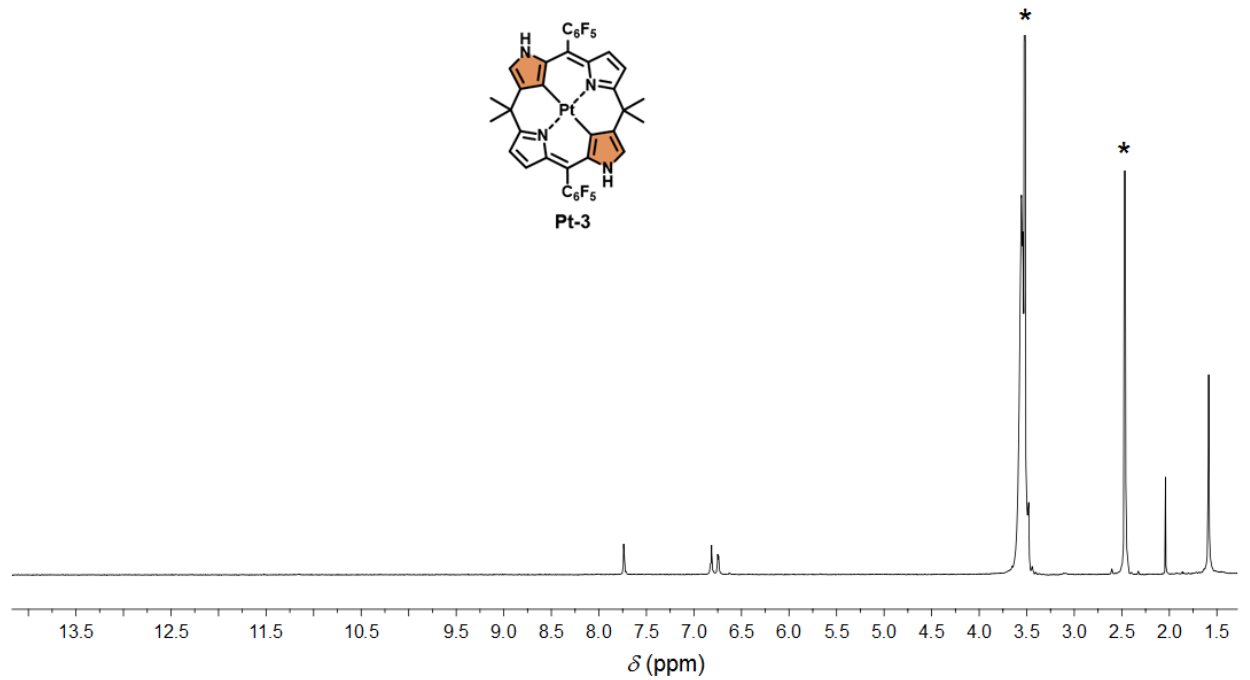

Figure S2-8: ^{1}H NMR spectrum of **Pt-3** in DMSO-d_6 after addition of D_2O. The outer NH peak (11.14 ppm) is disappeared.

Table S2-1. Crystallographic data of **8, 9,** and **10**

Compound	**8**	**9**	**10**
Empirical Formula	$C_{18}H_{13}F_5N_2O$	$C_{18}H_{13}F_5N_2O$	$C_{25}H_{12}F_{10}N_2O_2$
Crystal System	monoclinic	monoclinic	triclinic
Space Group	$C2/c$	$P2_1/c$	$P\bar{1}$
R_1 ($I > 2.00\sigma(I)$)	0.0526	0.0435	0.0435
wR_2 (All reflections)	0.1339	0.1130	0.1010
GOF	1.076	1.059	1.024
a [Å]	30.5480(10)	6.00333(17)	9.8387(3)
b [Å]	11.3136(3)	11.4287(3)	9.9746(3)
c [Å]	10.1565(3)	22.8144(7)	12.8952(3)
α [°]	90	90	72.828(2)
β [°]	96.885(3)	93.836(3)	74.855(2)
γ [°]	90	90	68.577(3)
V [Å^3]	3484.85(18)	1561.80(8)	1108.68(6)
Z	8	4	2
T [K]	100	100	100
D_{calc} [g/cm^3]	1.404	1.566	1.684
F_{000}	1504.00	752.00	564.00
$2\theta_{max}$ [°]	56.0	56.0	56.0
no. reflns measd. (unique)	4201	3741	5325
no. params.	237	237	354
CCDC no.	1566514	1566513	1566517

(a)

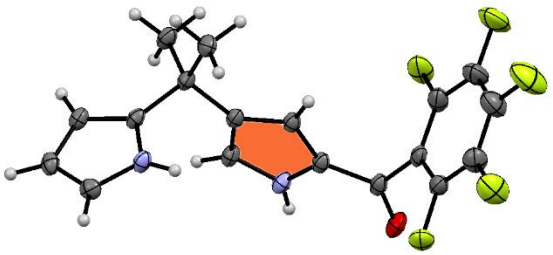

(b)

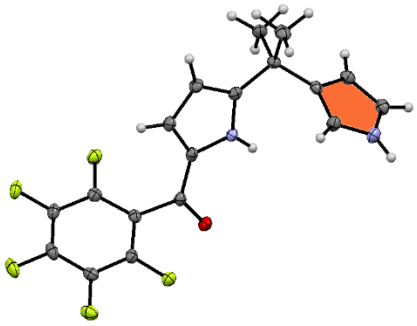

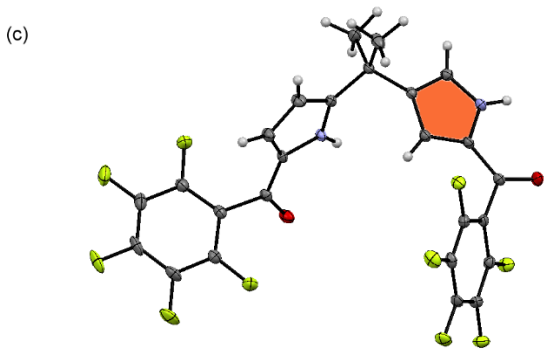

Figure S2-9. X-ray single crystal structures of the acylated dipyrromethanes: (a) **8**, (b) **9**, and (c) **10**. Co-crystallized solvent molecule(s) are omitted for clarity.

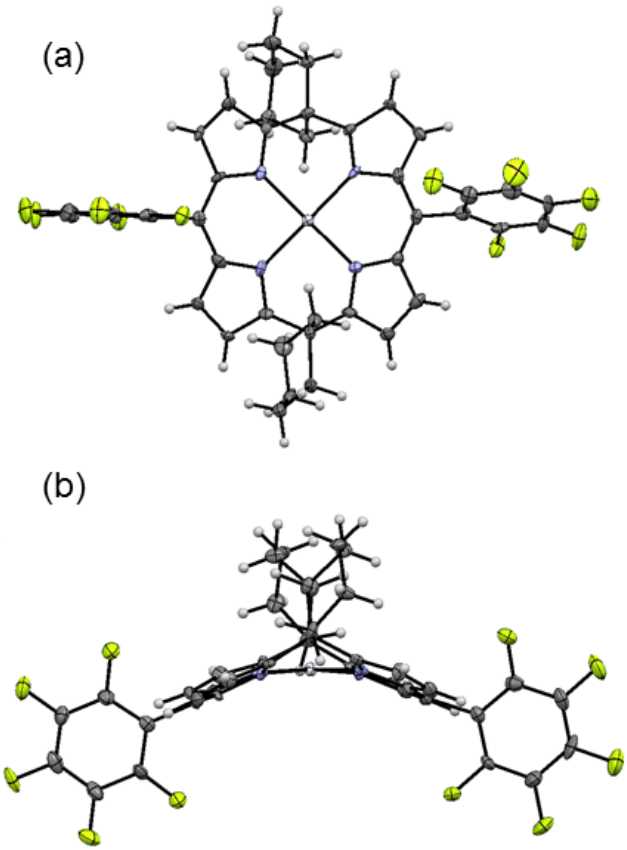

Figure S2-10. X-ray single crystal structures of **Pt-1c** (CCDC 682908)[24]: (a) top view, (b) side view. Co-crystallized solvent molecule(s) are omitted for clarity.

Table S2-2. Crystallographic data of **Pt-2** and **Pt-3**.

	Pt-2	**Pt-3**
Empirical Formula	$C_{36}H_{20}F_{10}N_4Pt$	$C_{47}H_{34}C_{l3}F_{10}N_5Pt_{1.5}$
Crystal System	monoclinic	monoclinic
Space Group	$P2_1/c$	$I2/a$
R_1 ($I>2.00\sigma(I)$)	0.0308	0.0489
wR_2 (All reflections)	0.0630	0.1169
GOF	1.058	1.042
a [Å]	14.8635(6)	23.4004(7)
b [Å]	10.5899(4)	14.9914(4)
c [Å]	10.0188(4)	26.4194(7)
α [°]	90	90
β [°]	109.655(4)	101.650(3)
γ [°]	90	90
V [Å^3]	1485.11(11)	9077.1(4)
Z	2	8
T [K]	100	100
D_{calc} [g/cm^3]	1.998	1.841
F_{000}	864.00	4872.00
$2\theta_{max}$ [°]	56.0	53.0
no. reflns measd. (unique)	3575	9401
no. params.	235	632
CCDC no.	1566518	1566511

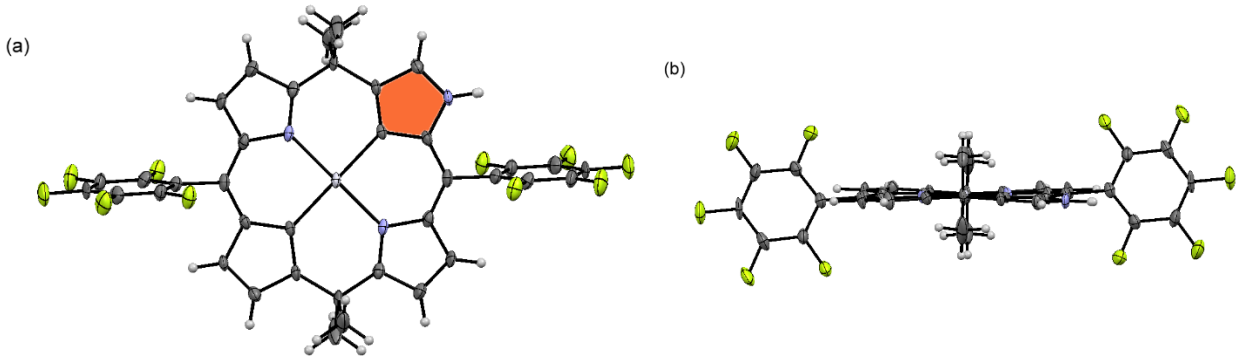

Figure S2-11. X-ray single crystal structures of complexes **Pt-2**: (a) top view, (b) side view. Co-crystallized solvent molecule was omitted for clarity. The confused rings are highlighted in orange.

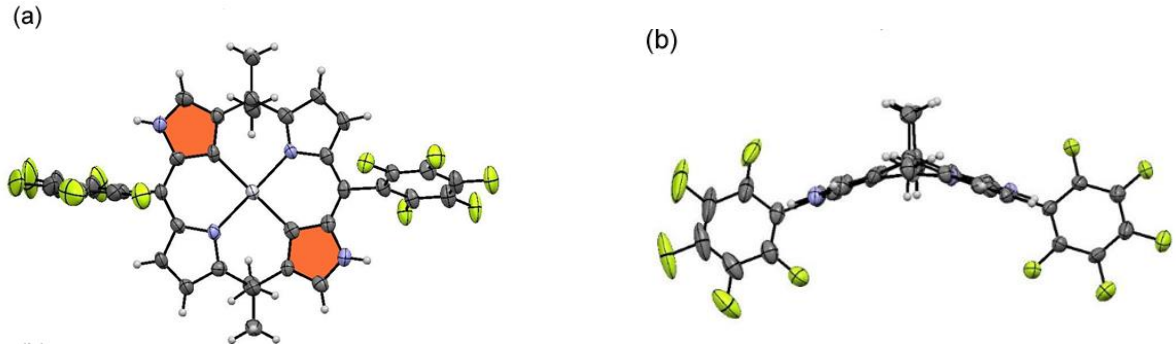

Figure S2-12. X-ray single crystal structures of complexes **Pt-3**: (a) top view, (b) side view. The co-crystalized solvent molecule(s) were omitted for clarity. The confused rings are highlighted in orange.

Table S2-3. Selected TD-DFT calculated oscillator strengths, symmetry and compositions of the major electronic transitions of **Pt-1**.

Wavelength (nm)	Osc. Strength, *f*	Symmetry	Major contributions
517.5713	0.0198	Singlet-A	H-3->LUMO (37%), H-1->LUMO (57%)
490.8321	0.0016	Singlet-A	H-3->LUMO (46%), H-1->LUMO (14%), HOMO->L+1 (36%)
489.5143	0.048	Singlet-A	H-2->LUMO (95%)
426.4289	0.0006	Singlet-A	H-2->L+1 (98%)
423.8486	0.0001	Singlet-A	H-3->L+1 (53%), H-1->L+1 (41%)
416.8517	0.0017	Singlet-A	H-4->LUMO (99%)
381.8541	0.0013	Singlet-A	H-4->L+1 (100%)
377.0465	0.7936	Singlet-A	H-3->LUMO (14%), H-1->LUMO (28%), HOMO->L+1 (56%)
346.3633	0.0003	Singlet-A	H-6->LUMO (97%)
324.2858	0.0048	Singlet-A	H-8->L+1 (12%), H-7->LUMO (71%), H-5->L+1 (15%)

323.5833	0.001	Singlet-A	H-8->LUMO (82%), H-7->L+1 (17%)
321.9532	0.0033	Singlet-A	H-6->L+1 (94%)
320.6875	0.0002	Singlet-A	H-7->LUMO (11%), H-5->L+1 (81%)
309.5658	0.02	Singlet-A	H-1->L+2 (35%), HOMO->L+3 (63%)
308.1654	0.0725	Singlet-A	H-10->LUMO (78%), H-9->L+1 (17%)
307.9205	0.0096	Singlet-A	H-10->L+1 (17%), H-9->LUMO (78%)
289.5609	0.0002	Singlet-A	H-8->LUMO (17%), H-7->L+1 (82%)
289.3987	0.0001	Singlet-A	H-8->L+1 (82%), H-7->LUMO (17%)
286.5295	0.0001	Singlet-A	H-1->L+3 (62%), HOMO->L+2 (33%)
286.5229	0.0016	Singlet-A	H-1->L+2 (61%), HOMO->L+3 (34%)
283.6842	0.0252	Singlet-A	H-1->L+5 (33%), HOMO->L+4 (66%)

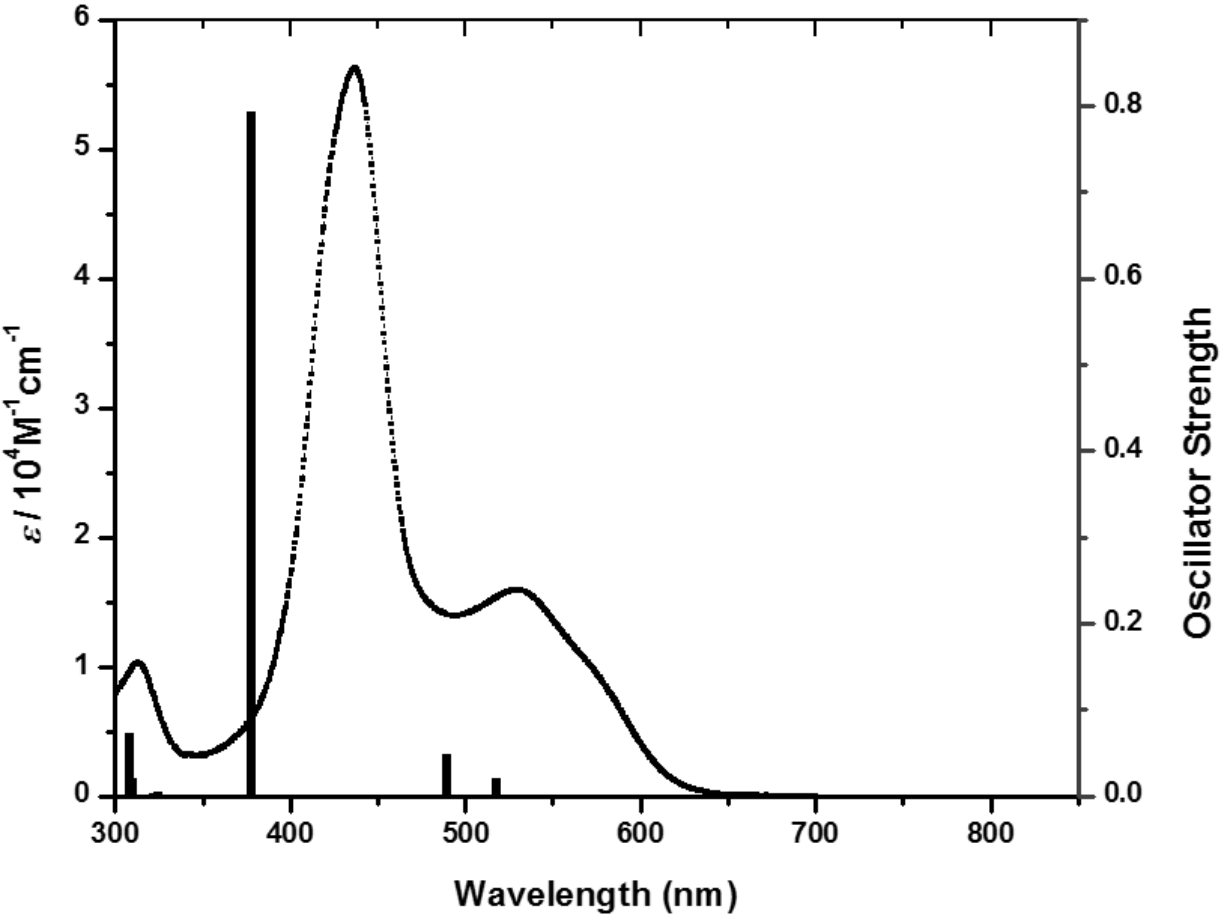

`**Figure S2-13.** Absorption spectrum of **Pt-1** recorded in CH_2Cl_2 along with the calculated stick spectrum obtained by TD-DFT (B3LYP) method.

Table S2-4. Selected TD-DFT calculated oscillator strengths, symmetry and compositions of the major electronic transitions of **Pt-2**.

Wavelength (nm)	Osc. Strength, *f*	Symmetry	Major contributions
594.4773	0.0093	Singlet-A	HOMO->LUMO (84%)
580.695	0.0068	Singlet-A	H-2->LUMO (27%), H-1->LUMO (55%), HOMO->LUMO (12%)
526.8525	0.0681	Singlet-A	H-2->LUMO (58%), H-1->LUMO (27%)
479.5552	0.0045	Singlet-A	H-4->LUMO (10%), H-2->L+1 (10%), H-1->L+1 (66%)
474.508	0.0021	Singlet-A	H-4->LUMO (83%)
452.3815	0.0099	Singlet-A	H-3->LUMO (32%), H-2->L+1 (27%), HOMO->L+1 (23%)
436.2875	0.0134	Singlet-A	H-3->LUMO (19%), H-2->L+1 (55%), HOMO->L+1 (13%)
400.4399	0.0412	Singlet-A	H-4->L+1 (54%), H-3->L+1 (35%)
395.1436	0.1095	Singlet-A	H-4->L+1 (44%), H-3->L+1 (33%), HOMO->L+1 (15%)
377.4252	0.5188	Singlet-A	H-3->LUMO (24%), H-3->L+1 (27%), HOMO->L+1 (22%)
372.6046	0.017	Singlet-A	H-6->LUMO (30%), H-5->LUMO (62%)
365.7243	0.0465	Singlet-A	H-6->LUMO (62%), H-5->LUMO (28%)
337.2068	0.0208	Singlet-A	H-1->L+2 (97%)
330.9422	0.0009	Singlet-A	H-6->L+1 (12%), H-5->L+1 (85%)
324.8636	0.0017	Singlet-A	HOMO->L+2 (99%)
323.1195	0.0037	Singlet-A	H-7->LUMO (54%), H-6->L+1 (32%)
321.2941	0.0012	Singlet-A	H-7->LUMO (29%), H-6->L+1 (51%), H-5->L+1 (10%)
316.8925	0.0111	Singlet-A	HOMO->L+4 (98%)
311.0023	0.0242	Singlet-A	H-10->LUMO (43%), H-8->LUMO (40%)
309.9915	0.0057	Singlet-A	H-1->L+3 (96%)
306.808	0.0041	Singlet-A	H-9->LUMO (85%)
306.6714	0.0056	Singlet-A	H-10->LUMO (26%), H-9->LUMO (12%), H-8->LUMO (38%), H-8->L+1 (11%)
304.622	0.0024	Singlet-A	H-2->L+2 (93%)
301.474	0.0002	Singlet-A	HOMO->L+3 (100%)
299.7829	0.0012	Singlet-A	H-7->LUMO (15%), H-7->L+1 (83%)

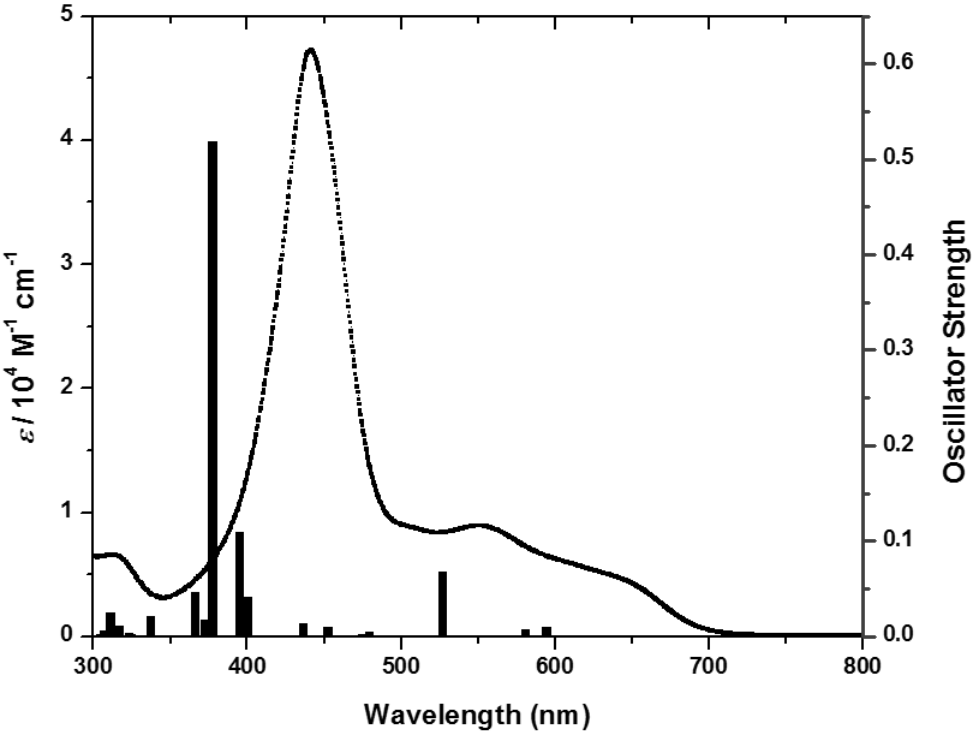

Figure S2-14. Absorption spectrum of **Pt-2** recorded in CH_2Cl_2 along with the calculated stick spectrum obtained by TD-DFT (B3LYP) method.

Table S2-5. Selected TD-DFT calculated oscillator strengths, symmetry and compositions of the major electronic transitions of **Pt-3**.

Wavelength (nm)	Osc. Strength,*f*	Symmetry	Major contributions
639.7533179	0.0397	Singlet-A	H-2->LUMO (21%), HOMO->LUMO (77%)
544.0766764	0.1045	Singlet-A	H-2->LUMO (75%), HOMO->LUMO (16%)
504.4929729	0.0002	Singlet-A	H-4->LUMO (16%), H-2->L+1 (35%), H-1->LUMO (46%)
495.1049957	0.002	Singlet-A	H-4->LUMO (83%), H-1->LUMO (12%)
469.7082627	0.0208	Singlet-A	H-3->LUMO (66%), H-1->L+1 (31%)
450.3603088	0.0027	Singlet-A	H-4->L+1 (97%)
405.2168285	0.0022	Singlet-A	H-3->L+1 (89%)
402.0500454	0.0071	Singlet-A	H-6->LUMO (96%)
380.3429444	0.6283	Singlet-A	H-3->LUMO (23%), H-1->L+1 (60%)
372.795096	0.0002	Singlet-A	H-7->LUMO (62%), H-5->LUMO (27%)
366.5785377	0.0003	Singlet-A	H-6->L+1 (91%)
352.5783962	0.0079	Singlet-A	H-7->L+1 (25%), H-5->L+1 (70%)

348.681571	0.0348	Singlet-A	HOMO->L+2 (90%)
337.4270439	0.0096	Singlet-A	H-7->L+1 (67%), H-5->L+1 (28%)
319.7611622	0.0091	Singlet-A	HOMO->L+5 (90%)
319.6292679	0.0008	Singlet-A	H-8->LUMO (52%), HOMO->L+4 (38%)
310.3561867	0.0156	Singlet-A	H-2->L+2 (71%), H-1->L+3 (23%)
308.9178847	0.0152	Singlet-A	H-2->L+2 (27%), H-1->L+3 (60%)

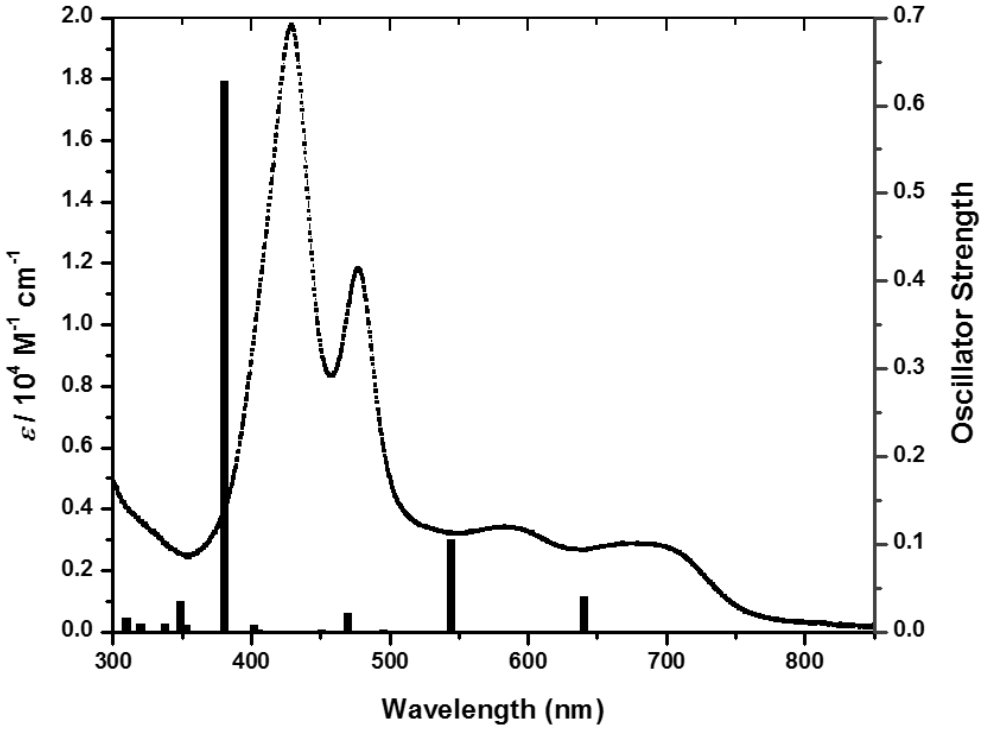

Figure S2-15. Absorption spectrum of **Pt-3** recorded in CH_2Cl_2 along with the calculated stick spectrum obtained by TD-DFT (B3LYP) method.

Emission studies

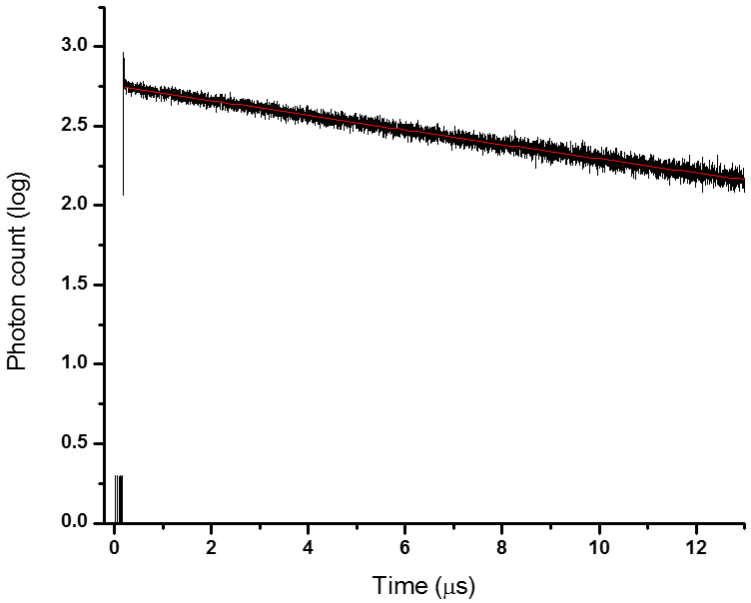

Figure S2-16: Time resolved phosphorescence decay of **Pt-1** in CH_2Cl_2; λ_{ex}= 532 nm.

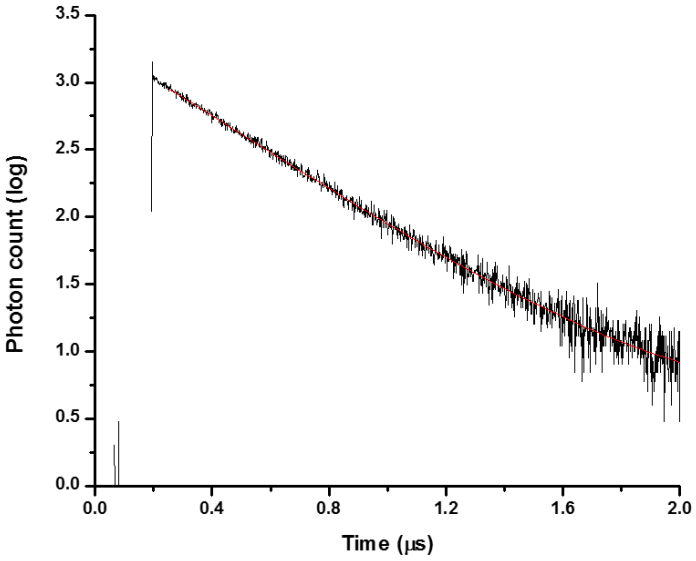

Figure S2-17: Time resolved phosphorescence decay of **Pt-2** in CH_2Cl_2; λ_{ex}= 532 nm

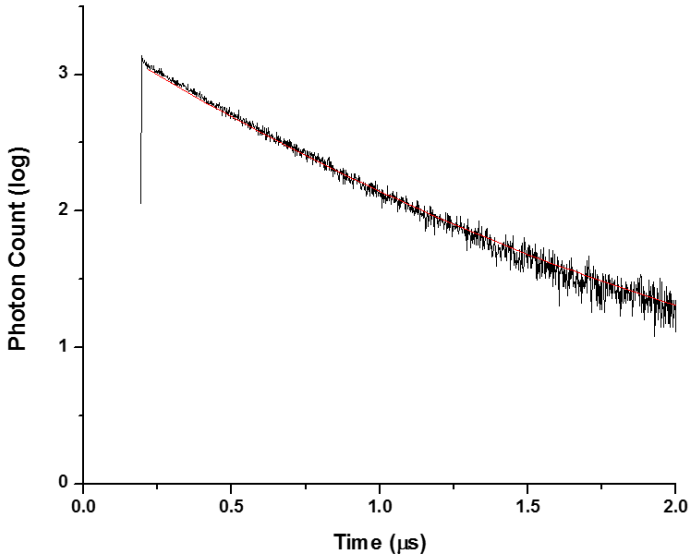

Figure S2-18: Time resolved phosphorescence decay of **Pt-3** in CH_2Cl_2: λ_{ex}= 532 nm

(a)

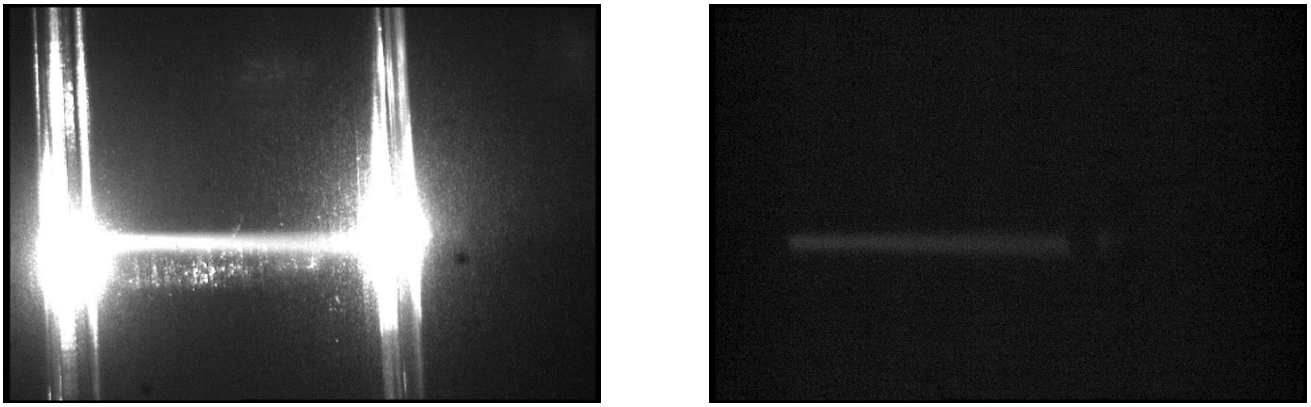

(b)

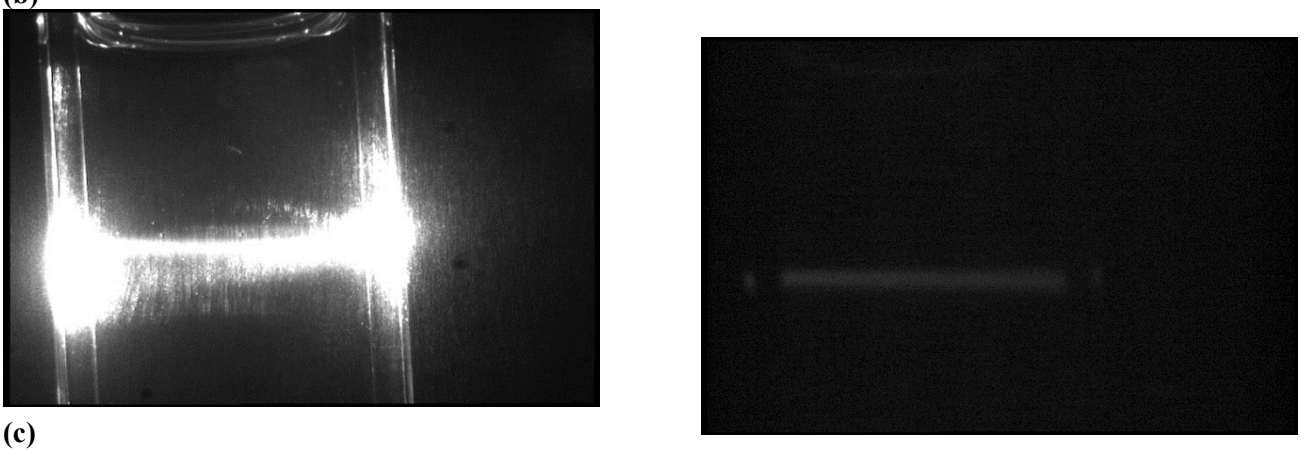

(c)

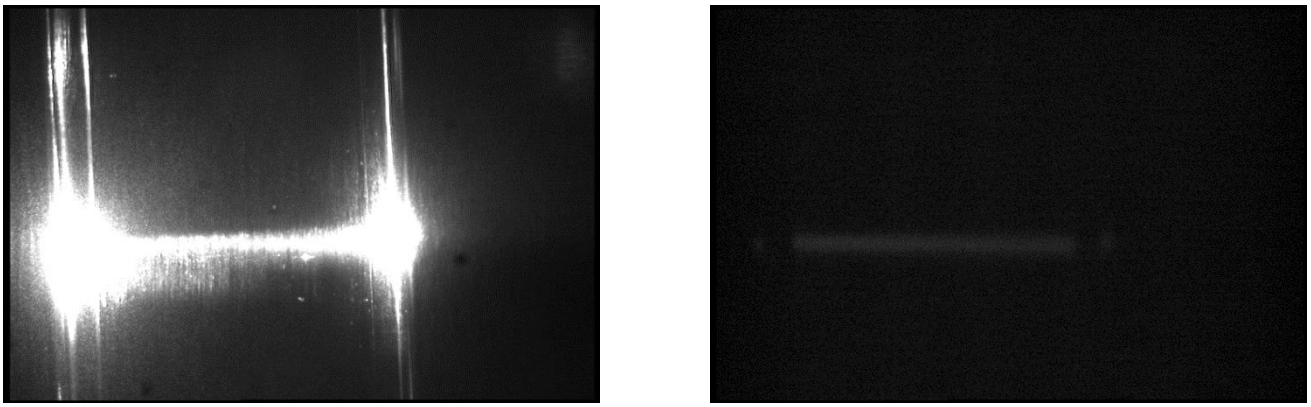

Figure S2-19: Photographs show excitation (λ_{ex}=445 nm, left) of (a) **Pt-1**, (b) **Pt-2**, (c) **Pt-3** and the observed NIR phosphorescence (right).

Singlet oxygen studies

The concentration of the oxygen scavenger, 1,3- diphenylisobenzofuran (DPBF) used in the measurements was 62 μM in methanol and the absorbance (at the intense absorption band) of the platinum complexes solution in methanol was kept in the range of 0.55-0.70 for the singlet oxygen studies.

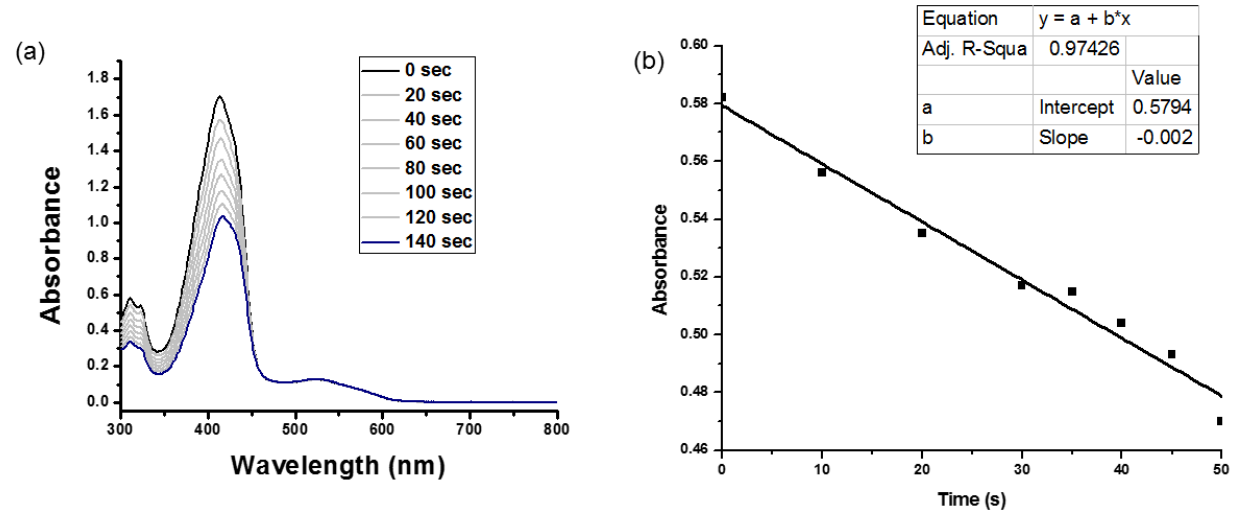

Figure S2-20. (a) UV/vis spectral change of **Pt-1** in MeOH upon photoirradiation at 535 nm and (b) the rate of decrease in absorption measured at 324 nm.

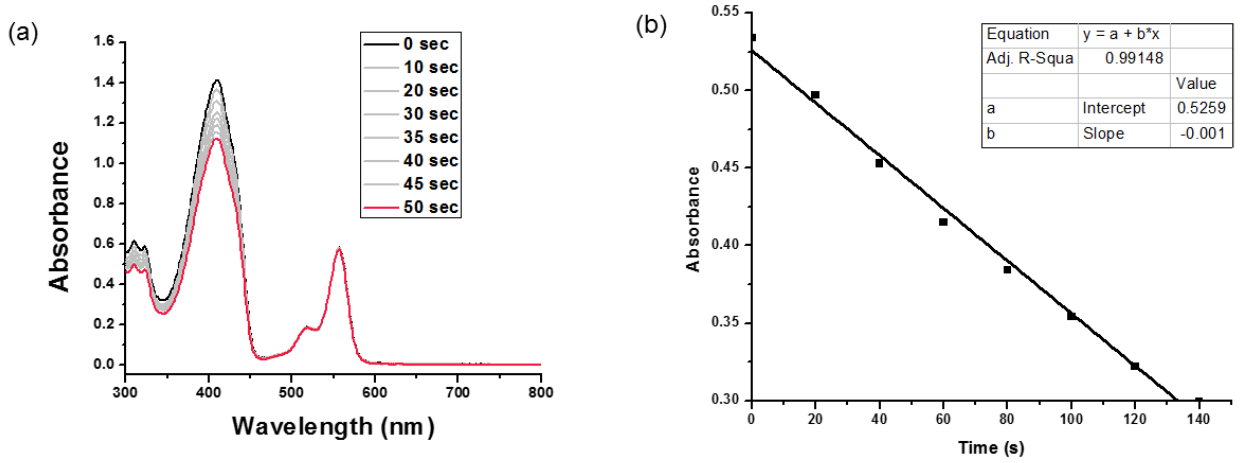

Figure S2-21. (a) UV/vis spectral change of Rose Bengal in MeOH upon photoirradiation at 535 nm and (b) the rate of decrease in absorption measured at 324 nm..

Φ_{Δ} = 0.76, for Rose Bengal in MeOH.

$\Phi_{\Delta(S)} = \Phi_{\Delta(S0)}$ x { Slope(S) / Slope(S0)}, where S is for sample and S0 is for standard

$\Phi_{\Delta(S)}$ = 0.76 x {0.0017/0.002} = 0.646

$\Phi_{\Delta(\mathbf{Pt\text{-}1})}$ = 64.6%

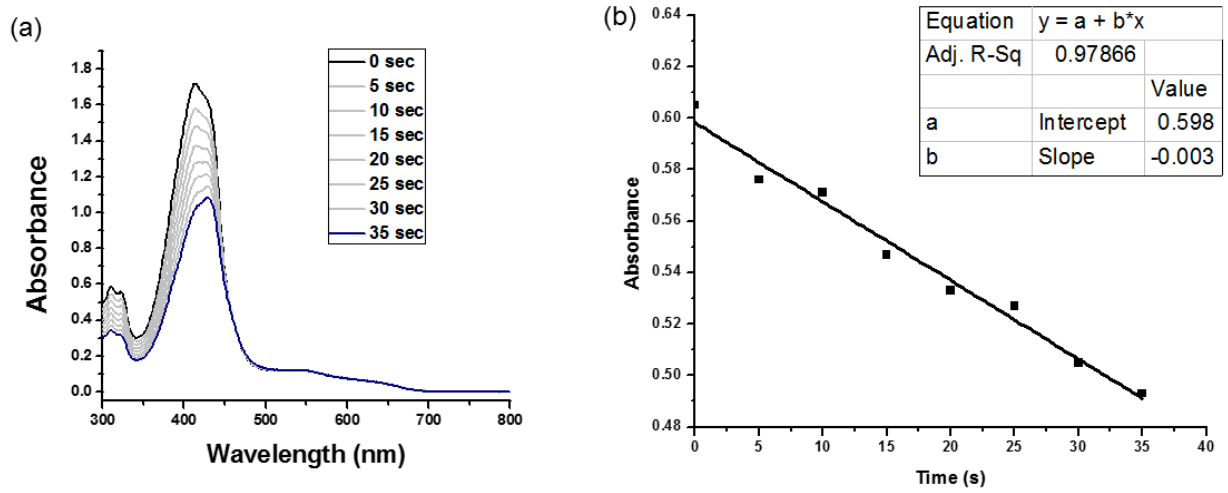

Figure S2-22. (a) UV/vis spectral change of **Pt-2** in MeOH upon photoirradiation at 531 nm and (b) the rate of decrease in absorption measured at 324 nm.

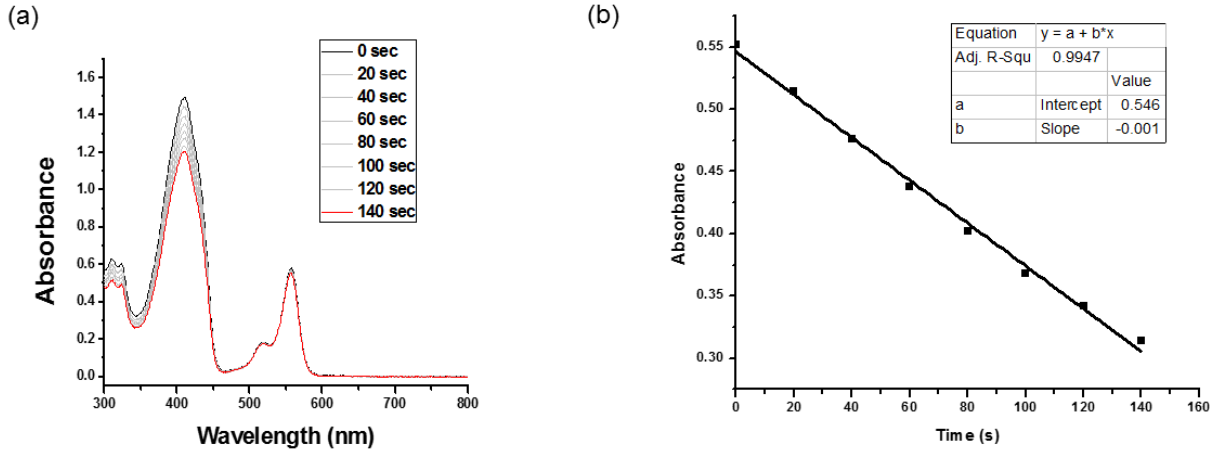

Figure S2-23. (a) UV/vis spectral change of Rose Bengal in MeOH upon photoirradiation at 531 nm and (b) the rate of decrease in absorption measured at 324 nm.

$\Phi_{\Delta(S)} = \Phi_{\Delta(S0)}$ x { Slope(S) / Slope(S0)},
where S is for sample and S0 is for standard
$\Phi_{\Delta(S)} = 0.76$ x {0.0017/0.0031} = 0.4168

$\Phi_{\Delta(\mathbf{Pt\text{-}2})} = 41.68\%$

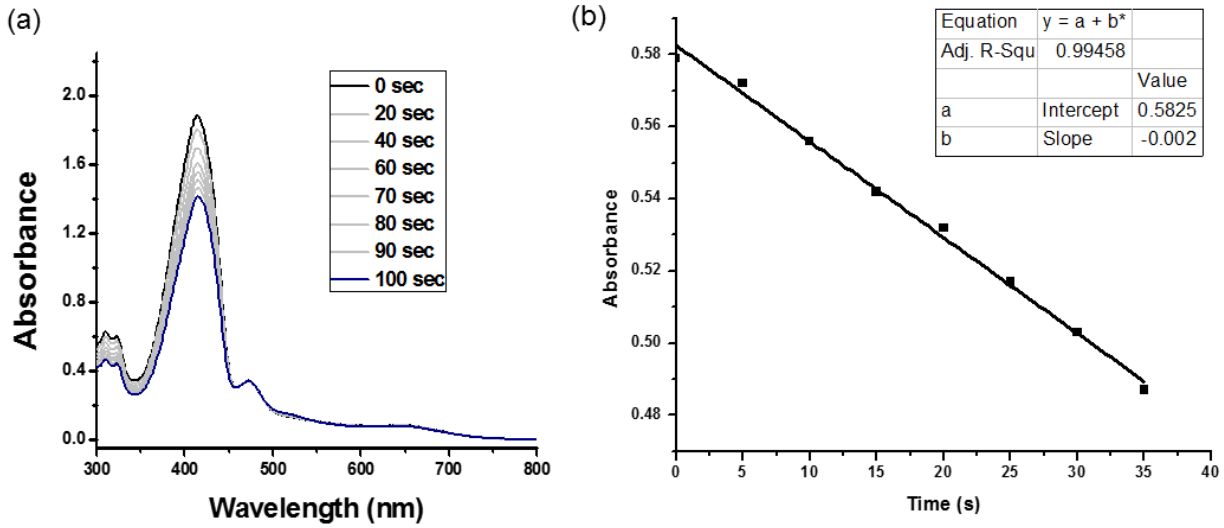

Figure S2-24. (a) UV/vis spectral change of **Pt-3** in MeOH upon photoirradiation at 533 nm and (b) the rate of decrease in absorption measured at 324 nm.

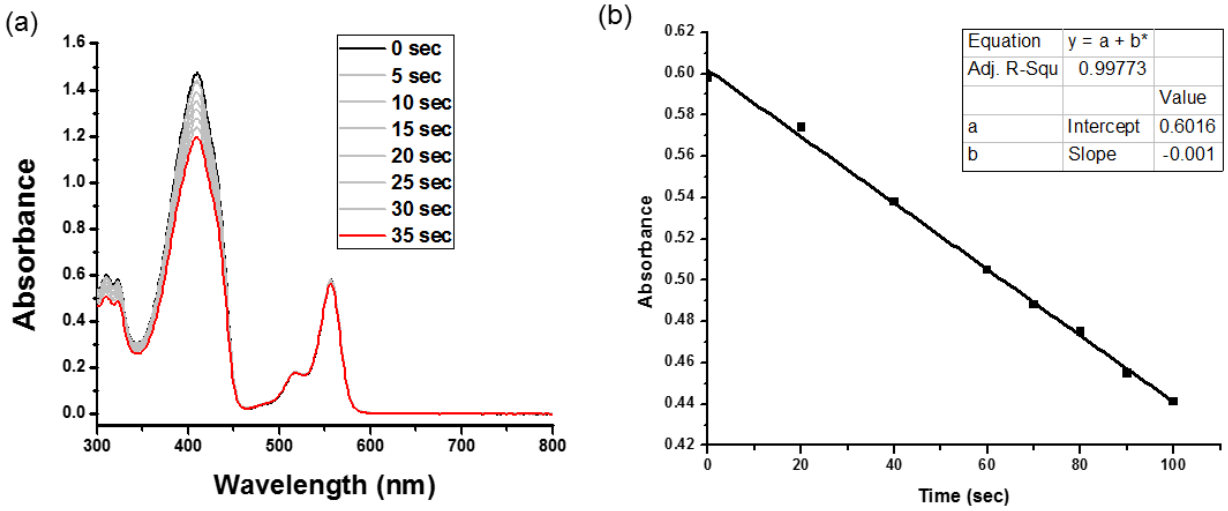

Figure S2-25. (a) UV/vis spectral change of Rose Bengal in MeOH upon photoirradiation at 533 nm and (b) the rate of decrease in absorption measured at 324 nm.

$\Phi_{\Delta(S)} = \Phi_{\Delta(S0)}$ x { Slope(S) / Slope(S0)},
where S is for sample and S0 is for standard
$\Phi_{\Delta(S)} = 0.76$ x {0.0016/0.0027} = 0.45

$\Phi_{\Delta(\mathbf{Pt\text{-}3})} = 45.04\%$

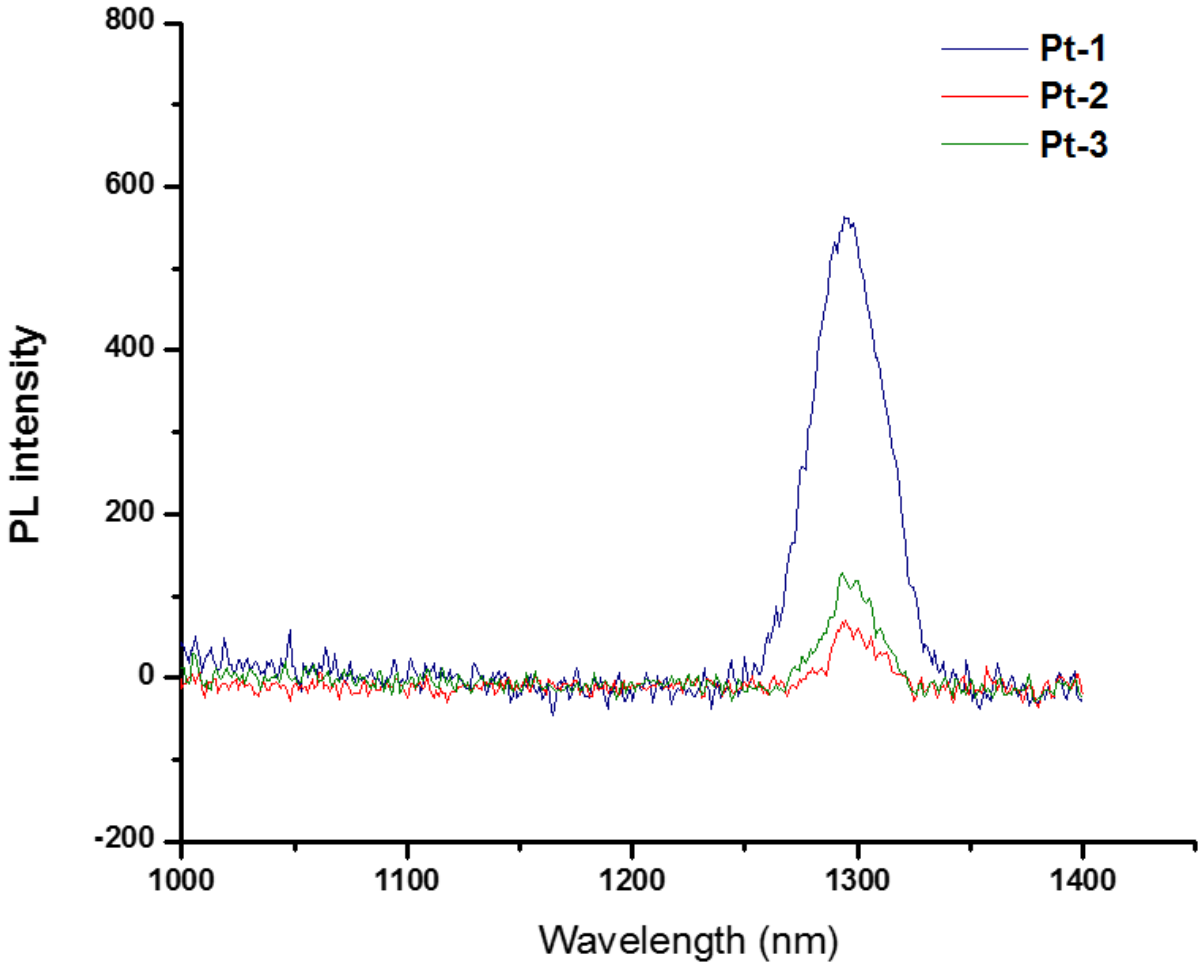

Figure S2-26. Emission spectra of **Pt-1**, **Pt-2**, and **Pt-3** under oxygen rich environment showing singlet oxygen emission peak around 1280 nm in MeOH (λ_{ex} – 535, 531 and 533 nm respectively).

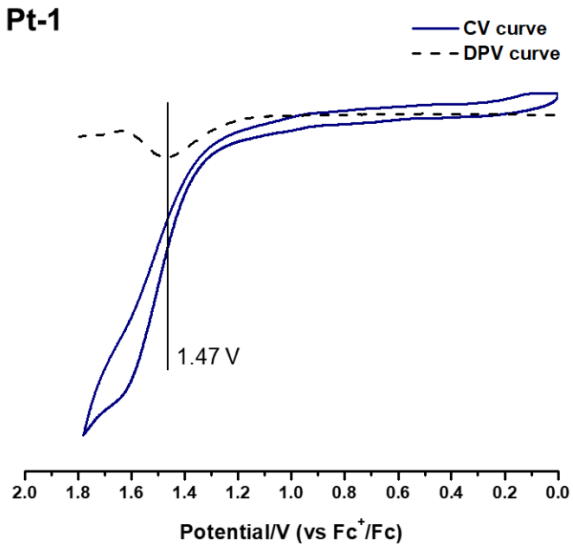

Figure S2-27. Cyclic voltammograms and DPV curve of **Pt-1,** showing the irreversible oxidation wave and E_{pa}.

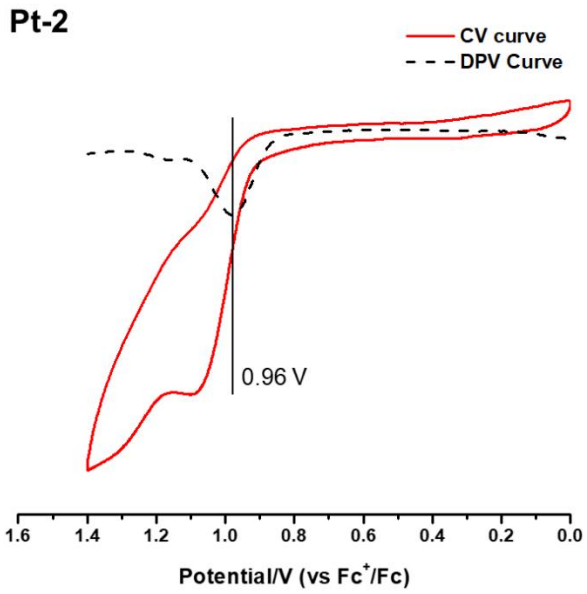

Figure S2-28. Cyclic voltammograms and DPV curve of **Pt-2,** showing the irreversible oxidation wave and E_{pa}.

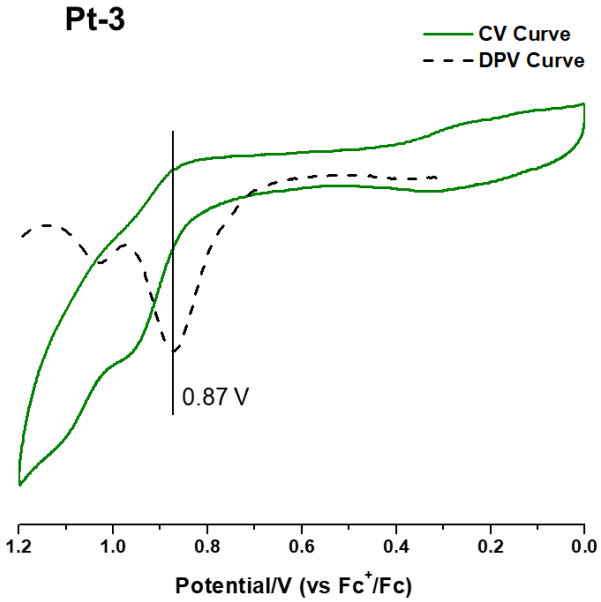

Figure S2-29. Cyclic voltammograms and DPV curve of **Pt-3,** showing the irreversible oxidation wave and E_{pa}.

2-9 References

[1] (a) D. A. K. Vezzu, D. Ravindranathan, A. W. Garner, L. Bartolotti, M. E. Smith, P. D. Boyle, S. Huo, *Inorganic Chemistry* **2011**, *50*, 8261-8273; (b) S. C. F. Kui, F.-F. Hung, S.-L. Lai, M.-Y. Yuen, C.-C. Kwok, K.-H. Low, S. S.-Y. Chui, C.-M. Che, *Chemistry – A European Journal* **2012**, *18*, 96-109.

[2] (a) P. Kit-Man Siu, D.-L. Ma, C.-M. Che, *Chemical Communications* **2005**, 1025-1027; (b) Y. Sun, Z. M. Hudson, Y. Rao, S. Wang, *Inorganic Chemistry* **2011**, *50*, 3373-3378.

[3] (a) J. Xuan, W.-J. Xiao, *Angewandte Chemie International Edition* **2012**, *51*, 6828-6838; (b) J. I. Goldsmith, W. R. Hudson, M. S. Lowry, T. H. Anderson, S. Bernhard, *Journal of the American Chemical Society* **2005**, *127*, 7502-7510.

[4] (a) F. Xue, Y. Lu, Z. Zhou, M. Shi, Y. Yan, H. Yang, S. Yang, *Organometallics* **2015**, *34*, 73-77; (b) M. Ethirajan, Y. Chen, P. Joshi, R. K. Pandey, *Chemical Society Reviews* **2011**, *40*, 340-362; (c)A. Gorman, J. Killoran, C. O'Shea, T. Kenna, W. M. Gallagher, D. F. O'Shea, *Journal of the American Chemical Society* **2004**, *126*, 10619-10631.

[5] (a) C. Huo, H. Zhang, H. Zhang, H. Zhang, B. Yang, P. Zhang, Y. Wang, *Inorganic Chemistry* **2006**, *45*, 4735-4742; (b) M. E. Köse, B. F. Carroll, K. S. Schanze, *Langmuir* **2005**, *21*, 9121-9129.

[6] M. C. DeRosa, R. J. Crutchley, *Coordination Chemistry Reviews* **2002**, *233-234*, 351-371.

[7] (a) H. Xiang, J. Cheng, X. Ma, X. Zhou, J. J. Chruma, *Chemical Society Reviews* **2013**, *42*, 6128-6185; (b) J. Zhao, W. Wu, J. Sun, S. Guo, *Chemical Society Reviews* **2013**, *42*, 5323-5351.

[8] (a) A. A. Abdel-Shafi, D. R. Worrall, A. Y. Ershov, *Dalton Transactions* **2004**, 30-36; (b) K. Ishii, *Coordination Chemistry Reviews* **2012**, *256*, 1556-1568.

[9] (a) S. J. Farley, D. L. Rochester, A. L. Thompson, J. A. K. Howard, J. A. G. Williams, *Inorganic Chemistry* **2005**, *44*, 9690-9703; (b) M. A. Baldo, D. F. O'Brien, Y. You, A. Shoustikov, S. Sibley, M. E. Thompson, S. R. Forrest, *Nature* **1998**, *395*, 151-154.

[10] (a) G. Cheng, S. C. F. Kui, W.-H. Ang, M.-Y. Ko, P.-K. Chow, C.-L. Kwong, C.-C. Kwok, C. Ma, X. Guan, K.-H. Low, S.-J. Su, C.-M. Che, *Chemical Science* **2014**, *5*, 4819-4830; (b) G. Cheng, P.-K. Chow, S. C. F. Kui, C.-C. Kwok, C.-M. Che, *Advanced Materials* **2013**, *25*, 6765-6770; (c) S. C. F. Kui, P. K. Chow, G. Cheng, C.-C. Kwok, C. L. Kwong, K.-H. Low, C.-M. Che, *Chemical Communications* **2013**, *49*, 1497-1499.

[11] R. H. Herber, M. Croft, M. J. Coyer, B. Bilash, A. Sahiner, *Inorganic Chemistry* **1994**, *33*, 2422-2426.

[12] (a) J. R. Sommer, A. H. Shelton, A. Parthasarathy, I. Ghiviriga, J. R. Reynolds, K. S. Schanze, *Chemistry of Materials* **2011**, *23*, 5296-5304; (b) Y. Matano, T. Miyajima, T. Nakabuchi, H. Imahori, N. Ochi, S. Sakaki, *Journal of the American Chemical Society* **2006**, *128*, 11760-11761; (c) F.

Niedermair, S. M. Borisov, G. Zenkl, O. T. Hofmann, H. Weber, R. Saf, I. Klimant, *Inorganic Chemistry* **2010**, *49*, 9333-9342.

[13] (a) L. Sessler Jonathan, S. Zimmerman Rebecca, C. Bucher, V. Král, B. Andrioletti, in *Pure and Applied Chemistry, 73*, **2001**, 1041-1057; (b) B. Dolenský, J. Kroulík, V. Král, J. L. Sessler, H. Dvořáková, P. Bouř, M. Bernátková, C. Bucher, V. Lynch, *Journal of the American Chemical Society* **2004**, *126*, 13714-13722.

[14] P. S. Salini, A. P. Thomas, R. Sabarinathan, S. Ramakrishnan, K. C. G. Sreedevi, M. L. P. Reddy, A. Srinivasan, *Chemistry – A European Journal* **2011**, *17*, 6598-6601.

[15] (a) G. Karthik, P. V. Krushna, A. Srinivasan, T. K. Chandrashekar, *The Journal of Organic Chemistry* **2013**, *78*, 8496-8501; (b) S. C. Jha, M. Lorch, R. A. Lewis, S. J. Archibald, R. W. Boyle, *Organic & Biomolecular Chemistry* **2007**, *5*, 1970-1974; (c) C. Bucher, R. S. Zimmerman, V. Lynch, V. Král, J. L. Sessler, *Journal of the American Chemical Society* **2001**, *123*, 2099-2100.

[16] H. Furuta, T. Ishizuka, A. Osuka, *Inorganic Chemistry Communications* **2003**, *6*, 398-401.

[17] (a) C. Bucher, D. Seidel, V. Lynch, V. Král, J. L. Sessler, *Organic Letters* **2000**, *2*, 3103-3106; (b) C. Bucher, R. S. Zimmerman, V. Lynch, J. L. Sessler, *Chemical Communications* **2003**, 1646-1647.

[18] (a) Y. Matano, H. Imahori, *Accounts of Chemical Research* **2009**, *42*, 1193-1204; (b) Y. Matano, T. Miyajima, N. Ochi, T. Nakabuchi, M. Shiro, Y. Nakao, S. Sakaki, H. Imahori, *Journal of the American Chemical Society* **2008**, *130*, 990-1002; (c) Y. Matano, M. Fujita, T. Miyajima, H. Imahori, *Organometallics* **2009**, *28*, 6213-6217.

[19] C.-M. Che, Y.-J. Hou, M. C. W. Chan, J. Guo, Y. Liu, Y. Wang, *Journal of Materials Chemistry* **2003**, *13*, 1362-1366.

[20] M. Toganoh, H. Furuta, *Chemical Communications* **2012**, *48*, 937-954.

[21] A. Muranaka, S. Homma, H. Maeda, H. Furuta, N. Kobayashi, *Chemical Physics Letters* **2008**, *460*, 495-498.

[22] Y. Chi, P.-T. Chou, *Chemical Society Reviews* **2010**, *39*, 638-655.

[23] M. Ishida, T. Omagari, R. Hirosawa, K. Jono, Y. M. Sung, Y. Yasutake, H. Uno, M. Toganoh, H. Nakanotani, S. Fukatsu, D. Kim, H. Furuta, *Angewandte Chemie International Edition* **2016**, *55*, 12045-12049.

[24] D.-H. Won, M. Toganoh, Y. Terada, S. Fukatsu, H. Uno, H. Furuta, *Angewandte Chemie International Edition* **2008**, *47*, 5438-5441.

[25] (a) J. P. Belair, C. J. Ziegler, C. S. Rajesh, D. A. Modarelli, *The Journal of Physical Chemistry A* **2002**, *106*, 6445-6451; (b) S. Vyas, C. M. Hadad, D. A. Modarelli, *The Journal of Physical Chemistry A* **2008**, *112*, 6533-6549.

[26] The absorption spectra of the complexes, **Pt-n** (n=1-3) were measured in various solvents (Figure

S18)

[27] D. S. McClure, *The Journal of Chemical Physics* **1949**, *17*, 905-913.

[28] For **Pt-1**, there is a shoulder appeared around 800 nm in the phosphorescence spectrum (Figure 6). The corresponding energy could be estimated to be ca. 1.5 eV.

[29] J. V. Caspar, E. M. Kober, B. P. Sullivan, T. J. Meyer, *Journal of the American Chemical Society* **1982**, *104*, 630-632.

[30] It is evident that the energy difference between the singlet state and triplet state energies for the complexes computed by TD-DFT method were estimated to be 0.822, 0.972, and 0.946 eV, respectively. The larger difference of **Pt-2** implies the large alteration of the electronic structure occurring during the excited decay process.

[31] C. Schweitzer, R. Schmidt, *Chemical Reviews* **2003**, *103*, 1685-1758.

[32] M. Wierzchowski, L. Sobotta, P. Skupin-Mrugalska, J. Kruk, W. Jusiak, M. Yee, K. Konopka, N. Düzgüneş, E. Tykarska, M. Gdaniec, J. Mielcarek, T. Goslinski, *Journal of Inorganic Biochemistry* **2013**, *127*, 62-72.

[33] Frisch, M. J.; Trucks, G. W.; Schlegel, H. B.; Scuseria, G. E.; Robb, M. A.; Cheeseman, J. R.; Scalmani, G.; Barone, V.; Mennucci, B.; Petersson, G. A.; Nakatsuji, H.; Caricato, M.; Li, X.; Hratchian, H. P.; Izmaylov, A. F.; Bloino, J.; Zheng, G.; Sonnenberg, J. L.; Hada, M.; Ehara, M.; Toyota, K.; Fukuda, R.; Hasegawa, J.; Ishida, M.; Nakajima, T.; Honda, Y.; Kitao, O.; Nakai, H.; Vreven, T.; Montgomery, J. A., Jr.; Peralta, J. E.; Ogliaro, F.; Bearpark, M.; Heyd, J. J.; Brothers, E.; Kudin, K. N.; Staroverov, V. N.; Kobayashi, R.; Normand, J.; Raghavachari, K.; Rendell, A.; Burant, J. C.; Iyengar, S. S.; Tomasi, J.; Cossi, M.; Rega, N.; Millam, J. M.; Klene, M.; Knox, J. E.; Cross, J. B.; Bakken, V.; Adamo, C.; Jaramillo, J.; Gomperts, R.; Stratmann, R. E.; Yazyev, O.; Austin, A. J.; Cammi, R.; Pomelli, C.; Ochterski, J. W.; Martin, R. L.; Morokuma, K.; Zakrzewski, V. G.; Voth, G. A.; Salvador, P.; Dannenberg, J. J.; Dapprich, S.; Daniels, A. D.; Farkas, Ö.; Foresman, J. B.; Ortiz, J. V.; Cioslowski, J.; Fox, D. J. Gaussian 09, Revision B.01; Gaussian, Inc: Wallingford, CT, 2009.

[34] (a) A. D. Becke, *The Journal of Chemical Physics* **1993**, *98*, 5648-5652;

[35] M. Bernátková, B. Andrioletti, V. Král, E. Rose, J. Vaissermann, *The Journal of Organic Chemistry* **2004**, *69*, 8140-8143.

Chapter 3. Doubly N-Confused Calix[6]phyrin Bis-Organopalladium Complexes: Photostable Triplet Sensitizers for Singlet Oxygen Generation.

3-1. Abstract

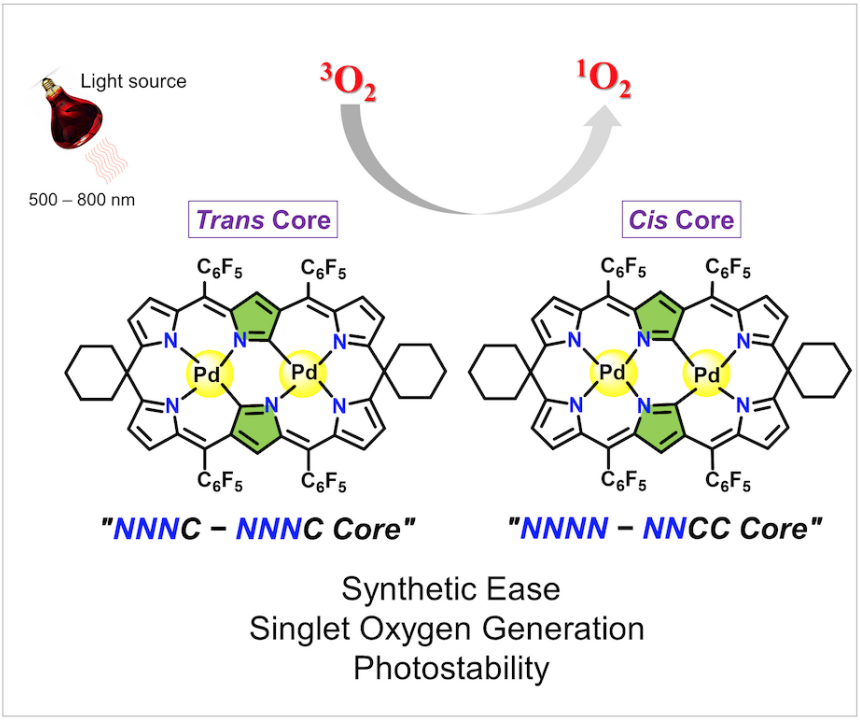

Triplet photosensitizers that generate singlet oxygen efficiently are attractive for applications such as photodynamic therapy (PDT). Extending the absorption band to a near-infrared (NIR) region (700 nm≈) with reasonable photostability is one of the major demands in the rational design of such sensitizers. The author prepared a series of mono- and bis-palladium complexes (**1-Pd-H$_2$**, **2-Pd-H$_2$**, **1-Pd-Pd**, and **2-Pd-Pd**) based on modified calix[6]phyrins as photosensitizers for singlet oxygen generation. These palladium complexes showed intense absorption profiles in the visible-to-NIR region (500-750 nm) depending on the number of central metals. Upon photoirradiation in the presence of 1,5-dihydroxynaphthalene (DHN) as a substrate for reactive oxygen species, the bis-palladium complexes generated singlet oxygen with high efficiency and excellent photostability. Singlet oxygen generation was confirmed from the characteristic spectral feature of the spin trapped complex in the EPR spectrum and the intact $^1O_2$ emission at 1270 nm.

3-2. Introduction

Singlet oxygen ($^1\Delta_g$) is the lowest excited electronic state of oxygen and is one of the most important reactive oxygen species (ROS) playing a key role in many photoinduced oxidative processes in biological/chemical systems.[1] Generally, singlet oxygen can be generated by using molecular oxygen ($^3O_2$) under UV illumination with triplet photosensitizers. The well accepted microscopic mechanism is such that, the characteristic species in the triplet state formed via intersystem crossing (ISC) from the photo-excited singlet state transfers the energy to $^3O_2$.[2] Such photosensitizers are thus useful in many applications such as photodynamic therapy (PDT),[3] oxygen sensing,[4] photocatalysis,[5] and triplet-triplet annihilation upconversion.[6] To date, many triplet sensitizers, such as heavy-atom-substituted organic chromophores (e.g., BODIPYs),[7] poly-pyridyl transition metal complexes (Pt^{II}, Ru^{II}, Ir^{II})[8] and metallo-macrocyclic complexes with porphyrin/phthalocyanine scaffolds[9] have gained much attention as they showed sufficient singlet oxygen generation capabilities. To attain higher efficiency for singlet oxygen generation, 1) strong absorption (in the near-infrared (NIR) biological window for PDT), 2) photostability, 3) high triplet state quantum yields (effective intersystem crossing (ISC)), 4) reasonably long-lived triplet state lifetime, and 5) solubility in appropriate media, are essentially required for the photosensitizers. For this purpose, the porphyrin-based chromophores have some benefits; tunable photophysical properties (i.e., molecular orbital symmetry and energy) by facile modification of the parent frameworks and changing the central metal cations in the macrocyclic ligand.[10] Largely, the metal complexes show reasonable durability even under the strong photo-irradiation.

Calixphyrin is a unique class of the porphyrin analogues containing one or multiple sp^3-hybridized *meso*-carbon bridges providing intrinsic molecular flexibility to endure facile cation bindings.[11] From the interest of the effect of the carbon-metal bond in the macrocyclic core for photosensitizers, Furuta and co-workers have been working on the modified (confused) carbaporphyrinoid and calix[4]phyrin(1.*1*.1.*1*) metal complexes.[12, 13] Despite the disrupted π-conjugation in the parent tetrapyrrolic scaffold, the NIR light absorption was achieved by electronic perturbation through an N-confusion modification of the platinum calix[4]phyrin complexes (Figure 1).[13c] The doubly N-confused derivative demonstrated the lowest energy absorption and subsequently good singlet oxygen generation. Using this modification strategy, Furuta *et al*., have also reported novel NIR luminescent dyes based on doubly N-confused calix[6]phyrin(1.1.*1*.1.1.*1*) bis-platinum complexes.[14] The core-expansion of the parent calix[4]phyrins induces the lower energy optical properties as there are more π-electrons in the scaffold. However due to the fact that the complexes possess relatively short triplet lifetimes (≈15 ns) and insufficient triplet energy that could otherwise allow the energy transfer to dioxygen, the photosensitization for singlet oxygen generation remains to be

achieved. Increasing the spin-orbit coupling decreases the triplet state lifetime and spin orbital coupling will increase with atomic

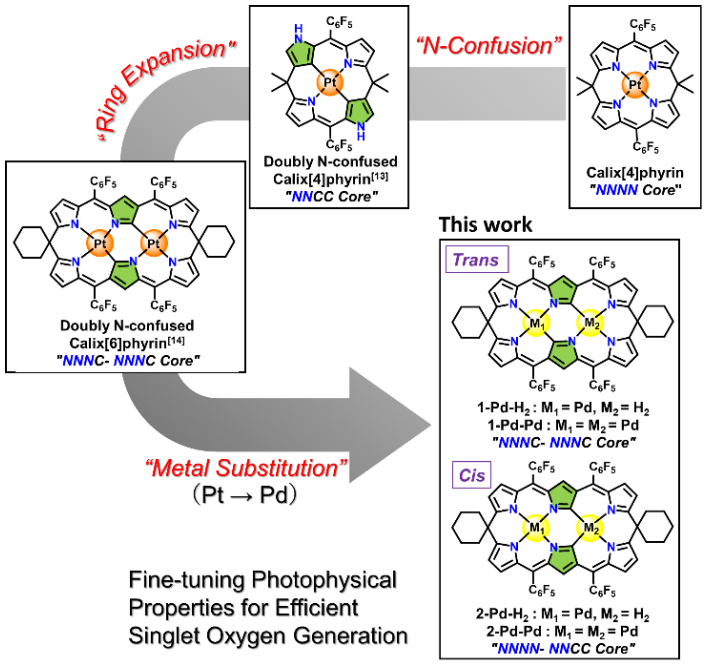

Figure 3-1. Strategic design of bis-Pd calix[6]phyrin complexes. Chemical structures of previously reported complexes, Pt-calix[4]phyrin, Pt-doubly N-confused calix[4]phyrin, bis-Pt calix[6]phyrin, and mono- and bis-Pd calix[6]phyrin complexes used in this work.

number.[15] Thus, the author envisioned that replacing the platinum metal with palladium, in the row right above in the group 10 element column, should allow one to longer triplet state lifetime for efficient sensitization of excited oxygen and increasing the conjugation to form calix[6]phyrin will fine tune the molecular orbitals with NIR photophysical properties. Moreover, the bis-palladium complex of doubly N-confused hexaphyrin exhibited a much lower energy absorption (≈1470 nm) which should discourage energy transfer to singlet oxygen even though it has advantage in the absorption profile in the NIR region.[16]

The author here report the facile synthesis of novel mono- and bis-organopalladium calix[6]phyrin complexes (**1-Pd-H$_2$**, **1-Pd-H$_2$**, **1-Pd-Pd**, and **2-Pd-Pd**) (Figure 1). The large π-conjugated scaffold based on the expanded calixphyrins attained prominent photophysical properties toward the NIR light region. The influence of the structural factors (e.g., coordination environment and the number of metal cations) on the photosensitized singlet oxygen generation were systematically investigated by X-ray crystallographic analysis, NMR, absorption, emission, and EPR spectroscopies.

3-3. Synthesis of Organopalladium complexes of calix[6]phyrin

The synthetic route of the mono- and bis-palladium complexes, **1-Pd-H$_2$**, **2-Pd-H$_2$**, **1-Pd-Pd**, and **2-Pd-Pd**, is shown in the Scheme 3-1. The freebase calix[6]phyrin ligands (*transoid*, **C6-1** and *cisoid*, **C6-2**)

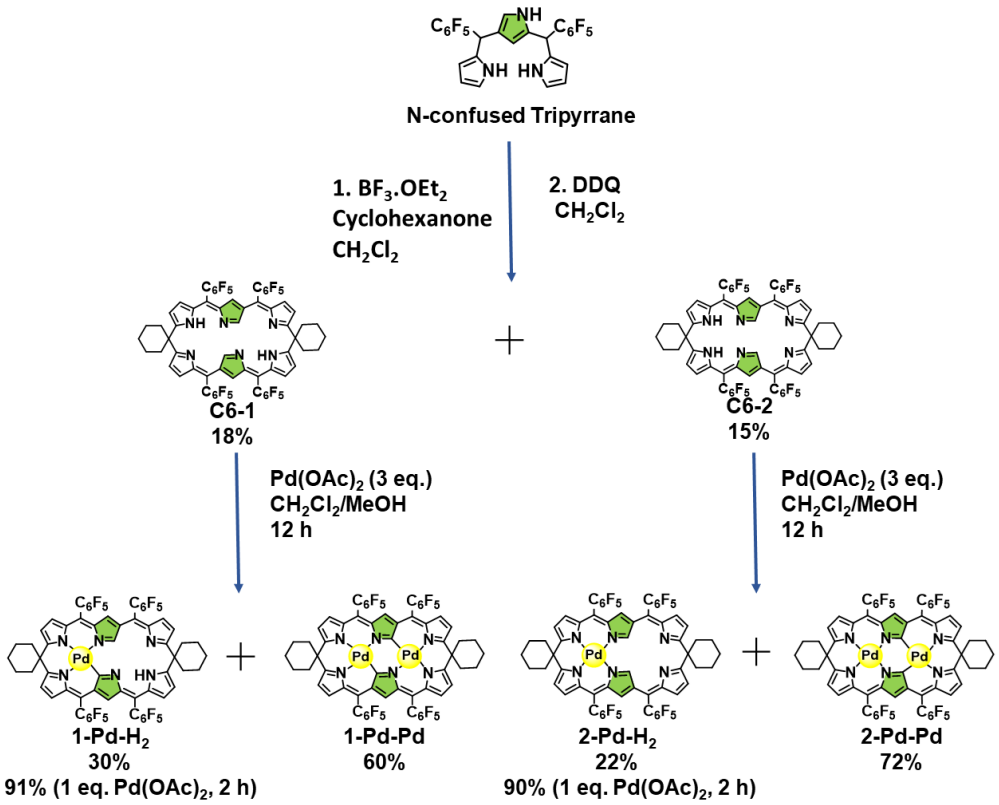

Scheme 3-1. Synthetic scheme of **1-Pd-H$_2$**, **2-Pd-H$_2$**, **1-Pd-Pd**, and **2-Pd-Pd.**

were previously reported by our group, which serve as the rectangular-shaped macrocyclic ligands.[14] The two isomeric macrocycles, **1** and **2**, in which the arrangement of the nitrogen atoms of the N-confused pyrrole rings (highlighted in green) is different, provide two organopalladium cation pockets surrounded by symmetrical and unsymmetrical coordination donor sites, "*NNNC-NNNC*" and "*NNNN-NNCC*", respectively. The corresponding bis-organopalladium metal complexes, **1-Pd-Pd** and **2-Pd-Pd**, were formed smoothly using 3 equivalents of $Pd(OAc)_2$ under reflux condition in a CH_2Cl_2/MeOH mixture, in 60 and 72 % yields, respectively. Along with the formation of bis-palladium complexes, the mono-palladium complexes, **1-Pd-H$_2$** and **2-Pd-H$_2$**, were also formed in 30 % and 22 % yields, respectively. When one equivalent of $Pd(OAc)_2$ was added into the solution containing a ligand **C6-1** or **C6-2**, mono-palladium complex, **1-Pd-H$_2$** or **2-Pd-H$_2$** was predominantly obtained in 80 and 75 % yields, respectively. The ^{1}H and ^{19}F NMR spectroscopy and high- resolution mass spectrometry support the expected structures

(Supporting Information). Specifically, the complex **1-Pd-H$_2$** shows two characteristic signals at δ=12.90 (inner NH) and 10.59 ppm (inner CH) (Figure S3-1). However, the complex **2-Pd-H$_2$** shows one sharp inner CH signal at 10.26 ppm reflecting the molecular symmetry in the ^{1}H NMR spectrum (Figure S3-2). The symmetry of **1-Pd-H$_2$** is also reflected in the ^{19}F NMR spectra; the splitting pattern of the *para*-substituted ^{19}F signals of the peripheral aryl groups in a 1:2:1 ratio for **1-Pd-H$_2$** and a 2:1:1 ratio for **2-Pd-H$_2$** verifies their *trans*/*cis* configurations (Figures S3-1 and S3-2). These results suggested the porphyrin-like N4 donor site in *cis*-configured **C6-2** can preferentially accommodate a palladium cation before subsequent second palladium metalation occurs, to give **2-Pd-Pd**. The absence of the inner protons in the low field region (beyond 8 ppm) in the ^{1}H NMR spectra implies the successful bis-metalation in the core. The peripheral β-protons appear in the typical sp^2-CH region due to the non-global π-conjugation as seen in the bis-platinum calixphyrin complexes.[14]

3-4. X-ray Crystallographic Data

The molecular structures of the complexes, **1-Pd-H$_2$**, **2-Pd-H$_2$**, **3-Pd-Pd**, and **4-Pd-Pd**, were characterized by X-ray crystallographic analysis (Figure 3-2 and S3-7, Table S3-1). The palladium cations reside in a square planar geometry in the inner coordination environments for all complexes. The coplanar tripyrrin planes are faced with tethering sp^3-hybridized *meso*-carbon centers located in the short

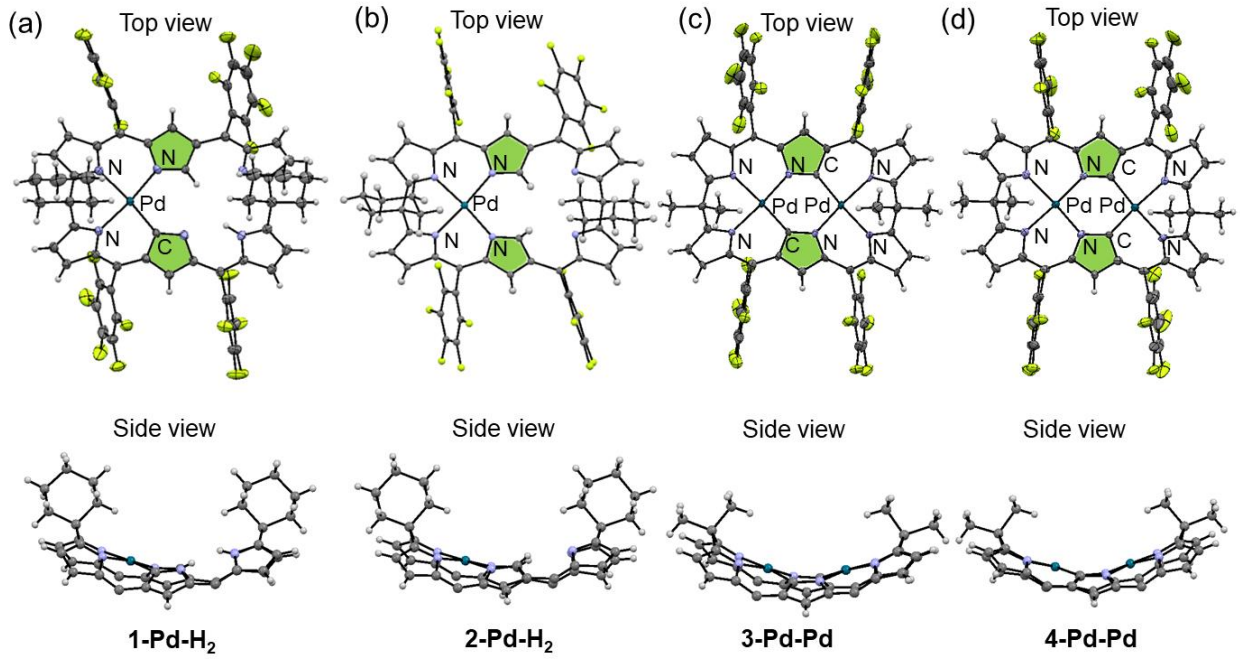

Figure 3-2. Top and side views of the X-ray crystal structures of (a) **1-Pd-H$_2$**, (b) **2-Pd-H$_2$**, (c) **3-Pd-Pd**, and (d) **4-Pd-Pd**. The confused rings are highlighted in green. In the side view, the meso-aryl rings are omitted for clarity.

axis side in the rectangular geometry. The overall core structures of the complexes exhibit bent-distortions along the longer molecular axis with the angles of 83-86°. The values for mean plane deviations (used with 36 core atoms) were estimated to be 0.717, 0.671, 0.743, and 0.770 Å for **1-Pd-H$_2$**, **2-Pd-H$_2$**, **3-Pd-Pd**, and **4-Pd-Pd**, respectively (Table 3-1). The formation of the organopalladium bonds may play an important role in the stabilization of the complexes as well as in the tuning of their electronic structures. Unfortunately, the disorder of the inner nitrogen versus adjacent carbon atoms of the confused pyrrole rings in the complexes hampered us to gain the discrete bonding information of the organopalladium complexes.

Table 3-1. Selected structural parameters of the palladium complexes

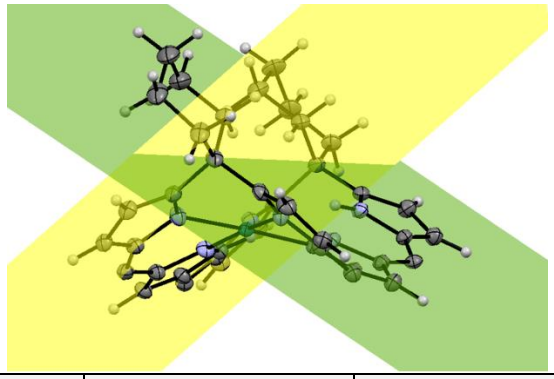

Complex	Bent Angle[a] (°)	Mean Plane Deviation[b] (Å)
1-Pd-H$_2$	86	0.717
2-Pd-H$_2$	83	0.671
3-Pd-Pd	84	0.743
4-Pd-Pd	84	0.770

[a]The bent angles (°) between the half skeleton of the tripyrrin planes are estimated. [b]The mean deviation (Å) values were defined using the 36 atoms of the core skeleton of the complexes.

The stronger bonding character of the Pd-C linkages than that of the Pd-N was speculated due to the intrinsic donor character of the anionic carbon sites.[17] The theoretical structures of the complexes obtained from the density functional calculations reproduced the experimental structures (vide infra, Figure 3-5).

3-5. Studies on Molecular orbital and Optical properties

With the purpose of studying the optical properties of the complexes, UV/Vis-NIR spectra were recorded in toluene (Figure 3-3). All the complexes exhibit the intense absorption bands in the visible region

(λ_{abs} = 500 − 700 nm) and tailing bands in the NIR region. The peak maxima of the mono-Pd complexes, **1-Pd-H$_2$** and **2-Pd-H$_2$**, appear around 560 nm ($\varepsilon \approx 80\ 000$ M^{-1} cm^{-1}), whereas the peaks for the bis-Pd complexes, **1-Pd-Pd** and **2-Pd-Pd**, are seen in the lower energy region beyond 600 nm with relatively high absorption coefficient ($\varepsilon \approx 90\ 000$ M^{-1} cm^{-1}) (Table 3-2). Interestingly, depending on the molecular symmetry, the *trans*-configured complexes show relatively intense shoulder bands in the lower energy region.

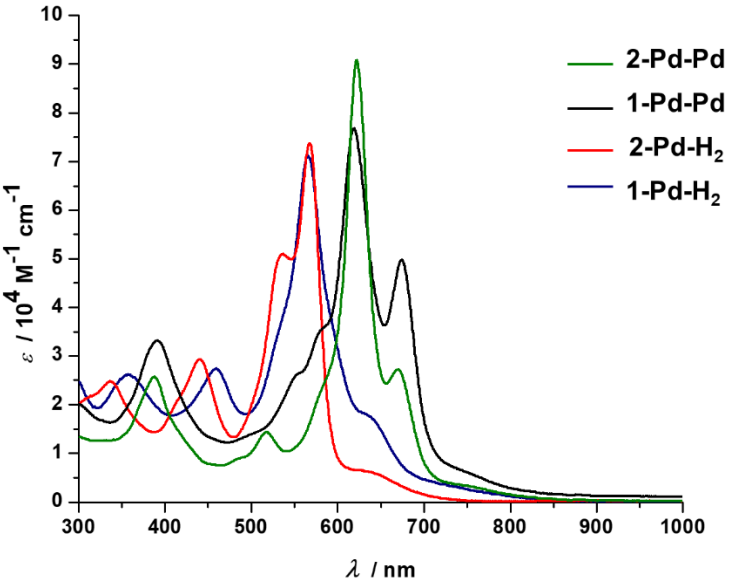

Figure 3-3. UV-vis-NIR absorption spectra of Pd complexes; **1-Pd-H$_2$** (blue line), **2-Pd-H$_2$** (red), **1-Pd-Pd** (black), and **2-Pd-Pd** (green) in toluene.

Owing to the severely broadened absorption features in the NIR region, the HOMO-LUMO energy gap of the complexes was analyzed using cyclic voltammetry (CV) and differential pulse voltammetry (DPV) in dichloromethane containing 0.1 M tetrabutylammonium hexafluorophosphate ($TBAPF_6$) as the supporting electrolyte (Figures 3-4, S3-12, and S3-13). In fact, the bis-palladium complexes represent the similar redox profile: the quasi-reversible oxidation waves and irreversible reduction waves were observed at E_{ox} = 0.57 and 0.54 V (vs. ferrocene/ferrocenium couple) and E_{red} = -1.07 and -1.09 V, respectively. The corresponding energy gaps are thus calculated to be 1.64 and 1.63 V for **1-Pd-Pd** and **2-Pd-Pd**, respectively. In contrast, the irreversible oxidations at E_{ox}=0.65 and 0.69 V, and the reduction at E_{red} = -0.95 and -1.24 V were observed for the mono-palladium complexes, **1-Pd-H$_2$** and **2-Pd-H$_2$**, respectively. The remarkably narrow HOMO−LUMO gap of **1-Pd-H$_2$** is originated from the anodic shift of the reduction wave than that of **2-Pd-H$_2$**, which implies the alteration of the electronic structures of the macrocycles.

In an effort to further elucidate the electronic structures of the complexes, density functional theory (DFT) calculations were carried out using B3LYP/6-31G**+SDD method. The π-electron present in the

frontier molecular orbital diagrams was found to be delocalized over the π-ligands for all complexes except for **1-Pd-H$_2$** (Figure 3-5). The LUMO pair of **1-Pd-H$_2$** indicated the partial localization on the tripyrrin moieties, which induces the broken-degeneracy of the LUMO/LUMO+1 pair. The feature in the

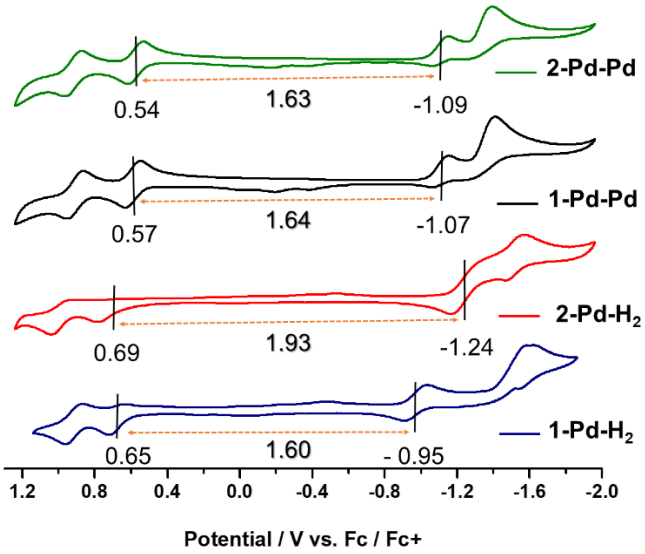

Figure 3-4. Cyclic voltammograms of **1-Pd-H$_2$**, **2-Pd-H$_2$**, **3-Pd-Pd**, and **4-Pd-Pd** in CH_2Cl_2 containing 0.1m $TBAPF_6$. The scan rate is 100 mVs^{-1}, and the concentration was set to 1 mm.

remarkably stabilized LUMO causes the intrinsically narrower HOMO-LUMO gap of 2.07 V than that of the corresponding isomer **2-Pd-H$_2$** with the gap of 2.63 V. The surrounding metal-coordination environment can also contribute to the HOMO energy profiles; the palladium-carbon bonding nature within the *NNNC* sphere in **1-Pd-H$_2$** destabilizes the energy as reported for other porphyrinoids.[18] The partial contribution from the d-orbital (d_{yz}) of organopalladium center in HOMO for **1-Pd-H$_2$** may influence the electronic alteration (but not for **2-Pd-H$_2$**). Similarly, the influence of metal d-electron in the ground state molecular orbitals for the organopalladium complexes was speculated through the Pd - C bond linkage. There is a partial contribution from d-orbital in HOMO and HOMO-1, which should reflect the optical properties.

The spectral features were analyzed using time-dependent (TD)-DFT calculations with B3LYP method (Figures S8 − S11, Tables S2 − S5). As discussed above, the *trans*-configured complexes, **1-Pd-H$_2$** and **1-Pd-Pd**, show intensified shoulder peaks compared to their *cis*-form counterparts, **2-Pd-H$_2$** and **2-Pd-Pd**, respectively. The TD-DFT calculations suggest that the transition from HOMO-1 to LUMO orbital contributes mostly and the oscillator strength of this transition is larger for the *trans*-form. Interestingly, partial MLCT contribution exists in the *trans*-forms more than in the *cis*-form. Moreover, calculations also suggest the bathochromic shifts for bis-palladium complexes. As is the case with bis-platinum

calix[6]phyrin complexes (λ_{em}≈1020 nm), a series of the palladium complexes indeed showed phosphorescence in the NIR region at room temperature in deaerated toluene (Figure 3-6 and Table 3-2). In terms of the energies, the bis-Pd complexes showed similar spectral feature (E≈1.27 eV). In contrast, the mono-Pd complexes indicated the varied emission energies in the order, **2-Pd-H$_2$** (1.56 eV) >**1-Pd-H$_2$** (1.40 eV) depending on the molecular symmetry.

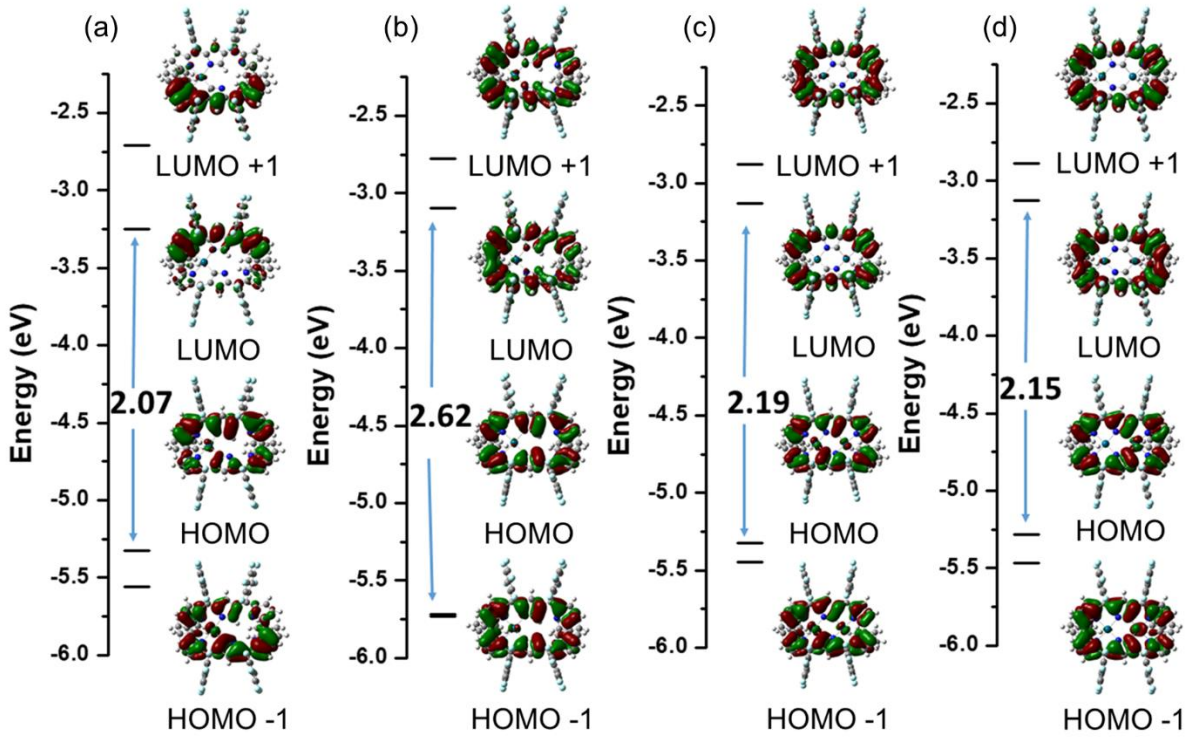

Figure 3-5. Molecular orbital energy diagrams of (a) **1-Pd-H$_2$**, (b) **2-Pd-H$_2$**, (c) **1-Pd-Pd** and (d) **2-Pd-Pd** obtained from DFT calculations (B3LYP/6-31G**/SDD level).

The phosphorescence quantum yields and lifetimes of the series of complexes were determined to analyze the triplet state behaviors (Figures S3-13 - S3-17). The phosphorescence lifetimes of bis-palladium complexes, **1-Pd-Pd** and **2-Pd-Pd**, are determined to be 183 and 174 ns, respectively, which are significantly larger than the photoluminescent lifetimes of Pt-calix[6]phyrin complexes.[14] Platinum calix[6]phyrin complexes **1-Pt-Pt** and **2-Pt-Pt** shows absorption similar to bis-palladium complexes **1-Pd-Pd** and **2-Pd-Pd** up to 800 nm with absorption maxima in the around 650 nm. The problem is its triplet state characteristics. These molecules shows triplet state energy of corresponding to 1010 and 1029 nm which is enough to sensitize singlet oxygen but the energy is very low which in turn increases the non-radiative transitions. Due to this and stronger heavy atom effect of platinum these molecules shows smaller triplet state lifetime. **1-Pt-Pt** and **2-Pt-Pt** shows 29 and 20 ns lifetime which is very short to sensitize singlet oxygen efficiently.

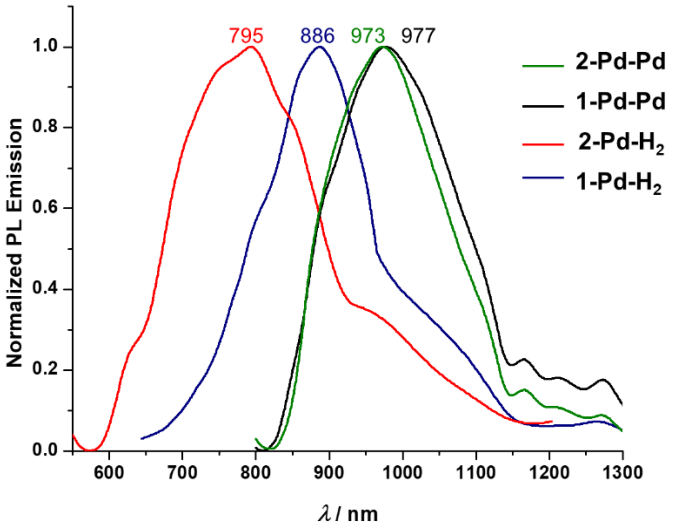

Figure 3-6. Phosphorescence spectra of **1-Pd-H$_2$**, **2-Pd-H$_2$**, **1-Pd-Pd**, and **2-Pd-Pd** in deaerated toluene at r.t. (λ_{ex}=532 nm).

In the case of the mono-palladium complexes, there is an apparent difference between the isomers; **2-Pd-H$_2$** possesses a significantly longer triplet state lifetime of 536 ns, whereas **1-Pd-H$_2$** has a short lifetime in the sub-microsecond time scale. In this regard, the phosphorescence quantum yields of **2-Pd-H$_2$** (Φ_{PL}=3.9×10^{-3}) is significantly larger than that of **1-Pd-H$_2$**. In the decay process, excited-state intramolecular proton transfer (ESIPT) of the pyrrolic NH moiety with adjacent pyrrole imine could be attributed for **1-Pd-H$_2$**. In contrast, the intrinsic strong C-H bonding nature of the N-confused pyrrole ring in **2-Pd-H$_2$** could have hindered this process.[20] In the case of **1-Pd-Pd** and **2-Pd-Pd**, slightly smaller values of Φ_{PL} than that of **2-Pd-H$_2$** were obtained for both the bis-palladium complexes, probably due to the smaller energy gap.[21] Notably the *cis*-isomer was more luminescent than the *trans*-isomer as observed for bis-platinum complexes,[14] although a further study is necessary to clarify the effect of the symmetrical/unsymmetrical coordination environments on the excited state dynamics.

3-6. Singlet Oxygen Generation Studies

The emission due to the singlet oxygen ($^1\Delta_g$) was observed at 1270 nm from the solution of palladium complexes during the phosphorescence measurements under the aerobic conditions (Figure S3-24). The palladium complexes in the triplet state could sensitize the generation of singlet oxygen upon photoirradiation. The efficiency of sensitization was systematically studied by monitoring the UV-vis spectral changes of a well-known singlet oxygen scavenger, 1,5-dihydroxynaphthalene (DHN: λ~340 nm) in the presence of the photosensitizers (**1-Pd-H$_2$**, **2-Pd-H$_2$**, **1-Pd-Pd, 2-Pd-Pd**, and methylene blue (**MB**)

Table 3-2. Summary of the photophysical parameters for the palladium complexes.

Complex	λ_{abs} (nm) (ε/ 10^4 M^{-1} cm^{-1})	λ_{em} (nm)	Φ_{PL} [a] (1×10^{-3})	τ_{PL}(ns)[b]	k_r (10^3 s^{-1})	k_{nr} (10^6 s^{-1})	Φ_{Δ} [c]
1-Pd-H$_2$	566 (7.11)	886	0.56	127	4.4	7.8	0.05
2-Pd-H$_2$	568 (6.29)	795	3.9	536	7.3	1.8	0.83
1-Pd-Pd	619 (7.67)	977	1.2	183	6.5	5.4	0.30
2-Pd-Pd	622 (9.07)	973	2.1	174	11.9	5.7	0.27
1-Pt-Pt	649	1010	0.68	29	-	-	-
2-Pt-Pt	657	1029	1.2	20	-	-	-

[a] Quantum yield was calculated using **4-Pt-Pt** (Φ_{PL} = 0.0027 in toluene, λ_{ex} = 532 nm) as reference [14]. [b] Determined by TCSPC method with excitation at 532 nm. [c] Singlet oxygen quantum yield measured in CH_2Cl_2/MeOH with methylene blue as standard.[19]

as a reference) in CH_2Cl_2/MeOH (Figures S3-18 − S3-23). Singlet oxygen generated in situ can oxidize DHN to juglone upon Xe lamp irradiation (λ_{ex}; 450-800 nm) (Table 3-3).[22] The singlet oxygen quantum yields were calculated using the following Equation (1).[23]

$$\Phi_{\Delta}=\Phi_{\Delta}^{std}\times(v_i I^{std}/v_i^{std} I), \quad (1)$$

where Φ_{Δ} is the singlet oxygen quantum yield (Φ_{Δ}^{std}=0.74, for **MB**) in CH_2Cl_2/MeOH, v_i is the initial rate of DHN consumption, and I is the relative number of photons absorbed.[19] v_i is determined from the slope of the graph $\ln(C_t/C_0)$ in the initial 3 minutes (Figure 3-7 a). As the result, the quantum yields for singlet oxygen generation using the palladium complexes were estimated to be 0.83 (**2-Pd-H$_2$**)>0.30 (**1-Pd-Pd**)>0.27 (**2-Pd-Pd**)>0.05 (**1-Pd-H$_2$**) based on the reference value 0.74 (**MB**) (Table 3-2). The long-lived triplet excited state of photosensitizer has a higher probability to undergo bimolecular collision with ground state oxygen to generate singlet oxygen.[2] The huge acceleration in the conversion could be thus related to the triplet-state lifetime of the photosensitizer.

To confirm the singlet oxygen generation in the photosensitization, the author conducted the EPR measurements using spin labelling agents, 2,2,6,6-tetramethylpiperidine (TEMP) and 5,5-dimethyl-1-pyrroline-*N*-oxide (DMPO), respectively (Figure 3-7 d). Photoirradiation of an air-saturated toluene solution containing photosensitizer and TEMP resulted in the characteristic three-line EPR spectrum after 3 min. The hyperfine coupling constants, a_N is 16.0 G which can be assigned to TEMPO (TEMP and $^1\Delta_g$ react to form TEMPO).[24] The TEMPO signal intensity is in the order **2-Pd-H$_2$**>**1-Pd-Pd**>**2-Pd-Pd**>**1-Pd-H$_2$**, which is well correlated to the quantum yields of singlet oxygen generation. In contrast, no reaction

occurred in the presence of another spin labelling reagent, DMPO, indicating no other reactive oxygen species (e.g., peroxide, superoxide) are generated under this condition.[25]

Table 3-3. Chemical yield of conversion of DHN to juglone in the presence of sensitizer after 60 minutes.

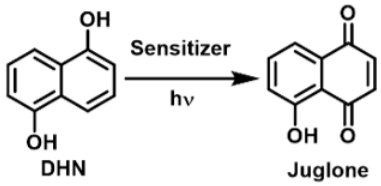

Complex	Chemical yield (%)	% degradation (60 min)
1-Pd-H_2	73	3.1
2-Pd-H_2	83	48.7
1-Pd-Pd	97	2.6
2-Pd-Pd	92	2.7
MB	98	30.1

Importantly, the author tested the durability of the sensitizers under the identical conditions and bis-palladium complexes, **1-Pd-Pd** and **2-Pd-Pd**, were found to be remarkably stable under photoirradiation (Figure 3-7 b, Table 3-3).[19] As a result, the actual chemical yields of juglone using the bis-palladium complexes, **1-Pd-Pd** (97 %) and **2-Pd-Pd** (92 %), were found to be larger than that of **2-Pd-H_2** (83 %) in spite of its higher singlet oxygen quantum yield (Figure 3-7 c). Interestingly, the relatively less effective **1-Pd-H_2** generated juglone gradually but in high yield after 60 min irradiation. In the case of most reactive **2-Pd-H_2**, juglone was rapidly formed but the yield was saturated after 20 min, presumably due to the instability of the complex under the condition used. Based on the above analysis, the photostability of the sensitizers is seen to be one of the most important factors for practical use in applications such as PDT. Without sensitizers the product was obtained only in 2 % yield after 60 minutes, indicating the critical role of photosensitizer in this reaction.

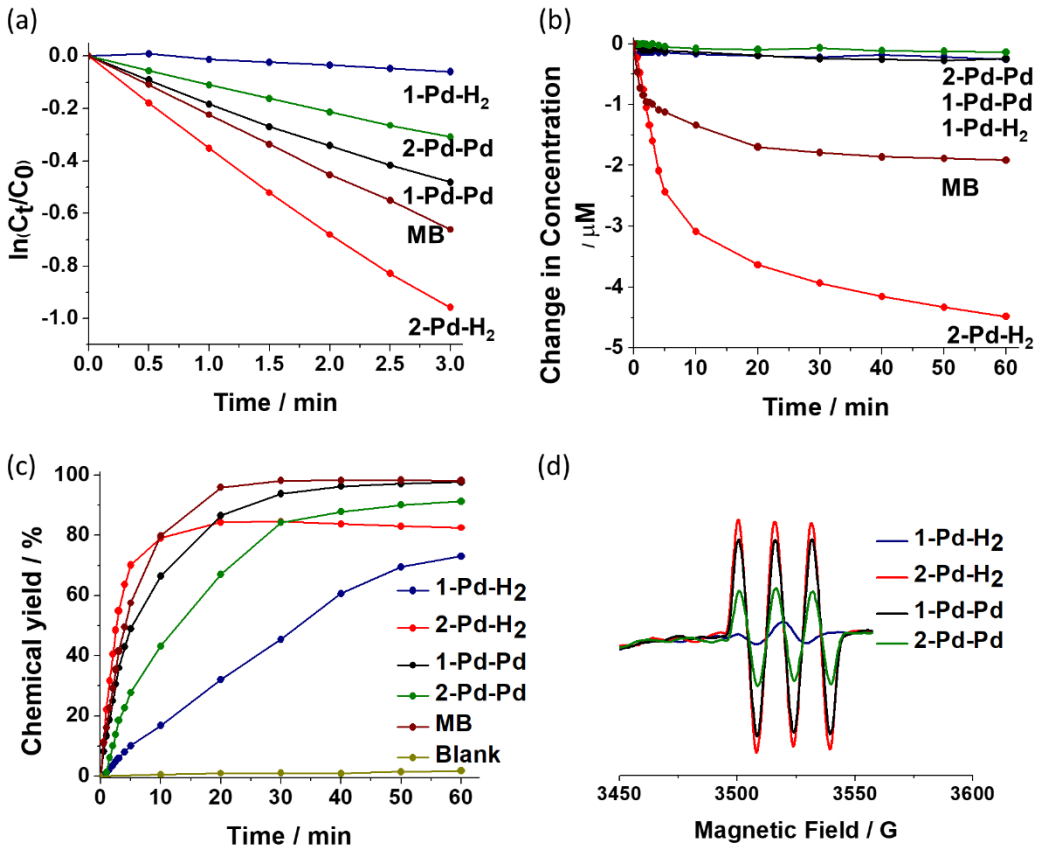

Figure 3-7. (a) Plot of ln(Ct/C0) versus irradiation time for palladium complexes (**1-Pd-H$_2$**, **2-Pd-H$_2$**, **1-Pd-Pd, 2-Pd-Pd**) and methylene blue (**MB**). (b) Change in concentrations of the photosensitizers under the irradiation condition. (c) Kinetics of chemical yields of juglone with respect to irradiation time in CH_2Cl_2/MeOH. (d) EPR spectra of the spin trapped species using TEMP in the presence of the palladium complexes in oxygen-saturated toluene solution recorded after 3 minutes of light irradiation (450–800 nm).

3-7. Conclusions

In summary, the author have synthesized a series of novel triplet photosensitizers based on mono- and bis-palladium calix[6]phyrin complexes, **1-Pd-H$_2$**, **2-Pd-H$_2$**, **1-Pd-Pd**, and **2-Pd-Pd**, for singlet oxygen generation**.** These complexes have broad absorption spectra from the visible to NIR region and appropriate triplet energy (800-1000 nm) and reasonably longer lifetimes (≈540 ns) for the sensitization of singlet oxygen generation. The metal number and coordination environment of the complexes play an important role in modulation of the optical properties as well as photostability. Because of the facile synthesis, good singlet oxygen generation capability, and photostability, the current calix[6]phyrin-based photosensitizers would hold promise for applications such as PDT, photo-redox catalysts and so on.

3-8. Experimental Section

3-8-1. Materials and Instruments: All reactions were performed in dried vessels under Ar or N_2. Commercially available solvents and reagents were used without further purification unless otherwise mentioned. CH_2Cl_2 was dried by passing through a pad of alumina. Thin-layer chromatography (TLC) was performed on an aluminum sheet coated with silica gel 60 F_{254} (Merck). Preparative separation was performed by silica gel flash column chromatography (KANTO silica gel 60 N, spherical, neutral, 40-50 μm) or silica gel gravity column chromatography (KANTO Silica Gel 60 N, spherical, neutral, 63-210 μm). ^{1}H and ^{19}F NMR spectra were recorded in $CDCl_3$ solutions on a JEOL ECX500 NMR spectrometer (500 MHz for ^{1}H and 470 MHz for ^{19}F). Chemical shifts were reported relative to $CDCl_3$ (δ=7.26 ppm) for ^{1}H in parts per million. Trifluoroacetic acid (0.02 % in $CDCl_3$) was used as an external reference for ^{19}F (δ=-76.5 ppm). UV-vis-NIR absorption spectra were measured on a Shimadzu UV-3150PC spectrometer. Fluorescence spectra were recorded on an SPEX Fluorolog-3-NIR spectrometer (HORIBA) with an NIR-PMT R5509 photomultiplier tube (Hamamatsu) in a 10 mm quartz fluorescence cuvette. High-resolution mass spectra (HRMS) were obtained in fast atom bombardment (FAB) mode with 3-nitrobenzyl alcohol (NBA) as a matrix on a JEOL LMS-HX-110 spectrometer.

3-8-2. **Singlet Oxygen Quantum Yields**: Singlet oxygen quantum yields (Φ_Δ) were determined in CH_2Cl_2/MeOH by using 5 mol % of mono- and bis-palladium complexes (**1-Pd-H$_2$**, **2-Pd-H$_2$**, **1-Pd-Pd**, and **2-Pd-Pd)** (9 μM) and methylene blue (**MB**) as the reference compound. The singlet oxygen scavenger, dihydroxynaphthalene (DHN, 181 μM) was used as the singlet oxygen scavenger. Alternately, emissions of the singlet oxygen sensitized by the palladium complexes in O_2 saturated toluene were recorded on an SPEX Fluorolog-3-NIR spectrometer (HORIBA). The solution of a sensitizer with DHN was bubbled with oxygen for 15 minutes to get oxygen saturated solution. Then the solution was irradiated with 450-800 nm light using a bandpass filter and photoirradiation was carried out using a Xe lamp of 300 W.

3-8-3. **Time-Resolved Emission Spectroscopy**: Time-resolved phosphorescence measurements were performed in the time-correlated single photon counting mode using a NIR-sensitive photomultiplier (Hamamatsu H10330-75). The excitation source was a 532 nm frequency-doubled passive-Q-switched Nd:YAG laser delivering a 1 μJ sub-nanosecond (<0.7 ns) pulse train at a repetition rate of 8 kHz. The sample solutions (toluene solvent) in the cell cuvette were carefully degassed by argon (gas) bubbling with septum.

3-8-4. **Theoretical Calculations**: DFT calculations were performed with the Gaussian16 program package without symmetry treatment.[26] Initial structures were based on the X-ray crystal structure of the related compounds. The geometries were fully optimized using Becke's three-parameter hybrid functional combined with the Lee-Yang-Parr correlation functional, denoted as the B3LYP level of DFT, with the 6-

31G(d,p), and SDD (for Pd) basis set for all calculations.[27] Experimental absorption spectra were analyzed by time-dependent DFT (TD-DFT) calculations with the same level. Ground-state geometries were verified by the frequency calculations, where no imaginary frequency was found. For visualization of the optimized geometries and the molecular orbitals, GaussView software was used.

3-8-5. X-ray Crystallography: Single-crystal X-ray structural analyses for **1-Pd-H$_2$**, **2-Pd-H$_2$**, **3-Pd-Pd**, and **4-Pd-Pd** were performed on a Saturn diffractometer equipped with a CCD detector (Rigaku) using $Mo_{K\alpha}$ (graphite, monochromatized, λ=0.71069 Å) radiation. The data were corrected for Lorentz, polarization, and absorption effects and refined using the SHELXS-2014/7 program.[28] All of the positional parameters and thermal parameters of non-hydrogen atoms were refined anisotropically on F^2 by the full-matrix least-squares method. Hydrogen atoms were placed at calculated positions and refined using a riding model on their corresponding carbon atoms. The crystal-to-detector distance was 45.00 mm.

3-8-6. Synthesis of Precursors: The freebase doubly N-confused calix[6]phyrins (**1-4**) were synthesized by following the procedure reported previously.[14] Detailed characterization data for **1-Pd-H$_2$**, **2-Pd-H$_2$**, **1-Pd-Pd**, and **2-Pd-Pd** is given in *Supporting Information.*

General method for synthesis of mono-palladium complexes (1-Pd-H$_2$): A mixture of free ligand, **1** (20 mg, 0.015 mmol) and $Pd(OAc)_2$ salt (3.8 mg, 0.017 mmol) in CH_2Cl_2/MeOH (2:1) was stirred under argon for 2 h under reflux conditions (40 °C). The solvents were removed in vacuo using high vacuum pump. The crude product was purified using silica gel column chromatography with CH_2Cl_2/hexane mixture.

The complex, **2-Pd-H$_2$** was also synthesized using **2** under the same conditions.

Data for **1-Pd-H$_2$**: yield=80 % (17.2 mg); ^{1}H NMR ($CDCl_3$): δ = 12.90 (s, 1 H), 10.59 (s, 1 H), 6.65 (d, J = 4.8 Hz, 1 H), 6.62 (d, J = 4.8 Hz, 1 H), 6.59 (s, 1 H), 6.54 (d, J = 4.5 Hz, 1 H), 6.48 (d, J = 4.4 Hz, 1 H), 6.36 (d, J = 4.3 Hz, 1 H), 6.33 (d, J = 4.3 Hz, 1 H), 6.19 (d, J = 4.2 Hz, 1 H), 5.98 (s, 1 H), 5.94 (s, 1 H), 3.29 (s, 2 H), 2.99 (s, 1 H), 2.54 (s, 1 H), 2.24 (s, 4 H), 1.82 (m, 4 H), 1.57 ppm (m, 8 H); ^{19}F NMR ($CDCl_3$): δ = -136.42 (s), -136.96 (s), -137.24 (s), -137.62 (s), -138.21 (s), -138.69 (s), -138.94 ≈ -139.15 (m), -150.99 (d, J = 38.5 Hz), -151.82 (d, J = 34.0 Hz), -152.41 (d, J = 39.5 Hz), -159.33 (s), -160.07 (s), -160.27 (d, J = 25.9 Hz), -160.70 (d, J = 64.1 Hz), -160.99 ppm (s); HRMS (FAB$^+$): m/z = 1371.1481 (found), 1371.1482 (Calcd for $C_{64}H_{33}F_{20}N_6Pd$), error -0.1 ppm.

Data for **2-Pd-H$_2$**: yield = 75 % (16.1 mg); ^{1}H NMR ($CDCl_3$): δ = 10.26 (s, 1 H), 6.65 (d, J = 4.6 Hz, 1 H), 6.50 (d, J = 4.6 Hz, 1 H), 6.41 (d, J = 4.6 Hz, 1 H), 6.36 (d, J = 4.5 Hz, 1 H), 5.93 (s, 1 H), 3.38 (s, 1 H), 2.88 (s, 1 H), 2.27 (s, 1 H), 2.21 (s, 1 H), 1.83 (s, 1 H), 1.62 ppm (m, 5 H); ^{19}F NMR ($CDCl_3$): δ = -136.69 (s), -137.28 (s), -138.57 (d, J = 23.9 Hz), -138.94 (s), -151.13 (s), -152.32 (d, J = 38.7 Hz), -159.82 (s), -

160.29 (s), -160.58 (s), -160.90 ppm (s); HRMS (FAB^+): *m*/*z* = 1371.1484 (found), 1371.1482 (Calcd for $C_{64}H_{33}F_{20}N_6Pd$), error + 0.1 ppm.

General method for synthesis of bis-palladium complexes (1-Pd-Pd): A mixture of free ligand **1** (20 mg, 0.015 mmol) and $Pd(OAc)_2$ (11.4 mg, 0.052 mmol) in CH_2Cl_2/MeOH (2:1) was stirred under argon for 12 h under reflux conditions (40 °C). The solvents were removed in vacuo using high vacuum pump. The crude product was purified using silica gel column chromatography with CH_2Cl_2/hexane mixture.

Data for **1-Pd-Pd**: yield = 60 % (14 mg); ^1H NMR ($CDCl_3$): δ = 6.59 (d, *J* = 4.5 Hz, 1 H), 6.55 (d, *J* = 4.7 Hz, 1 H), 6.48 (d, *J* = 4.6 Hz, 1 H), 6.41 (d, *J* = 4.4 Hz, 1 H), 5.90 (s, 1 H), 3.26 (s, 1 H), 3.06 (s, 1 H), 2.26 (m, 2 H), 1.83 (m, 2 H), 1.58 ppm (m, 4 H); ^{19}F NMR ($CDCl_3$): δ = -137.37 (s), -138.72 (d, *J* = 21.9 Hz), -139.13 (d, *J* = 24.7 Hz), -151.67 (d, *J* = 57.9 Hz), -159.73 (s), -160.08 (s), -160.61 (s), -160.93 ppm (s); HRMS (FAB^+): *m*/*z* = 1474.0290 (found), 1474.0282 (Calcd for $C_{64}H_{30}F_{20}N_6Pd_2$), error +0.5 ppm.

Data for **2-Pd-Pd**: yield = 71 % (16.5 mg); ^1H NMR ($CDCl_3$): δ = 6.64 (d, *J* = 4.7 Hz, 1 H), 6.48 (t, *J* = 5.2 Hz, 2 H), 6.38 (d, *J* = 4.4 Hz, 1 H), 5.93 (s, 1 H), 3.21 (s, 1 H), 3.09 (s, 1 H), 2.25 (m, 2 H), 1.80 (s, 2 H), 1.55 ppm (m, 4 H); ^{19}F NMR ($CDCl_3$): δ = -137.35 (d, *J* = 23.6 Hz), -138.71− -139.28 (m), -151.65 (d, *J*=37.5 Hz), -159.54 − -160.14 (m), -160.77 ppm (d, *J* = 87.8 Hz); HRMS (FAB^+): *m*/*z* = 1474.0285 (found), 1474.0282 (Calcd for $C_{64}H_{30}F_{20}N_6Pd_2$), error +0.2 ppm.

Data for **3-Pd-Pd**: ^1H NMR ($CDCl_3$): δ = 6.52 (m, 4 H), 6.48 (d, *J* = 4.7 Hz, 2 H), 6.40 (d, *J* = 4.4 Hz, 2 H), 5.94 (s, 2H), 2.27 (s, 6 H), 1.76 ppm (s, 6 H); ^{19}F NMR ($CDCl_3$): δ = -137.49 (s), -137.55 (d, *J* = 22.4 Hz), -138.88 (d, *J* = 22.9 Hz), -139.36 (d, *J* = 22.4 Hz), -139.40--139.55 (m), -151.52 (s), -151.57 (s), -151.61 (s), -151.68 (s), -151.74 (d, *J* = 19.0 Hz), -159.72 (t, *J* = 22.7 Hz), -160.06 (t, *J* = 18.8 Hz), -160.70 (s), -160.75 (s), -160.77 (d, *J* = 21.5 Hz), -160.72 − -161.52 ppm (m); HRMS (FAB^+): *m*/*z* = 1393.9684 (found), 1395.9656 (Calcd for $C_{58}H_{22}F_{20}N_6Pd_2$), error +2.0 ppm.

Data for **4-Pd-Pd**: ^1H NMR ($CDCl_3$): δ = 6.60 (m, 2 H), 6.47 (d, *J* = 4.6 Hz, 2 H), 6.42 (m, 2 H), 6.37 (d, *J* = 4.4 Hz, 2 H), 5.97 (s, 2 H), 2.27 (d, *J* = 10.1 Hz, 6 H), 1.75 ppm (d, *J* = 13.9 Hz, 6 H); ^{19}F NMR ($CDCl_3$): δ = -137.53 (m, 26.8 Hz), -138.95 (d, *J* = 28.3 Hz), -139.35 (d, *J* = 28.8 Hz), -151.65 (t, *J* = 22.9 Hz), -159.79 (t, *J* = 21.7 Hz), -159.99 (t, *J* = 21.8 Hz), -160.83 (t, *J* = 21.5 Hz), -161.04 ppm (t, *J* = 21.8 Hz); HRMS (FAB^+): *m*/*z* = 1393.9658 (found), 1395.9656 (Calcd for $C_{58}H_{22}F_{20}N_6Pd_2$), error +0.1 ppm.

3-9. Supporting Data

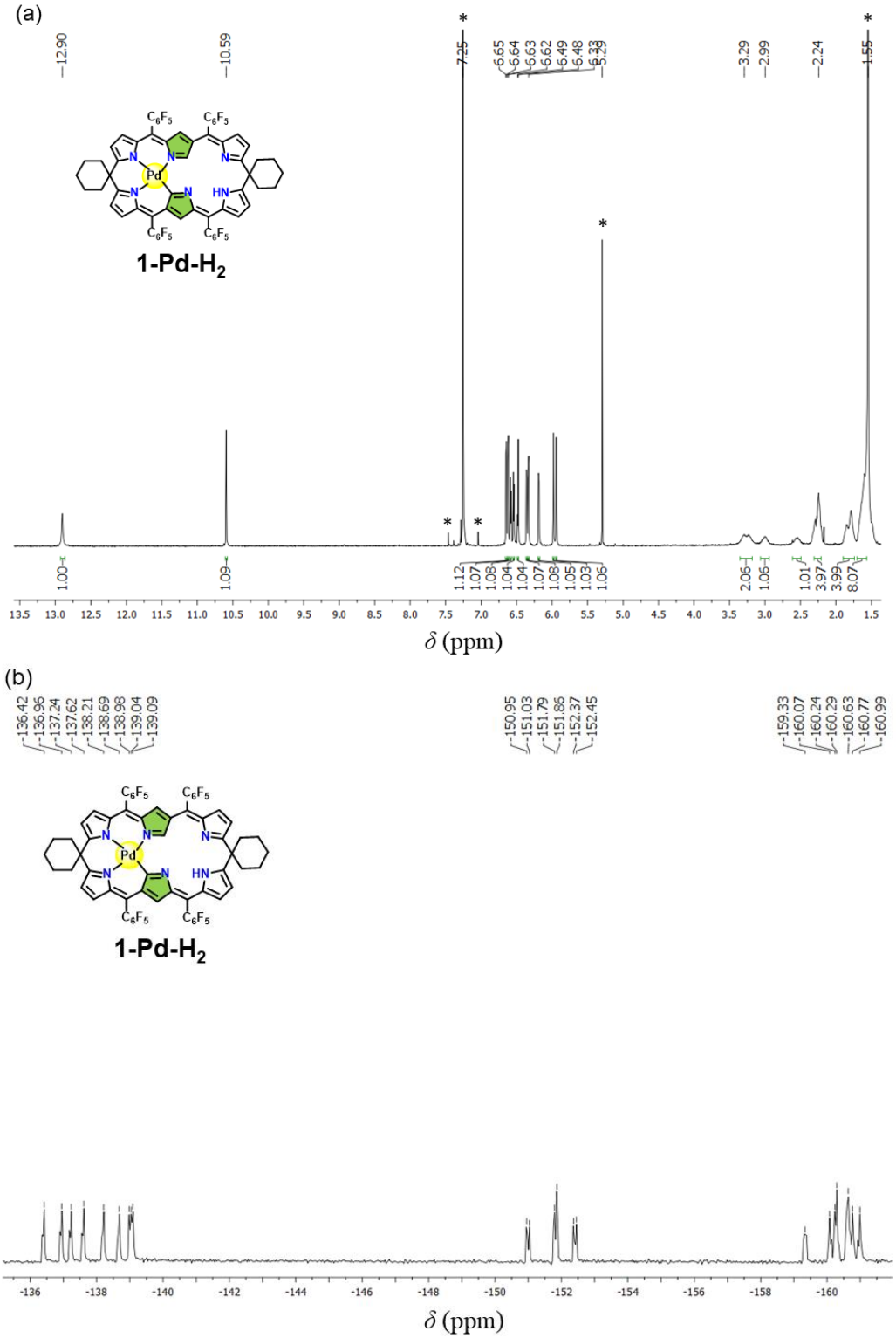

Figure S3-1. (a) ^{1}H and (b) ^{19}F NMR spectra of **1-Pd-H₂** in $CDCl_3$. Asterisks indicate the peaks of residual solvent and impurities.

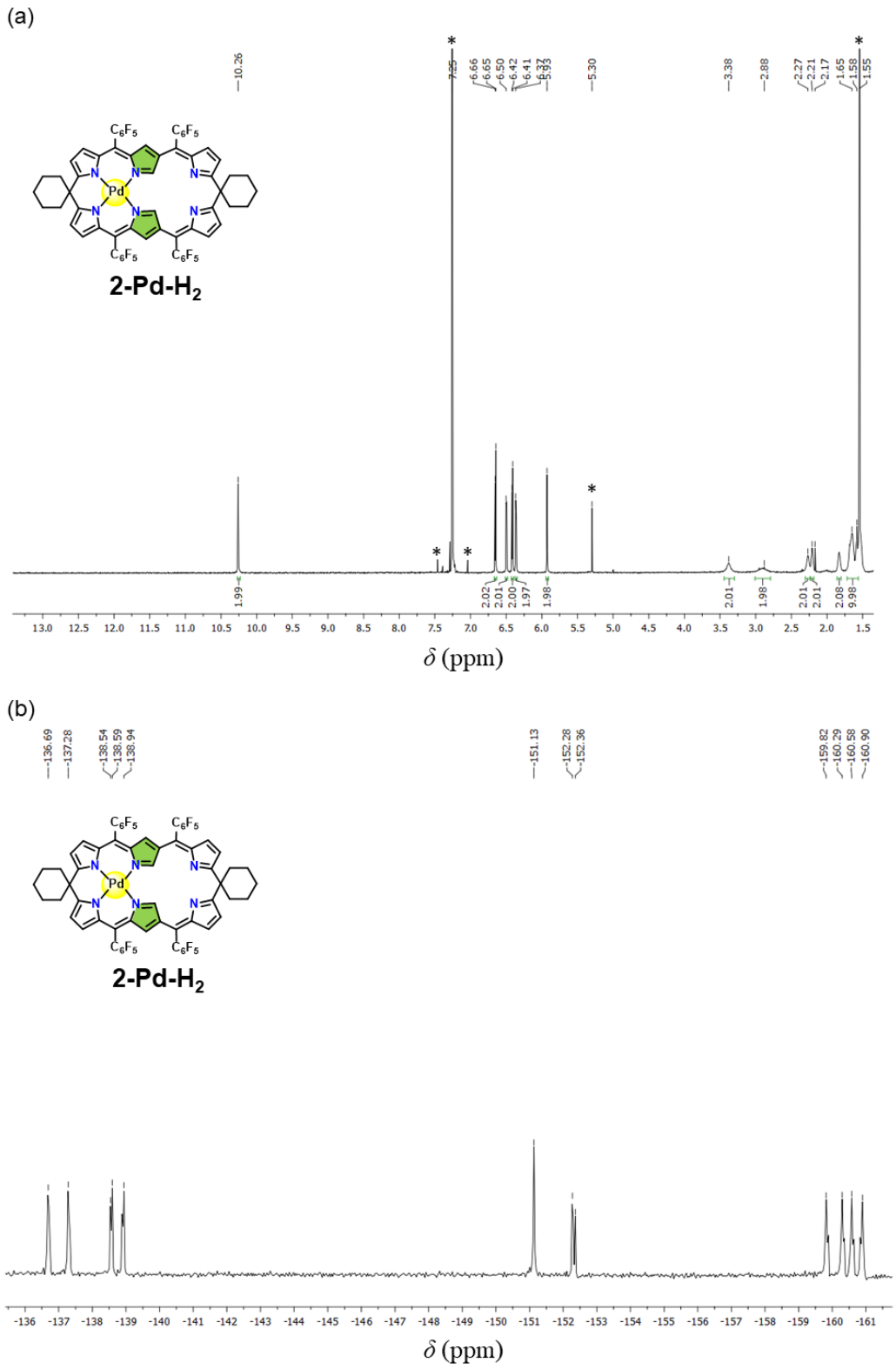

Figure S3-2. (a) ^{1}H and (b) ^{19}F NMR spectra of **2-Pd-H$_2$** in $CDCl_3$. Asterisks indicate the peaks of residual solvent and impurities.

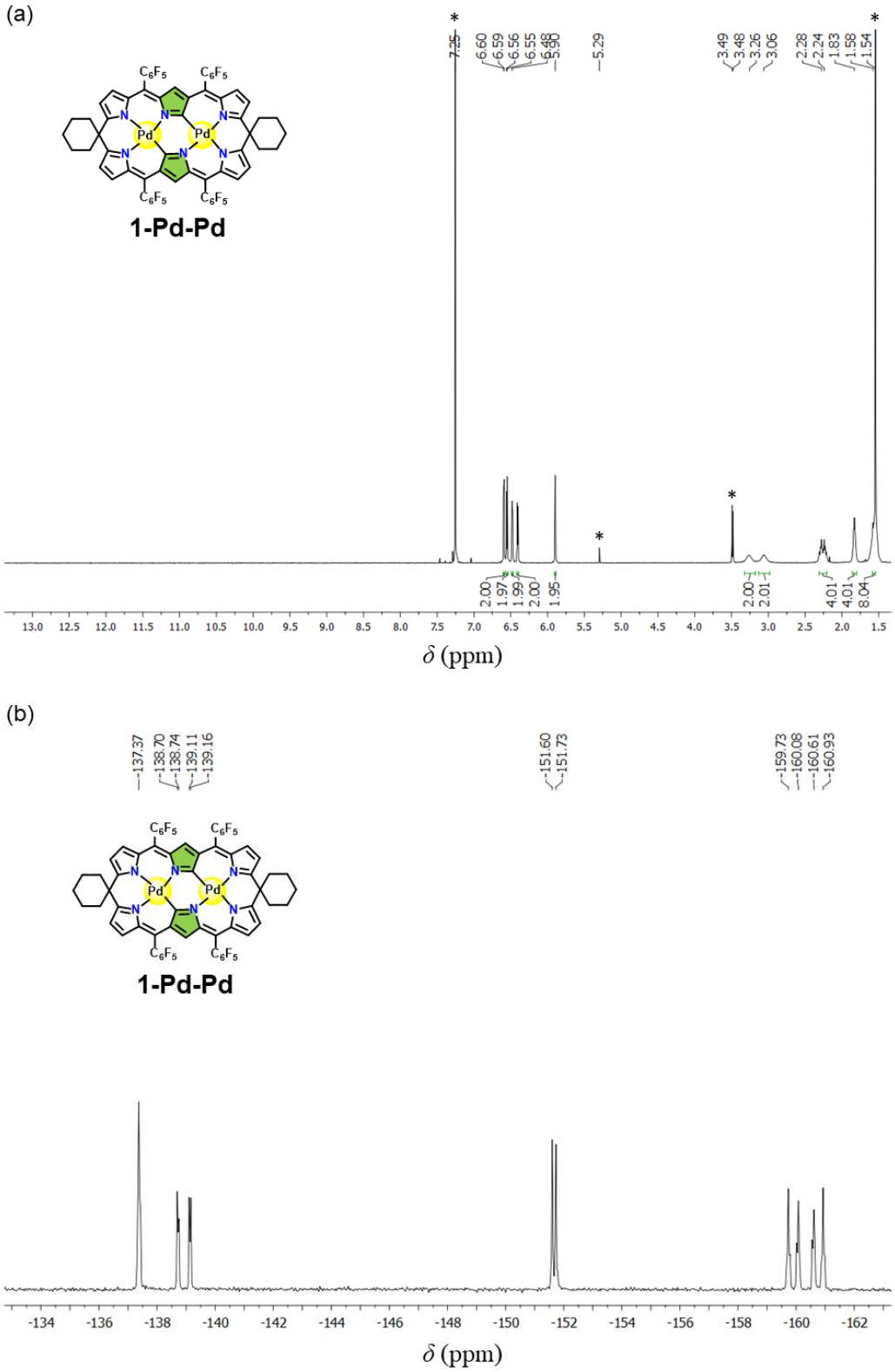

Figure S3-3. (a) ^{1}H and (b) ^{19}F NMR spectra of **1-Pd-Pd** in $CDCl_3$. Asterisks indicate the peaks of residual solvent and impurities.

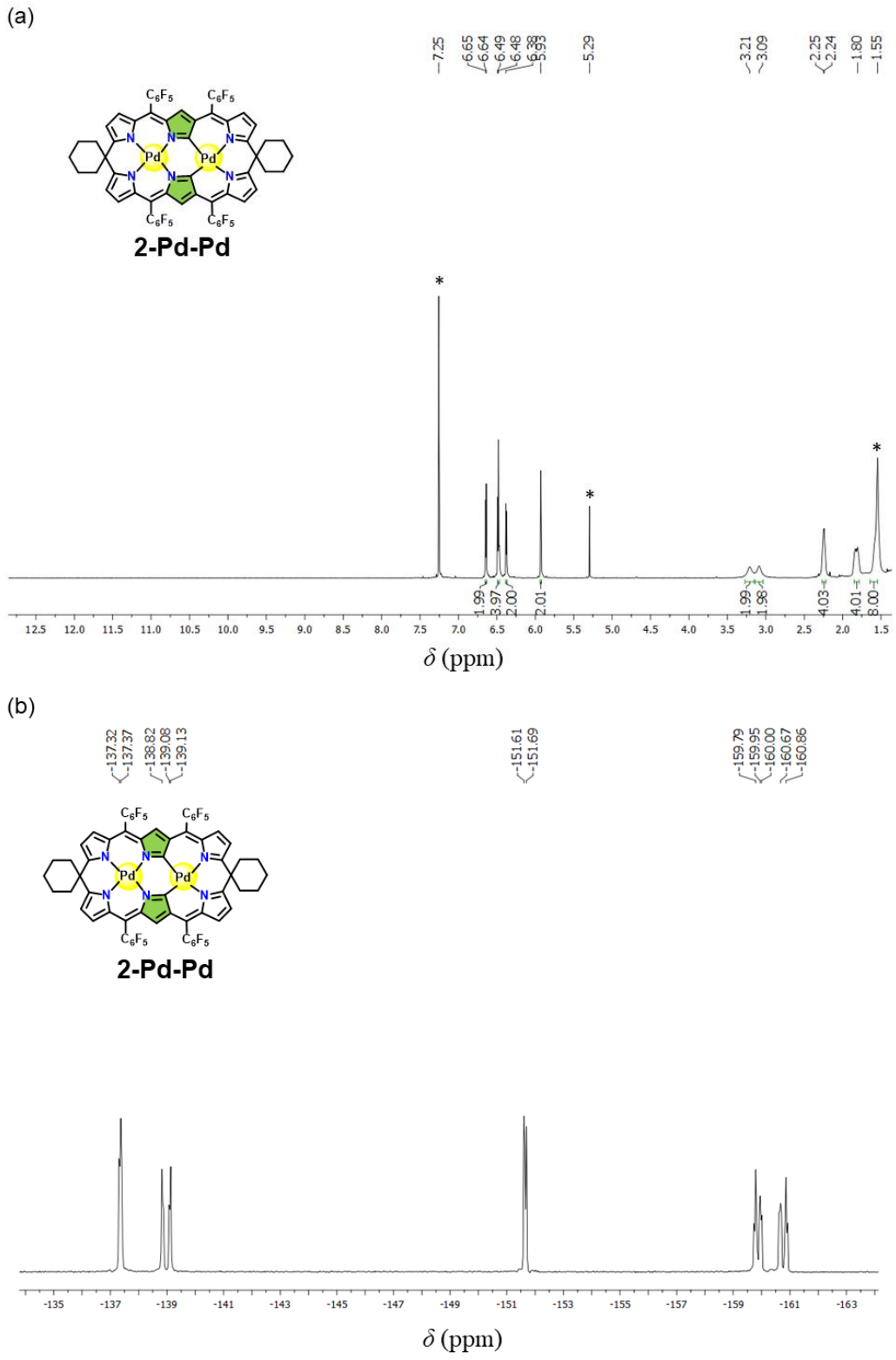

Figure S3-4. (a) ^{1}H and (b) ^{19}F NMR spectra of **2-Pd-Pd** in $CDCl_3$. Asterisks indicate the peaks of residual solvent and impurities.

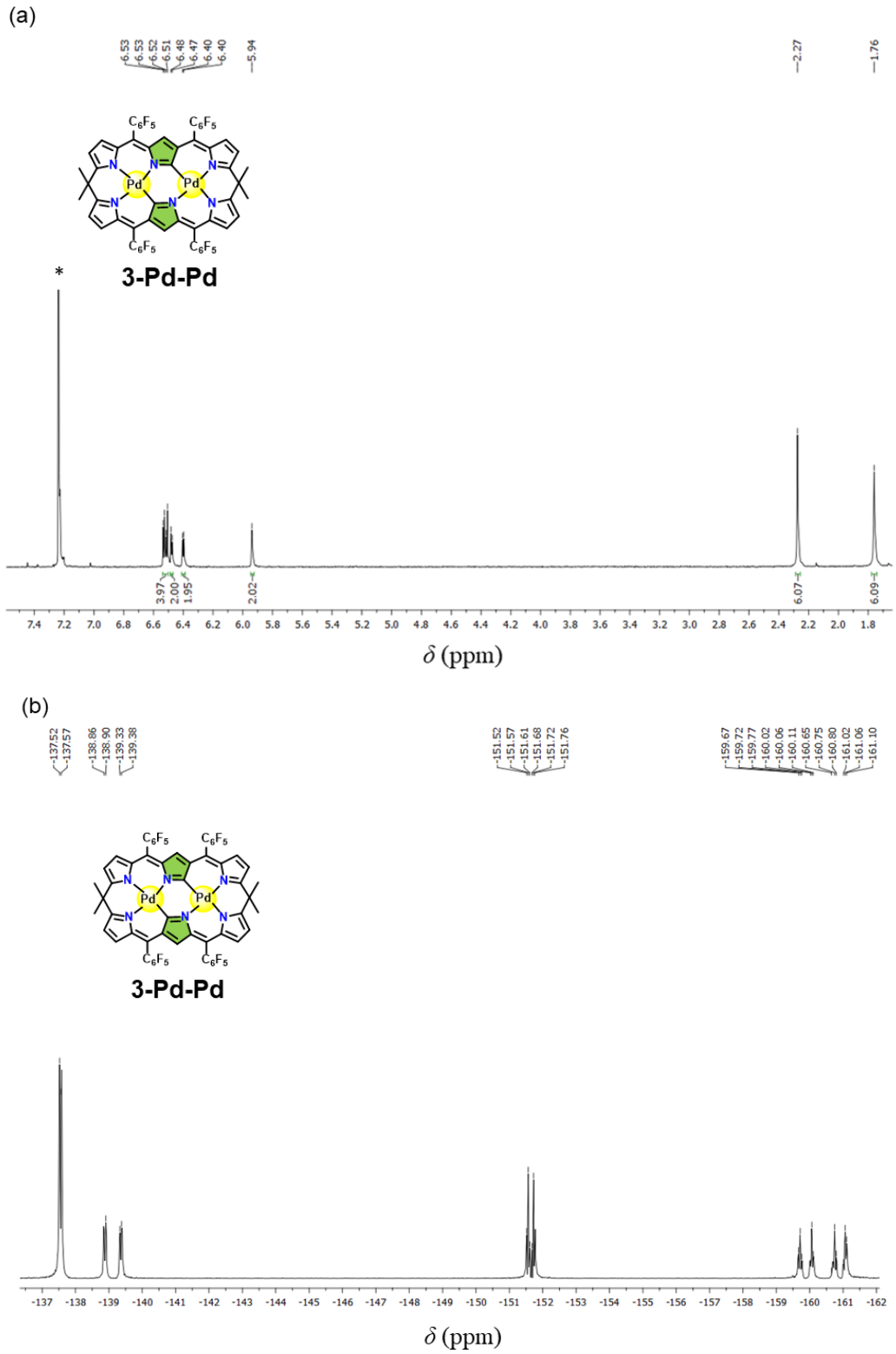

Figure S3-5. (a) ^{1}H and (b) ^{19}F NMR spectra of **3-Pd-Pd** in $CDCl_3$. Asterisks indicate the peaks of residual solvent and impurities.

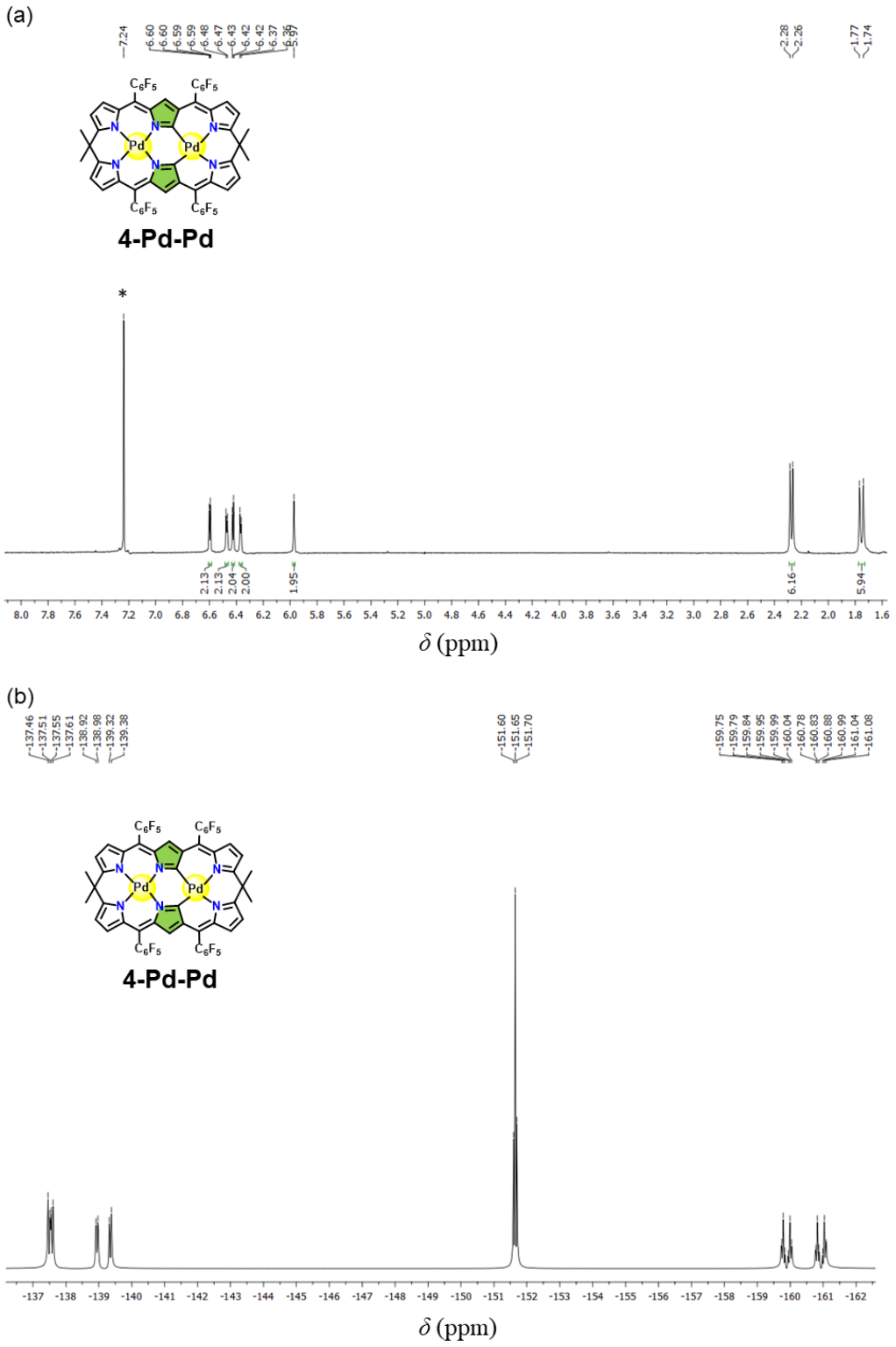

Figure S3-6. (a) ^{1}H and (b) ^{19}F NMR spectra of **4-Pd-Pd** in $CDCl_3$. Asterisks indicate the peaks of residual solvent and impurities.

Table S3-1: Crystallographic data of **1-Pd-H$_2$, 2-Pd-H$_2$, 3-Pd-Pd** and **4-Pd-Pd**

Compound	**1-Pd-H$_2$**	**2-Pd-H$_2$**	**3-Pd-Pd**	**4-Pd-Pd**
Empirical Formula	$C_{66.5}H_{42}F_{20}N_6O_{2.5}Pd$	$C_{64}H_{32}F_{20}N_6Pd$	$C_{68.5}H_{46}F_{20}N_6Pd_2$	$C_{144}H_{108}F_{40}N_{12}Pd_4$
Crystal System	orthorhombic	monoclinic	triclinic	triclinic
Space Group	*Pbca*	$P2_1/c$	$P\bar{1}$	$P\bar{1}$
R_1 ($I > 2.00\sigma(I)$)	0.0617	0.0995	0.0715	0.0677
wR_2 (All reflections)	0.1286	0.2459	0.1676	0.1696
GOF	1.113	1.033	1.008	1.030
a [Å]	28.2789(6)	15.2815(5)	12.2673(3)	12.3063(4)
b [Å]	23.3939(5)	23.7347(10)	15.2901(4)	15.4011(4)
c [Å]	17.5571(3)	17.2151(7)	17.0304(4)	17.1893(5)
α [°]	90	90	86.362(2)	85.501(2)
β [°]	90	93.234 (3)	89.338(2)	89.414(2)
γ [°]	90	90	78.354(2)	78.235(2)
V [Å^3]	11615.0(4)	6234.0 (4)	3122.29(14)	3179.57(16)
Z	8	4	2	1
T [K]	100	100	100	100
D_{calc} [g/cm^3]	1.660	1.461	1.644	1.667
F_{000}	5832	2736	1542	1600
$2\theta_{max}$ [°]	56	52	56	56
no. reflns measd. (unique)	14005	12247	29464	30299
no. params.	922	861	1878	1811
CCDC no.	1876970	1876971	1876972	1876973

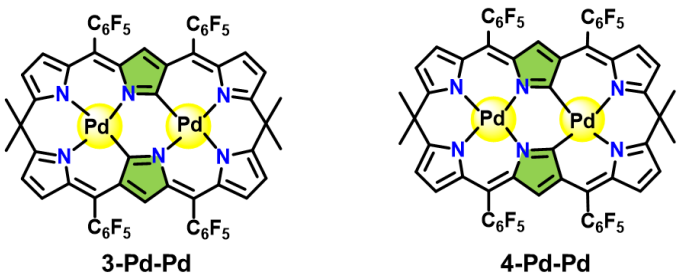

Figure S3-7: Chemical structures of **3-Pd-Pd** and **4-Pd-Pd**

Table S3-2. Selected TD-DFT calculated oscillator strengths, symmetry and compositions of the major electronic transitions of **1-Pd-H$_2$**.

Wavelength (nm)	Osc. Strength	Major contribs
770.3273875	0.0019	HOMO->LUMO (98%)
622.2231909	0.0786	H-1->LUMO (76%), HOMO->L+1 (21%)
522.6108287	0.0251	H-2->LUMO (79%)
515.3339416	0.2433	H-1->L+1 (36%), HOMO->L+1 (33%)
506.3059172	0.1643	H-4->LUMO (13%), H-1->L+1 (52%), HOMO->L+1 (19%)
484.4646492	0.071	HOMO->L+2 (79%)
466.3338963	0.1772	H-5->LUMO (32%), H-4->LUMO (48%)
448.0006974	0.355	H-5->LUMO (34%), H-4->LUMO (15%), H-1->L+2 (13%)
441.429106	0.0372	H-5->LUMO (10%), H-1->L+2 (62%)
439.0997061	0.0145	H-3->L+1 (79%)
427.2076115	0.0121	H-7->LUMO (48%), H-6->LUMO (18%), HOMO->L+3 (11%)
424.0225479	0.0462	H-7->LUMO (21%), H-2->L+1 (36%), HOMO->L+3 (11%)
417.9195504	0.0597	H-8->LUMO (56%)
403.3055527	0.0229	H-5->L+1 (17%), H-4->L+1 (38%), H-2->L+1 (11%), HOMO->L+3 (21%)
388.7626772	0.0112	H-5->L+1 (15%), H-4->L+1 (24%), H-2->L+2 (20%), H-1->L+3 (22%)
382.2779053	0.1745	H-5->L+1 (11%), H-2->L+2 (33%), H-1->L+3 (35%)
380.3196105	0.0513	H-6->L+1 (28%), H-5->L+1 (32%)
375.0845349	0.0312	H-11->LUMO (32%), H-10->LUMO (18%), H-6->L+1 (35%)
370.5112901	0.0449	H-7->L+1 (11%), H-6->L+1 (25%)

360.9227789	0.042	H-12->LUMO (37%), H-9->LUMO (47%)
360.3563129	0.0321	H-12->LUMO (36%), H-9->LUMO (47%)
356.5325464	0.088	H-10->LUMO (16%), H-7->L+1 (29%), H-4->L+2 (16%)
356.1740678	0.0931	H-15->LUMO (33%), H-7->L+1 (10%), H-4->L+2 (15%)

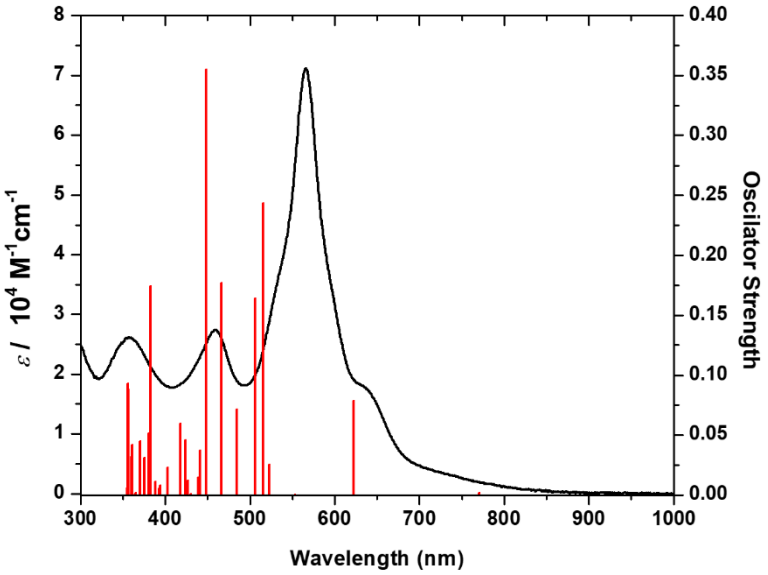

Figure S3-8. Absorption spectrum of **1-Pd-H₂** recorded in toluene along with the calculated stick (red) spectrum obtained by TD-DFT (B3LYP) method.

Table S3-3. Selected TD-DFT calculated oscillator strengths, symmetry and compositions of the major electronic transitions of **2-Pd-H₂**.

Wavelength (nm)	Osc. Strength	Major contribs
651.040711	0.0002	HOMO->LUMO (99%)
565.672931	0.0156	H-1->LUMO (65%), HOMO->L+1 (35%)
493.4694249	0.0113	H-1->L+1 (70%), HOMO->L+2 (26%)
485.0901562	0.5532	H-1->LUMO (23%), HOMO->L+1 (46%), HOMO->L+2 (12%)
479.7036022	0.0904	H-2->LUMO (11%), H-1->L+1 (24%), HOMO->L+2 (50%)
450.3603088	0.0942	H-2->LUMO (78%)
437.3957278	0.1064	H-1->L+2 (75%), HOMO->L+3 (11%)
426.9428134	0.0151	H-5->LUMO (15%), H-4->LUMO (30%), H-3->LUMO (45%)
420.3138959	0.2409	H-4->LUMO (15%), H-3->LUMO (17%), HOMO->L+3 (19%), HOMO->L+4 (28%)

418.1027619	0.0169	H-4->LUMO (15%), H-2->L+1 (23%), HOMO->L+4 (41%)
409.5537047	0.0503	H-2->L+1 (39%), HOMO->L+3 (20%), HOMO->L+4 (18%)
408.0575073	0.0344	H-5->LUMO (63%), H-4->LUMO (11%)
406.1992367	0.0445	H-8->LUMO (50%), H-7->LUMO (39%)
397.1433839	0.0125	H-6->LUMO (59%), H-3->L+1 (14%)
387.3416633	0.0355	H-8->LUMO (33%), H-7->LUMO (47%)
366.1779527	0.0178	H-8->L+1 (23%), H-1->L+3 (34%)
361.8497345	0.0203	H-8->L+4 (18%), H-7->L+1 (28%), H-5->L+1 (13%)
360.4401216	0.0101	H-7->L+1 (16%), H-5->L+1 (24%), H-5->L+4 (13%), H-2->L+4 (10%)
353.2816441	0.1764	H-5->L+4 (14%), H-2->L+4 (12%)

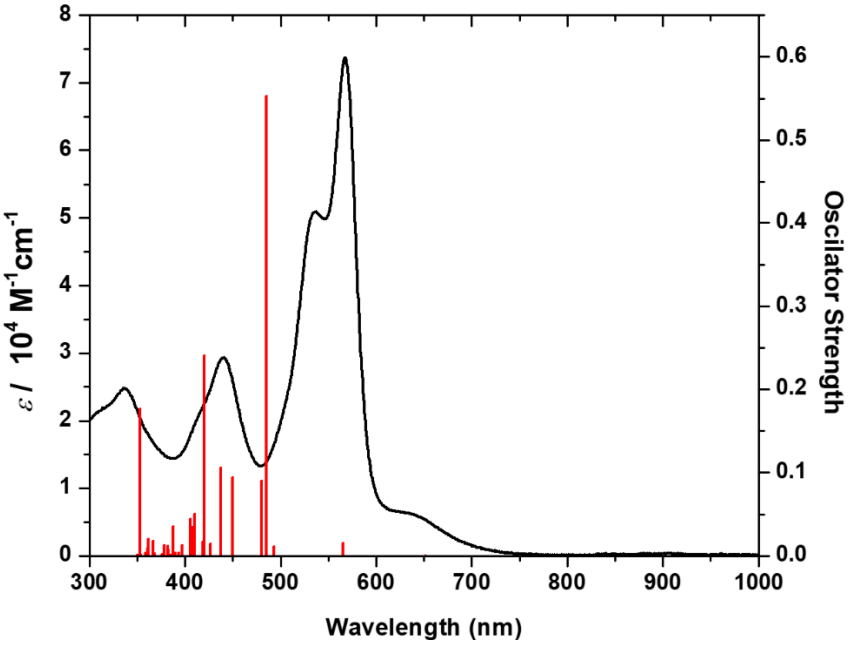

Figure S3-9. Absorption spectrum of **2-Pd-H₂** recorded in toluene along with the calculated stick (red) spectrum obtained by TD-DFT (B3LYP) method.

Table S3-4. Selected TD-DFT calculated oscillator strengths, symmetry and compositions of the major electronic transitions of **1-Pd-Pd**.

Wavelength (nm)	Osc. Strength	Major contribs
654.028554	0.0305	H-1->LUMO (71%), HOMO->L+1 (28%)

570.882185	0.0002	H-1->L+1 (97%)
545.897292	0.3312	H-2->LUMO (11%), H-1->LUMO (13%), HOMO->L+1 (43%), HOMO->L+2 (20%)
528.784889	0.0464	H-3->LUMO (84%)
505.500848	0.0816	H-2->LUMO (79%)
495.243431	0.3481	HOMO->L+1 (16%), HOMO->L+2 (68%)
446.725492	0.0381	H-4->L+1 (90%)
429.829062	0.0218	H-6->LUMO (67%), H-1->L+3 (12%)
421.987655	0.0122	H-5->L+1 (86%)
414.067371	0.2064	H-8->LUMO (79%)
379.783719	0.434	H-5->L+2 (12%), H-4->L+2 (61%)
378.427473	0.0136	H-10->LUMO (18%), H-8->L+1 (26%), H-6->L+1 (34%)
374.801067	0.1468	H-5->L+2 (76%), H-4->L+2 (12%)
366.806287	0.0639	H-9->L+1 (77%)
356.43005	0.0493	H-10->LUMO (64%)

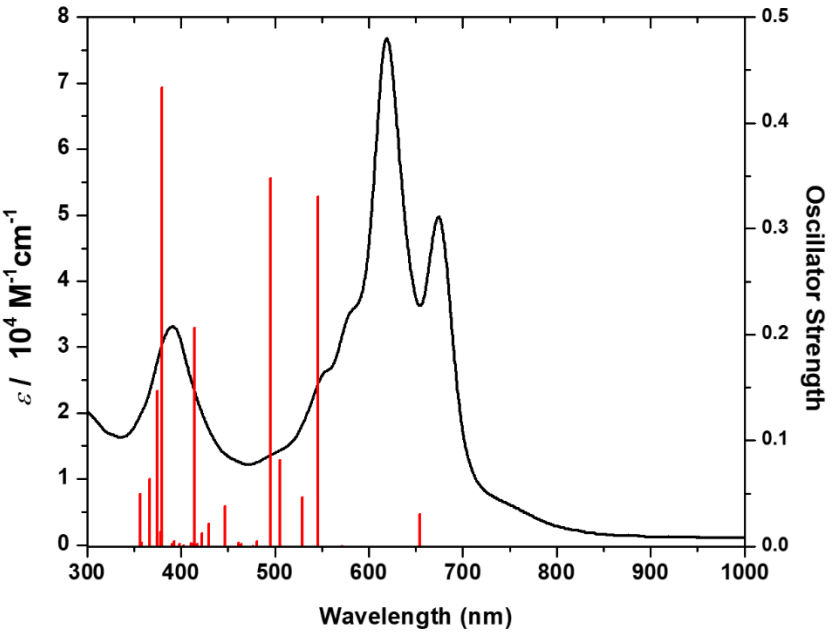

Figure S3-10. Absorption spectrum of **1-Pd-Pd** recorded in toluene along with the calculated stick (red) spectrum obtained by TD-DFT (B3LYP) method.

Table S3-5. Selected TD-DFT calculated oscillator strengths, symmetry and compositions of the major electronic transitions of **2-Pd-Pd**.

Wavelength (nm)	Osc. Strength	Major contribs
729.2758838	0.0023	HOMO->LUMO (99%)
655.0998257	0.0112	H-1->LUMO (65%), HOMO->L+1 (34%)
568.1614564	0.0037	H-1->L+1 (96%)
552.5388521	0.0698	H-2->LUMO (82%)
542.4579673	0.4351	H-2->LUMO (16%), H-1->LUMO (18%), H-1->L+2 (14%), HOMO->L+1 (42%)
500.8450536	0.026	H-3->LUMO (87%)
481.2303719	0.2162	H-4->LUMO (55%), H-1->L+2 (21%)
470.9750922	0.0537	H-4->LUMO (30%), H-1->L+2 (51%), HOMO->L+3 (12%)
455.5897443	0.0949	H-3->L+1 (80%)
450.6222033	0.0236	H-6->LUMO (64%), H-2->L+2 (21%)
424.3418202	0.0334	H-7->LUMO (28%), H-5->LUMO (35%), H-3->L+2 (15%), H-1->L+3 (12%)
421.1276554	0.1454	H-8->LUMO (85%)
397.6146271	0.0492	H-9->LUMO (60%), H-5->L+1 (22%)
383.235018	0.0315	H-9->LUMO (12%), H-5->L+1 (24%), H-4->L+2 (13%), HOMO->L+4 (30%)
374.0773383	0.2165	H-5->L+1 (13%), H-4->L+2 (32%), HOMO->L+4 (19%)
373.1092176	0.3362	H-4->L+2 (38%), HOMO->L+4 (42%)
366.2861326	0.0452	H-9->L+1 (63%), H-2->L+3 (16%)

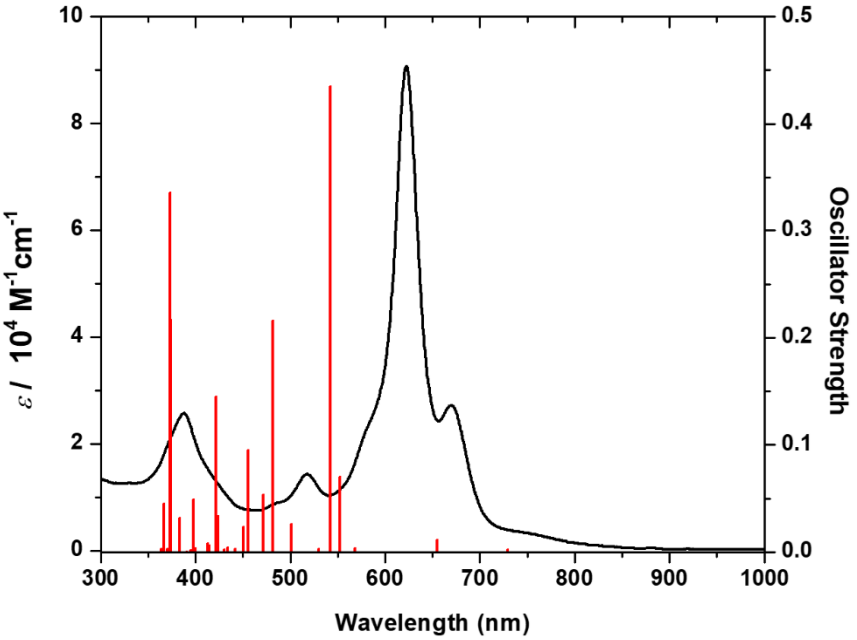

Figure S3-11. Absorption spectrum of **2-Pd-Pd** recorded in toluene along with the calculated stick (red) spectrum obtained by TD-DFT (B3LYP) method.

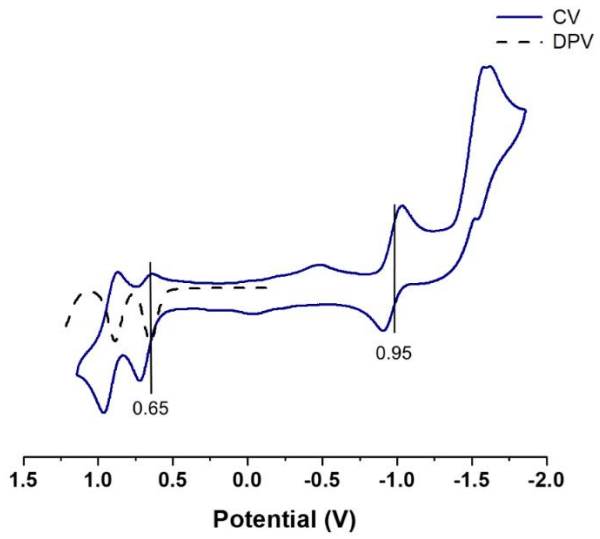

Figure S3-12. Cyclic voltammograms and DPV curve of **1-Pd-H$_2$** in CH_2Cl_2 containing 0.1 M $TBAPF_6$.

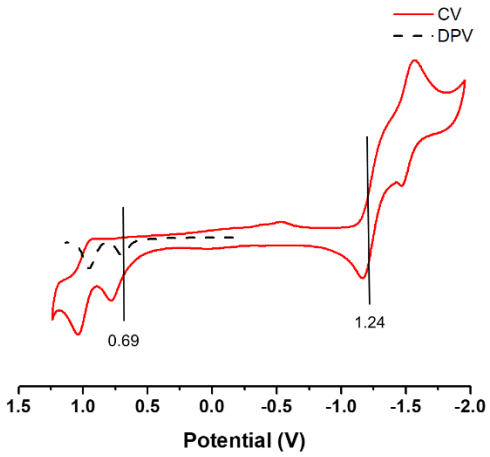

Figure S3-13. Cyclic voltammograms and DPV curve of **2-Pd-H$_2$** in CH_2Cl_2 containing 0.1 M $TBAPF_6$.

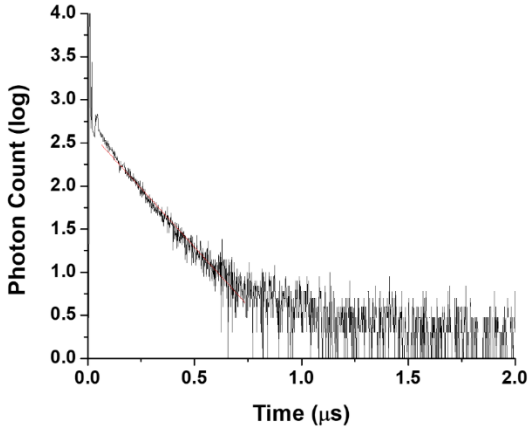

Figure S3-14. Time resolved phosphorescence decay of **1-Pd-H$_2$** in toluene; λ_{ex}= 532 nm. The line (in red) is a least-squares fit assuming a single exponential.

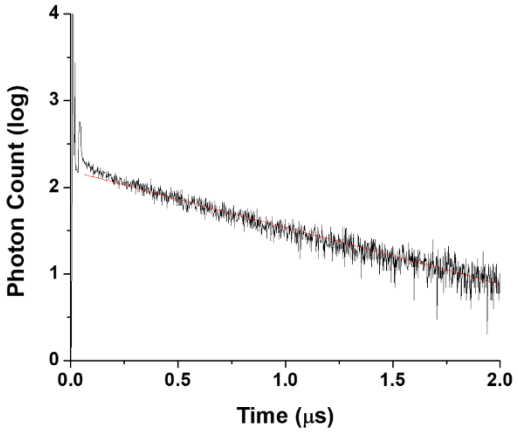

Figure S3-15. Time resolved phosphorescence decay of **2-Pd-H$_2$** in toluene; λ_{ex}= 532 nm. The line (in red) is a least-squares fit assuming a single exponential.

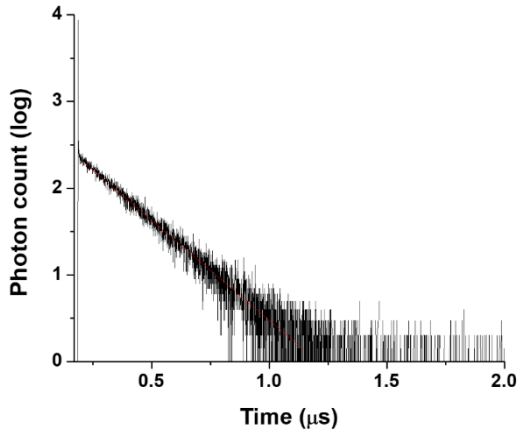

Figure S3-16. Time resolved phosphorescence decay of **1-Pd-Pd** in toluene; λ_{ex}= 532 nm. The line (in red) is a least-squares fit assuming a single exponential.

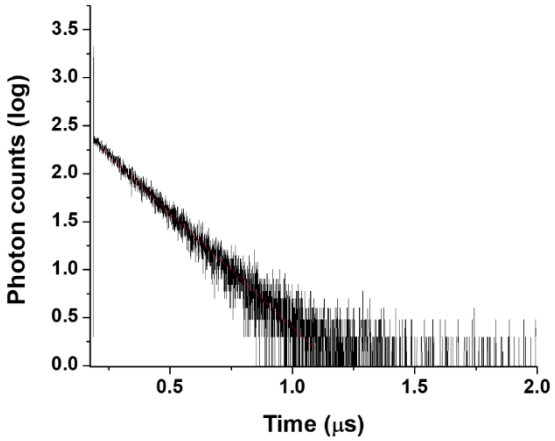

Figure S3-17. Time resolved phosphorescence decay of **2-Pd-Pd** in toluene; λ_{ex}= 532 nm. The line (in red) is a least-squares fit assuming a single exponential.

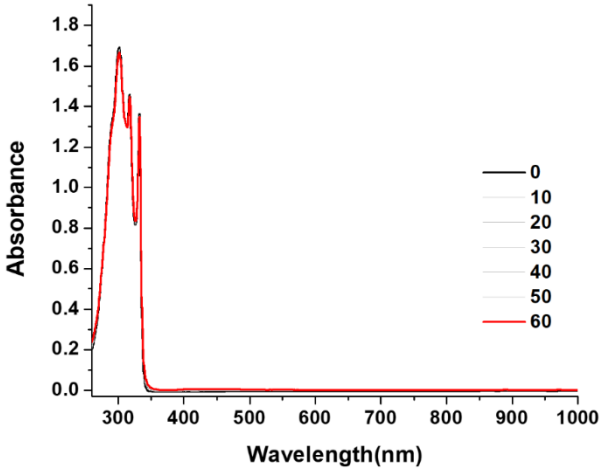

Figure S3-18. UV-Vis spectral change of DHN in the light irradiation (450 – 800 nm) in CH_2Cl_2/MeOH.

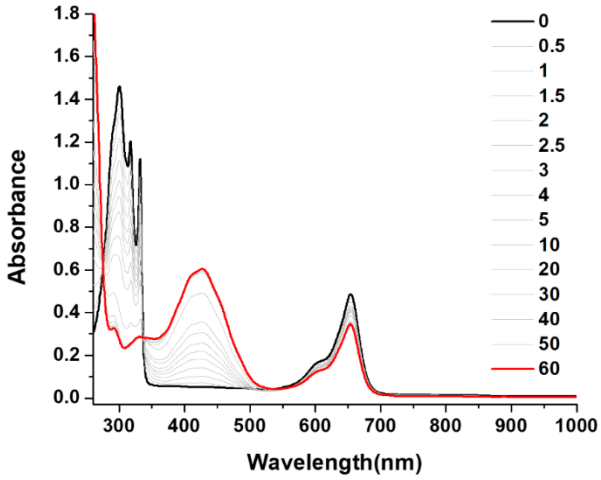

Figure S3-19. UV-Vis spectral change of DHN in the presence of **MB** (5 mol%) upon light irradiation (450 – 800 nm) in CH_2Cl_2/MeOH.

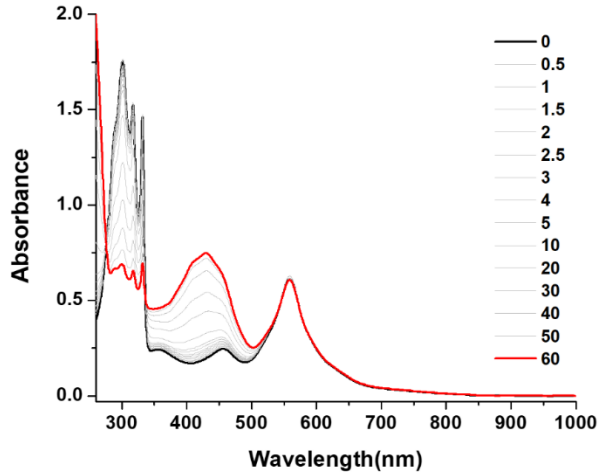

Figure S3-20. UV-Vis spectral change of DHN in the presence of **1-Pd-H_2** (5 mol%) upon light irradiation (450 – 800 nm) in CH_2Cl_2/MeOH.

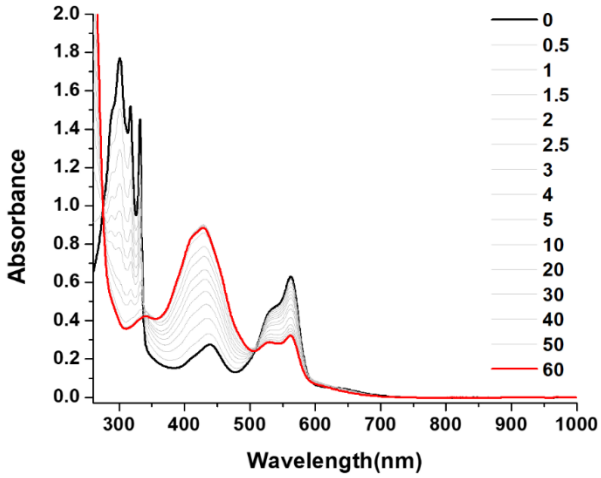

Figure S3-21. UV-Vis spectral change of DHN in the presence of **2-Pd- H_2** (5 mol%) upon light irradiation (450 – 800 nm) in CH_2Cl_2/MeOH.

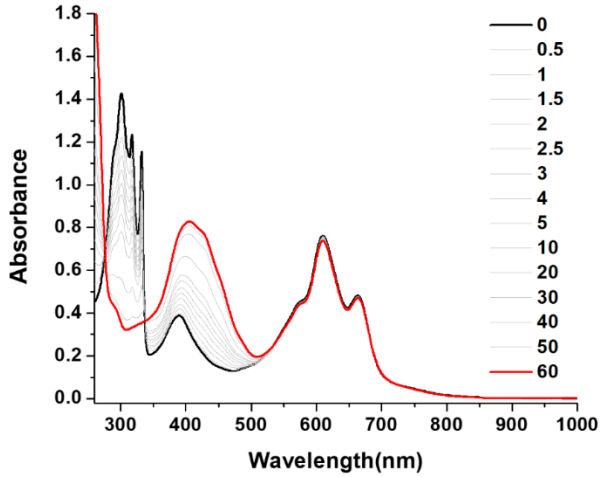

Figure S3-22. UV-Vis spectral change of DHN in the presence of **1-Pd-Pd** (5 mol%) upon light irradiation (450 – 800 nm) in CH_2Cl_2/MeOH.

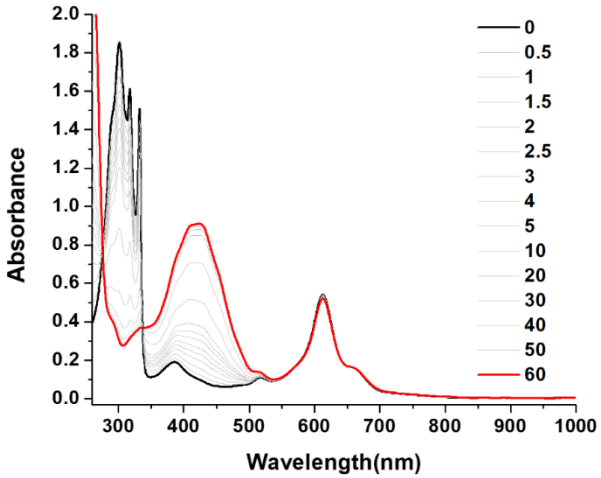

Figure S3-23. UV-Vis spectral change of DHN in the presence of **2-Pd-Pd** (5 mol%) upon light irradiation (450 – 800 nm) in CH_2Cl_2/MeOH.

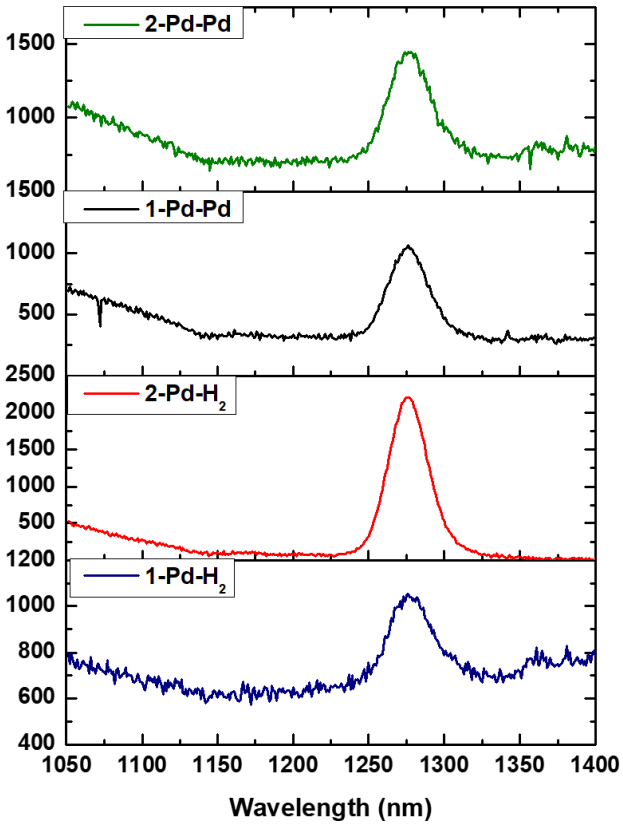

Figure S3-24. Emissions of the singlet oxygen sensitized by the palladium complexes in O_2 saturated toluene.

3-10. References

[1] (a) J. J. Liang, C. L. Gu, M. L. Kacher, C. S. Foote, *Journal of the American Chemical Society* **1983**, *105*, 4717-4721; (b) J. L. Ravanat, P. Di Mascio, G. R. Martinez, M. H. Medeiros, J. Cadet, *The Journal of biological chemistry* **2000**, *275*, 40601-40604; (c) M. C. DeRosa, R. J. Crutchley, *Coordination Chemistry Reviews* **2002**, *233-234*, 351-371.

[2] C. Schweitzer, R. Schmidt, *Chemical Reviews* **2003**, *103*, 1685-1758.

[3] (a) D. E. J. G. J. Dolmans, D. Fukumura, R. K. Jain, *Nature Reviews Cancer* **2003**, *3*, 380; (b) C. A. Robertson, D. H. Evans, H. Abrahamse, *Journal of Photochemistry and Photobiology B: Biology* **2009**, *96*, 1-8; (c) M. C. Issa, M. Manela-Azulay, *Anais brasileiros de dermatologia* **2010**, *85*, 501-511.

[4] (a) C. Huo, H. Zhang, H. Zhang, H. Zhang, B. Yang, P. Zhang, Y. Wang, *Inorganic Chemistry* **2006**, *45*, 4735-4742; (b) X. Jiang, J. Peng, J. Wang, X. Guo, D. Zhao, Y. Ma, *ACS Applied Materials & Interfaces* **2016**, *8*, 3591-3600.

[5] (a) O. Suchard, R. Kane, B. J. Roe, E. Zimmermann, C. Jung, P. A. Waske, J. Mattay, M.

Oelgemöller, *Tetrahedron* **2006**, *62*, 1467-1473; (b) L. Huang, J. Zhao, S. Guo, C. Zhang, J. Ma, *The Journal of Organic Chemistry* **2013**, *78*, 5627-5637; (c) W.-P. To, Y. Liu, T.-C. Lau, C.-M. Che, *Chemistry – A European Journal* **2013**, *19*, 5654-5664.

[6] (a) T. N. Singh-Rachford, F. N. Castellano, *Coordination Chemistry Reviews* **2010**, *254*, 2560-2573; (b) X. Cui, J. Zhao, P. Yang, J. Sun, *Chemical Communications* **2013**, *49*, 10221-10223.

[7] (a) W. Wu, H. Guo, W. Wu, S. Ji, J. Zhao, *The Journal of Organic Chemistry* **2011**, *76*, 7056-7064; (b) T. Yogo, Y. Urano, Y. Ishitsuka, F. Maniwa, T. Nagano, *Journal of the American Chemical Society* **2005**, *127*, 12162-12163.

[8] (a) D. N. Kozhevnikov, V. N. Kozhevnikov, M. Z. Shafikov, A. M. Prokhorov, D. W. Bruce, J. A. Gareth Williams, *Inorganic Chemistry* **2011**, *50*, 3804-3815; (b) X. Wang, S. Goeb, Z. Ji, N. A. Pogulaichenko, F. N. Castellano, *Inorganic Chemistry* **2011**, *50*, 705-707; (c) F. Heinemann, J. Karges, G. Gasser, *Accounts of Chemical Research* **2017**, *50*, 2727-2736.

[9] (a) T. N. Singh-Rachford, F. N. Castellano, *The Journal of Physical Chemistry A* **2008**, *112*, 3550-3556; (b) M. Ethirajan, Y. Chen, P. Joshi, R. K. Pandey, *Chemical Society Reviews* **2011**, *40*, 340-362; (c) Y. Che, W. Yang, G. Tang, F. Dumoulin, J. Zhao, L. Liu, Ü. İşci, *Journal of Materials Chemistry C* **2018**, *6*, 5785-5793.

[10] (a) A. Srinivasan, H. Furuta, *Accounts of Chemical Research* **2005**, *38*, 10-20; (b) J. R. Sommer, A. H. Shelton, A. Parthasarathy, I. Ghiviriga, J. R. Reynolds, K. S. Schanze, *Chemistry of Materials* **2011**, *23*, 5296-5304; (c) M. Toganoh, H. Furuta, *Chemical Communications* **2012**, *48*, 937-954; (d) V. V. Roznyatovskiy, C.-H. Lee, J. L. Sessler, *Chemical Society Reviews* **2013**, *42*, 1921-1933; (e) T. Chatterjee, V. S. Shetti, R. Sharma, M. Ravikanth, *Chemical Reviews* **2017**, *117*, 3254-3328; (f) S. Hiroto, Y. Miyake, H. Shinokubo, *Chemical Reviews* **2017**, *117*, 2910-3043.

[11] (a) A. Singhal, in *Top Curr Chem (Cham), Vol. 376*, **2018**, p. 21; (b) L. Sessler Jonathan, S. Zimmerman Rebecca, C. Bucher, V. Král, B. Andrioletti, in *Pure and Applied Chemistry, 73*, **2001**, 1041-1057; (c) A. C. Y. Tay, B. J. Frogley, D. C. Ware, P. J. Brothers, *Dalton Transactions* **2018**, *47*, 3388-3399.

[12] (a) K. Araki, F. M. Engelmann, I. Mayer, H. E. Toma, M. S. Baptista, H. Maeda, A. Osuka, H. Furuta, *Chemistry Letters* **2003**, *32*, 244-245; (b) F. M. Engelmann, I. Mayer, K. Araki, H. E. Toma, M. c. S. Baptista, H. Maeda, A. Osuka, H. Furuta, *Journal of Photochemistry and Photobiology A: Chemistry* **2004**, *163*, 403-411.

[13] (a) P. Pushpanandan, Y. K. Maurya, T. Omagari, R. Hirosawa, M. Ishida, S. Mori, Y. Yasutake, S. Fukatsu, J. Mack, T. Nyokong, H. Furuta, *Inorganic Chemistry* **2017**, *56*, 12572-12580; (b) H. Furuta, T. Ishizuka, A. Osuka, *Inorganic Chemistry Communications* **2003**, *6*, 398-401; (c) H. Furuta, T. Ishizuka, A. Osuka, Y. Uwatoko, Y. Ishikawa, *Angewandte Chemie International Edition*

2001, *40*, 2323-2325.

[14] D.-H. Won, M. Toganoh, Y. Terada, S. Fukatsu, H. Uno, H. Furuta, *Angewandte Chemie International Edition* **2008**, *47*, 5438-5441.

[15] (a) E. l. G. Azenha, A. C. Serra, M. Pineiro, M. M. Pereira, J. Seixas de Melo, L. G. Arnaut, S. J. Formosinho, A. M. d. A. Rocha Gonsalves, *Chemical Physics* **2002**, *280*, 177-190; (b) S. Drouet, C. O. Paul-Roth, V. Fattori, M. Cocchi, J. A. G. Williams, *New Journal of Chemistry* **2011**, *35*, 438-444; (c) S. M. Borisov, G. Zenkl, I. Klimant, *ACS Applied Materials & Interfaces* **2010**, *2*, 366-374; (d) M. Gouterman, F. P. Schwarz, P. D. Smith, D. Dolphin, *The Journal of Chemical Physics* **1973**, *59*, 676-690.

[16] S. Gokulnath, K. Nishimura, M. Toganoh, S. Mori, H. Furuta, *Angewandte Chemie International Edition* **2013**, *52*, 6940-6943.

[17] (a) H. Furuta, H. Maeda, A. Osuka, M. Yasutake, T. Shinmyozu, Y. Ishikawa, *Chemical Communications* **2000**, 1143-1144; (b) H. Furuta, N. Kubo, H. Maeda, T. Ishizuka, A. Osuka, H. Nanami, T. Ogawa, *Inorganic Chemistry* **2000**, *39*, 5424-5425.

[18] (a) S. Gokulnath, K. Yamaguchi, M. Toganoh, S. Mori, H. Uno, H. Furuta, *Angewandte Chemie International Edition* **2011**, *50*, 2302-2306; (b) J. H. Kwon, T. K. Ahn, M.-C. Yoon, D. Y. Kim, M. K. Koh, D. Kim, H. Furuta, M. Suzuki, A. Osuka, *The Journal of Physical Chemistry B* **2006**, *110*, 11683-11690.

[19] S.-y. Takizawa, R. Aboshi, S. Murata, *Photochemical & Photobiological Sciences* **2011**, *10*, 895-903.

[20] B. Dolenský, J. Kroulík, V. Král, J. L. Sessler, H. Dvořáková, P. Bouř, M. Bernátková, C. Bucher, V. Lynch, *Journal of the American Chemical Society* **2004**, *126*, 13714-13722.

[21] J. V. Caspar, E. M. Kober, B. P. Sullivan, T. J. Meyer, *Journal of the American Chemical Society* **1982**, *104*, 630-632.

[22] D. Murtinho, M. Pineiro, M. M. Pereira, A. M. d. A. Rocha Gonsalves, L. G. Arnaut, M. d. G. Miguel, H. D. Burrows, *Journal of the Chemical Society, Perkin Transactions 2* **2000**, 2441-2447.

[23] A. Ogunsipe, T. Nyokong, *Journal of Molecular Structure* **2004**, *689*, 89-97.

[24] (a) J. Moan, E. Wold, *Nature* **1979**, *279*, 450-451; (b) Y. Lion, M. Delmelle, A. Van De Vorst, *Nature* **1976**, *263*, 442-443.

[25] J. Wang , Y. Hou, W. Lei, Q. Zhou, C. Li, B. Zhang, X. Wang, *ChemPhysChem* **2012**, *13*, 2739-2747.

[26] M. J. Frisch, G. W. Trucks, H. B. Schlegel, G. E. Scuseria, M. A. Robb, J. R. Cheeseman, G. Scalmani, V. Barone, G. A. Petersson, H. Nakatsuji, X. Li, M. Caricato, A. V. Marenich, J. Bloino, B. G. Janesko, R. Gomperts, B. Mennucci, H. P. Hratchian, J. V. Ortiz, A. F. Izmaylov, J. L.

Sonnenberg, Williams, F. Ding, F. Lipparini, F. Egidi, J. Goings, B. Peng, A. Petrone, T. Henderson, D. Ranasinghe, V. G. Zakrzewski, J. Gao, N. Rega, G. Zheng, W. Liang, M. Hada, M. Ehara, K. Toyota, R. Fukuda, J. Hasegawa, M. Ishida, T. Nakajima, Y. Honda, O. Kitao, H. Nakai, T. Vreven, K. Throssell, J. A. Montgomery Jr., J. E. Peralta, F. Ogliaro, M. J. Bearpark, J. J. Heyd, E. N. Brothers, K. N. Kudin, V. N. Staroverov, T. A. Keith, R. Kobayashi, J. Normand, K. Raghavachari, A. P. Rendell, J. C. Burant, S. S. Iyengar, J. Tomasi, M. Cossi, J. M. Millam, M. Klene, C. Adamo, R. Cammi, J. W. Ochterski, R. L. Martin, K. Morokuma, O. Farkas, J. B. Foresman, D. J. Fox, Wallingford, CT, **2016**.

[27] (a) P. J. Stephens, F. J. Devlin, C. F. Chabalowski, M. J. Frisch, *The Journal of Physical Chemistry* **1994**, *98*, 11623-11627; (b) A. D. Becke, *The Journal of Chemical Physics* **1993**, *98*, 5648-5652.

[28] (a) G. Sheldrick, *Acta Crystallographica Section A* **2015**, *71*, 3-8; (b) G. Sheldrick, *Acta Crystallographica Section C* **2015**, *71*, 3-8; (c) G. Sheldrick, *Acta Crystallographica Section A* **2008**, *64*, 112-122.

Chapter 4. Conclusion and Future Plan

In this thesis, the author describes wide scope of non-conjugated analogue of porphyrin, calixphyrin and the effect of employing modifications such as N-confusion and π-expansion which can give rise to interesting electronic properties derived from the inner reactivity of carbon in the confused pyrrolic rings participating in bonding with metal.

Chapter 1 presents a brief overview of chemistry of porphyrin analogues mainly focusing on the structural properties of calixphyrin, N-confused porphyrin, N-confused calixphyrins and its applications.

In chapter 2, the author has synthesized several organoplatinum(II) complexes, **Pt-1**, **Pt-2** and **Pt-3**. Single and double N-confusion mutation to the pyrrole rings are introduced to the parent calix[4]phyrin macrocycle. These molecules have been structurally characterized using Mass, NMR and X-ray crystallographic analysis. Due to the sp^3 meso-carbon calixphyrin macrocycle shows a flexible, bent framework. Thus the MOs are refined to gain bathochromically shifted photophysical properties. On metalation the LUMO is stabilized in metalated calix[4]phyrin and introducing N-confusion modification leads to destabilization of HOMO leading to smaller HOMO-LUMO energy gap compared to metalloporphyrin. Moreover, the heavy atom effect of Pt results in efficient triplet state population and these complexes shows emission in the NIR region. These molecules also efficiently sensitized singlet oxygen and can be further utilized for photodynamic therapy applications.

In chapter 3, the author has synthesized palladium complexes of doubly n-confused calix[6]phyrin, **1-Pd-H_2**, **2-Pd-H_2**, **1-Pd-Pd**, and **2-Pd-Pd**. These molecules are characterized using NMR and X-ray crystallographic analysis. The unique structure of the expanded calixphyrin provides NNNC,NNNC and NNNN,NNCC coordination environment in the core. The structural relation to excited state dynamics were carefully studied using various techniques such as UV-Vis-NIR absorption spectroscopy, DFT/TD-DFT calculations, cyclic voltammetry. These palladium complexes showed intense absorption profiles in the visible-to-NIR region (500–750 nm) depending on the number of central metals. This can be accounted to the narrower HOMO-LUMO energy gap due to extension of π- conjugation in the system and improvising the rigidity of the macrocycle by metalation. The palladium metalation resulted in the increased triplet state life time due to smaller spin-orbit coupling of Pd than Pt. Thus upon photoirradiation in the presence of 1,5- dihydroxynaphthalene (DHN) as a substrate for reactive oxygen species, the bis-palladium complexes generated singlet oxygen with high efficiency and excellent photostability. The number of metal coordinated and coordination environment plays a major role in the photostability of the complex. Singlet oxygen generation was confirmed from the characteristic spectral feature of the spin trapped complex in the EPR spectrum and the intact $^1O_2$ emission at 1270 nm. The double N-confused bis-palladium complexes can be used for designing water soluble photosensitizers for further utilizing these molecules for biological

applications such as PDT.

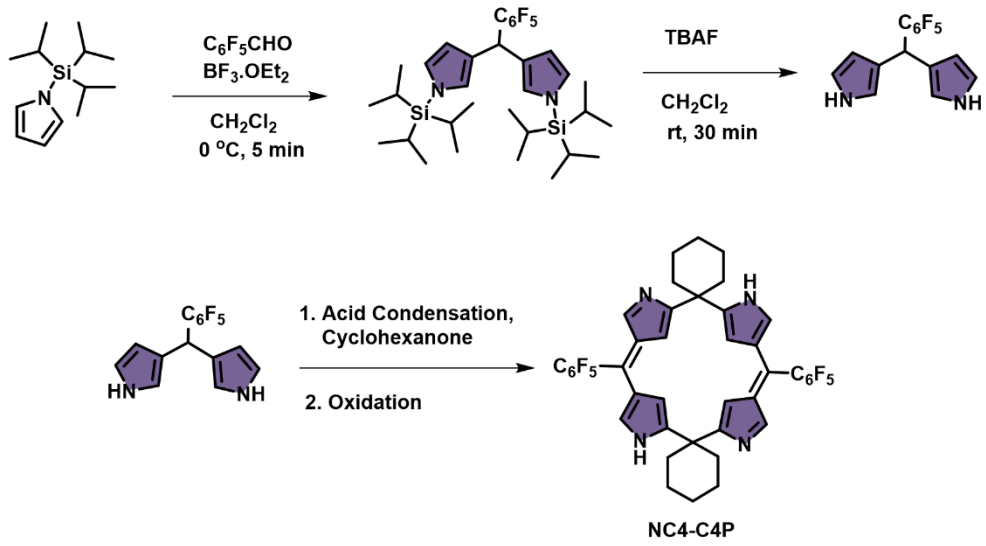

Scheme 4-1. Step-wise proposed synthesis scheme of quadraply N-confused calix[4]phyrin (**NC4-C4P**).

In the future, multiply N-confused calix[4]phyrin moieties can be designed and synthesized. Acid condensation of double N-confused dipyrromethane with cyclohexanone followed by oxidation should result in quadraply N-confused calix[4]phyrin (**NC4-C4P**) and higher analogues (Scheme 4-1). These molecules will have multiple carbon metal coordination sites and should be suitable for stabilizing metal complexes in higher oxidation state as carbon is a better donor altogether. Another direction which is interesting to pursue is the coordination chemistry of peripheral nitrogen groups. This opens wide possibilities for the novel ligand and can find application in sensing, catalysis, supramolecular chemistry and so on.

As a future perspective to chapter 3 designing calix[8]phyrin (**C[8]Ph**) with multiple metalation site is of much interest. The synthesis of double N-confused tetrapyrrole and followed by acid based condensation should result in the target compound, **C[8]Ph** (Scheme 4-2). The coordination chemistry and photophysical properties which the macrocycle can offer is very interesting to explore. The synthesis of this macrocycle is currently undergoing in the laboratory.

This thesis provides a wide scope of newly developed calixphyrin isomers which are superior organometallic ligands and possess a great ability to stabilize the transition metal complexes. The rationale design can be utilized to design more efficient triplet photosensitizers in the future.

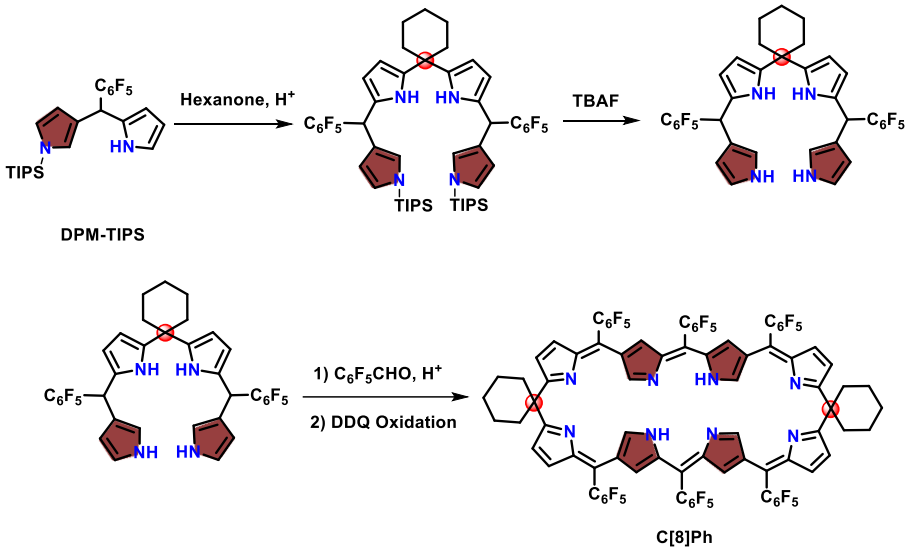

Scheme 4-2. Proposed synthesis scheme for the synthesis of c[8]ph

List of Publication

- Singly and Doubly N-Confused Calix[4]phyrin Organoplatinum(II) Complexes as Near-IR Triplet sensitizers. (**Chapter 2**)

  P. Pushpanandan, Y. K. Maurya, T. Omagari, R. Hirosawa, M. Ishida, S. Mori, Y. Yasutake, S. Fukatsu, J. Mack, T. Nyokong, H. Furuta., *Inorg. Chem*. **2017**, *56*, 12572−12580.

- Doubly N-Confused Calix[6]phyrin Bis-Organopalladium Complexes: Photostable Triplet Sensitizers for Singlet Oxygen Generation. (**Chapter 3**)

  P. Pushpanandan, D. H. Won, S. Mori, Y. Yasutake, S. Fukatsu, M. Ishida, H. Furuta., *Chem. Asian J.* **2019**, *14*, 1729 – 1736.

Acknowledgment

I would like to express my sincere gratitude to my supervisor Prof. Hiroyuki Furuta at the Department of Chemistry and Biochemistry, Graduated School of Engineering, Kyushu University for giving me the opportunity to work under his supervision. His excellent guidance, continuous encouragement and many helpful discussions throughout the investigation are the key foundation of my PhD work. I am also very grateful for the freedom of work he has always given to me to follow my ideas. I am also thankful for his gracious support, care and for always having time to listen and giving advices.

I would like to express my heartfelt appreciation to Prof. Nagao Kobayashi and Prof. Hisashi Shimakoshi for reviewing this thesis, and giving their valuable suggestions.

I am very grateful to my co-supervisor Prof. Masatoshi Ishida at the Department of Chemistry and Biochemistry, Graduated School of Engineering, Kyushu University for his enormous support and beneficial discussions throughout my work. His elaborated guidance, teaching lessons and advices taught me to strive for perfection in conducting experiments, writing manuscripts and this doctoral thesis. It has been a real pleasure and pleasant experience to work with him.

I also would like to express my heartiest gratitude to Prof. Soji Shimizu at the Department of Chemistry and Biochemistry, Graduated School of Engineering, Kyushu University for his helpful suggestions, and supervisions throughout my PhD tenure. I would also like to thank him for his productive, encouraging and inspiring discussions over the course of three years. I am also thankful to Dr. Takaaki Miyazaki for his helpful advices in the group meetings.

I also would like to thank all the collaborators for their enormous support and contributions they have provided to fulfill my research goals in this doctoral project. My special thanks goes to Prof. Shigeki Mori at Integrated Center for Sciences, Ehime University for his excellent support in the X-ray crystallographic analysis measurements. I would like to thank Prof. Susume Fukatsu and Prof. Yuhsuke Yasutake at University of Tokyo for their valuable contributions to my research. Also, I would like to thank Prof. Tebello Nyokong and Prof. John Mack of Rhodes University, South Africa for their valuable contribution towards singlet oxygen generation studies.

I am thankful to all the lab members, both the former and current members for their support, understanding, helpful discussions and creating a warm, friendly atmosphere, which made the whole work fun. To name a few, I am thankful to former members, Dr. Hisamune, Dr. Yogesh, Dr. Yang, and current members, Dr. Biju, Mr. Yamasumi, Mrs. Wang, Mr. Kage, Mr. Wang, Mr. Alex and all the other members in my lab.

I would like to thank my family and friends for their endless support, encouragement, and love.